Annual Report 2013

HI Jena

Helmholtz Institute Jena

Helmholtz Institute Jena
Fröbelstieg 3
07743 Jena
www.hi-jena.de

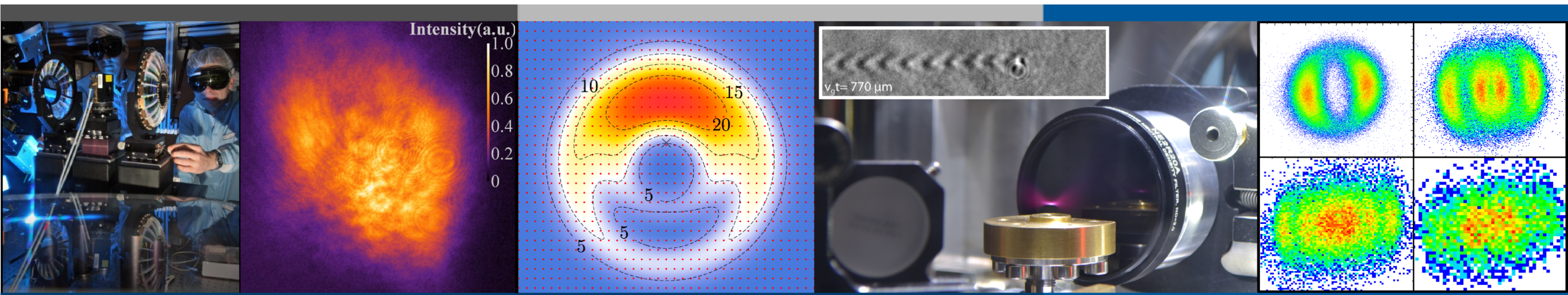

seit 1558

Helmholtz Institute Jena

Annual Report 2013

Contents

Introduction

The Helmholtz Institute Jena (HI-Jena), a branch of the GSI Helmholtz Center for Heavy Ion Research and located on the campus of the Friedrich Schiller University Jena (FSU), was founded in 2009 to bring together expertise on the development of high-intensity lasers, their applications for particle acceleration, as well as the detection and spectroscopy of high-energy photon and particle beams. Meanwhile, the HI-Jena has become a center of its own for the physics of strong fields. This Annual Report for the year 2013 documents the ongoing progress.

The Helmholtz Institute Jena also has established an important bridge between the Helmholtz Centers in Darmstadt, Dresden and Hamburg, for which it provides and transfers experience at the border between conventional particle-acceleration schemes and the rapidly evolving field of laser-induced particle acceleration. It benefits considerably from the strong involvement of the research groups at the Friedrich-Schiller University Jena working in the fields of high-power laser systems, X-ray spectroscopy techniques and on experiments in the realm of extreme electromagnetic fields. In particular, the HI-Jena has been found very valuable for planning and developing the research at the two large-scale accelerator projects for electrons and ions, the European XFEL and the International FAIR facilities.

The HI-Jena appreciates the successful application for a Helmholtz Young Investigator Group by Dr. Sergey Rykovanov, as well as for the funding within the framework of the Helmholtz Postdoc Program for Dr. Renate Märtin. The research at the institute includes the theoretical study of relativistic laser plasmas together with the generation of X-ray pulses, and X-ray spectroscopy. Furthermore, Prof. Dr. Stephan Fritzsche arrived in 2013 at the HI-Jena. He leads a group on theoretical atomic physics at the HI-Jena, and belongs to the "Theoretisch Physikalisches Institut" at the Friedrich-Schiller University. To highlight the strong theoretical involvement and support of ongoing experiments, we have included a dedicated section on theory in this Annual Report.

In addition, several workshops were held at the HI-Jena in 2013 and brought together international expertises from different fields. In particular let us mention the 10th SPARC workshop with more than 100 participants that connected the current research with the perspectives of the future "Facility for Antiproton and Ion Research" (FAIR) located at the GSI Helmholtz Center for Heavy Ion Research in Darmstadt.

Finally, we want to mention the Research School for Advanced Photon Science (RS-APS), the joint graduate school of the HI-Jena and the FSU, which was started successfully in 2012. Last year's highlight was the first joint lecture week with the Helmholtz Graduate School for Hadron and Ion Research (HGS-HIRe) in Ulrichshusen Manor. A detailed report on the status of the RS-APS follows on the next page.

Research School of Advanced Photon Science of the Helmholtz Institute Jena *

R. Märtin[1,2], *C. Spielmann*[3], *and Th. Stöhlker*[1,2,3]
[1]HI-Jena, Jena, Germany; [2]GSI, Darmstadt, Germany; [3]IOQ, University Jena, Jena, Germany

Among the most important tasks of the Helmholtz Institute Jena is the education and support of young scientists who are working in the research field of new laser-induced accelerator concepts, as well as in the investigation of intense photon and particle beams, including their interaction with matter. The Research School of Advanced Photon Science (RS-APS) provides structured PhD education adapted to the research profile and organizational structure of the HI Jena which is of major importance for the international FAIR project in Darmstadt and the European XFEL facility in Hamburg, both being currently in the construction phase.

Currently 20 PhD students are participating in the program of the research school who are supervised by 14 principal investigators belonging directly to the Helmholtz Institute Jena or to institutes of the cooperating University Jena. Here, the doctoral students have the possibility to participate in the academic program which is offered directly by the Helmholtz Institute Jena and moreover they have access to the broad spectrum of courses provided by the cooperating graduate programs. The RS-APS is member of the graduate academy of the Jena university and additionally, the school is in close cooperation with both the Abbe School of Photonics, which resides at the Department for Physics and Astronomy (PAF), and the DFG graduate college "Quantum and Gravitational Fields". Moreover since 2013 the RS-APS is member of the Helmholtz Graduate School for Hadron and Ion Research (HGS-HIRe) which promotes structured PhD education for research associated with FAIR and GSI.

In 2013 almost half of the students of the HI Jena participated in dedicated soft skill block courses offered by HGS-HIRe focusing on the strengthening the core competencies of young researchers. Furthermore students of the Helmholtz Institute were represented at so-called Power Weeks by HGS-HIRe. A Power Week is focused on a particular science topic. In contrast to a lecture week it is not interdisciplinary and therefore allows discussions on a much deeper level. In addition transferable skill courses offered on site by the graduate academy Jena have been visited, e.g. qualification in academic teaching.

One major event in 2013 was the first joint HGS-HIRe and RS-APS Lecture Week which took place in Ulrichshusen Manor from August 25-30, 2013. The whole week 25 students dealt intensively with "The physics of ultrashort laser pulses and laser matter interactions". Here the PhD students have been supervised by the lecturers Michael Geissler (U Belfast), Mark Prandolini (HI Jena and DESY), Christian Spielmann (HI Jena and U Jena) and Matt Zepf (HI Jena and U Belfast) (see Fig.1).

Figure 1: Participants of the joint lecture week of HGS-HIRe and RS-APS.

The Research School of the HI Jena is not only supporting its students financially through scholarships but also every student has it own annual travel budget which he can spend individually. In 2013 two third of the doctoral candidates took use of this money for visiting international workshops and conferences to present their research results.

* Work supported by HI Jena

High Power Laser Development

16.6 J chirped femtosecond laser pulses from the 5^{th} diode pumped Yb:CaF_2 amplifier of POLARIS laser system *

A. Kessler[1,2], M. Hornung[1,2], S. Keppler[2], F. Schorcht[1], M. Hellwing[2], A. Sävert[2], J. Hein[1,2], and M. C. Kaluza[1,2]

[1]HI-Jena, Jena, Germany; [2]Institute of Optics and Quantum Electronics (IOQ), Jena, Germany

Diode-pumped, chirped pulse amplification using Yb^{3+}-doped amplification materials is envisioned to be an efficient approach for generating high peak power laser pulses both with high repetition rate and high pulse energy [1, 2]. $Yb{:}CaF_2$ is a promising candidate supporting the generation of short pulses with duration in 100 fs region. We report results using the 5^{th} amplifier of the POLARIS laser system [3, 4] which uses $Yb{:}CaF_2$ as the amplification medium.

The pump engine currently includes 120 (of 240 possible) laser diode stacks (LDS). Each LDS (Jenoptik AG) emits an optical peak power of 2.5 kW at a pump wavelength of 940 nm. For a 2.7 ms long pump pulse a total pump energy of 810 J can be applied to the laser material.

For anticipated output energies of up to 50 J, the diameter of the laser pulses in the last amplifier had to be increased to 35 mm (FWHM), requiring an amplification crystal with a diameter of more than 60 mm to avoid clipping. As the active material, we use a <111>-cut, 2.3 at.% doped $Yb{:}CaF_2$ crystal made by Hellma Materials GmbH with a diameter of d=65 mm and a thickness of t=34 mm (90 % pump absorption). Both flat surfaces are anti-reflective coated for both pump (935 nm - 950 nm) and laser wavelengths (1020 nm - 1045 nm) with R<0.15%.

For energy extraction a multi-pass configuration with 9 passes through the active medium has been installed. The passes are assembled in a cone of beams with a separation angle of $8°$. The amplifier is seeded by stretched nanosecond pulses at a central wavelength of 1033 nm and a bandwidth of 11.5 nm (FWHM). A pulse energy of E_{out}=16.6 J has been achieved with a seed pulse energy of E_{seed}=2.7 J corresponding to a gain factor of g=6.1, agreeing with our numerical simulation. These are to our knowledge the most energetic laser pulses achieved from a diode pumped chirped pulse amplifier so far.

Fig. 1 presents the results of the actual amplification measurements. In Fig. 1 a) the near field profile of an amplified laser pulse, in b) spectral intensity distribution compared to the seed pulse spectrum. The inset displays the near-field distribution of the seed pulse.

In agreement with our simulation, the input pulses (λ_c=1033 nm) are slightly red-shifted to λ_c=1034 nm during the amplification while their FWHM bandwidth is reduced from 11.5 nm to 10 nm due to gain narrowing.

While the seed energy from the amplifier A4 could be increased up to 6.5 J (cf. [2]) the A5-output energy is currently limited by the maximum fluence of $2\,\mathrm{J/cm^2}$ on the $Yb{:}CaF_2$-crystal in order to avoid laser induced damage of the coating ($F_{damage}=3.4\,\mathrm{J/cm^2}$). However, $Yb{:}CaF_2$ crystals AR coated with a damage fluence of more than $10\,\mathrm{J/cm^2}$ will be available soon which is likely to triple the output energy of this amplifier in the future. The next steps will be to compress and focus the amplified pulses in order to ultimately use them in high-intensity laser matter experiments.

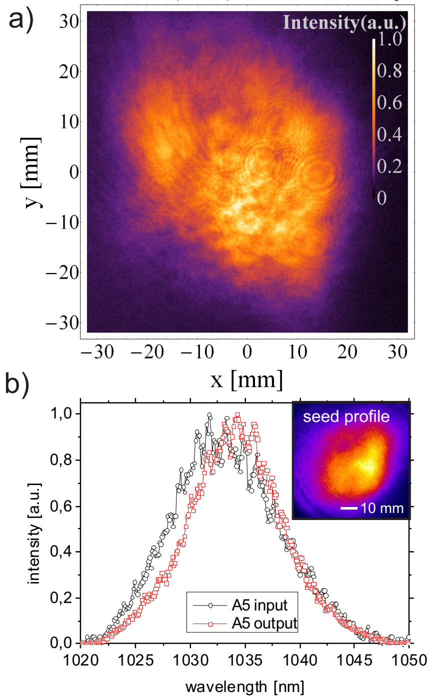

Figure 1: Measurements of the amplified laser pulses. a) Near field distribution of a laser pulse with 16.6 J pulse energy at the output of A5. b) Spectral intensity distribution of the seed pulses (black) and the amplified laser pulses (red). The inset shows the near-field distribution of the seed pulse.

References

[1] M. Siebold et al., Appl.Phys. B **90**, 431-437 (2008).

[2] M. Hornung et al., Optics Letters **38** [5], 718-720 (2013).

[3] A. Kessler et al., annual report HI-Jena **2011**, p18.

[4] A. Kessler et al., Optics Letters, accepted (2014)

* Work supported by HI-Jena and FSU-Jena IOQ, EC's 7^{th} Framework Programme (LASERLAB-EUROPE, grant n° 228334) and from the BMBF (03ZIK445 and 03Z1H531)/

Temporal characterization of the on-target ASE intensity from POLARIS*

S. Keppler† [1], M. Hornung[1,2], H. Liebetrau[1,2], A. Kessler[1,2], M. Hellwing[1], F. Schorcht[1,2], J. Hein[1,2], and M. C. Kaluza[1,2]

[1]Institute of Optics and Quantum Electronics, Jena, Germany; [2]Helmholtz Institute Jena, Germany

State-of-the-art high-intensity laser systems generating focused intensities I_0 of up to $10^{20}\ \mathrm{W/cm^2}$ are predestined to be used in acceleration schemes for charged particles, e.g. for electrons or protons and heavier ions. However, for a comprehensive description of the physics dominating the various interaction scenarios a precise characterization of the laser pulse parameters and the target conditions at the beginning of the high-intensity interaction is mandatory. In addition to wavelength, energy, duration, and peak intensity of the laser pulse, the temporal evolution of the pulse contrast is another crucial parameter. Both amplified spontaneous emission (ASE) of laser radiation within the laser amplifier chain and short prepulses strongly influence the evolution of the contrast before and after the main pulse and thus significantly alter the target conditions. Hence, a complete characterization and the improvement of the pulse contrast are among the key issues when optimizing high-power laser systems for laser-matter experiments.

Since the saturation fluence of Yb:glass, which is used as the amplifying medium at the fully diode-pumped POLARIS laser, is much higher than the laser induced damage threshold, the amplifiers cannot be operated in saturation. This fact allows for the independent characterization of the ASE generated by each individual amplifier without the seed pulse from the oscillator.

For the temporal characterization, the ASE of both regenerative amplifiers A1 and A2 and of the subsequent multipass amplifiers A2.5, A3, and A4 was measured behind the compressor. For the measurement of the ASE of a particular amplifier, the seed was blocked at the entrance of the respective amplifier, while all subsequent amplifiers were operating with their usual parameters.

Fig. 1 shows a combination of two log-log plots (a) for times $-10\,\mathrm{ms} \leq t \leq -10\,\mathrm{fs}$ and (b) for times $10\,\mathrm{fs} \leq t \leq 10\,\mathrm{ms}$. The axis of symmetry, represented by the vertical dashed black line, provides the artificially added time $t = 0$, which was used as the absolute time reference during the measurement. The main pulse was measured with a 3^{rd}-order crosscorrelator while the ASE contributions of the several amplifiers were measured with a photo diode/oscilloscope setup with a temporal resolution of $0.7\,\mathrm{ns}$ and calibrated ND-filters [2]. Note that the ASE duration τ of the regenerative amplifiers A1 and A2 is mainly determined by the round-trip time of $13.25\,\mathrm{ns}$, while τ of the main amplifiers is determined by the pump duration of $2.7\,\mathrm{ms}$ and the fluorescence lifetime of $1.4\,\mathrm{ms}$ for Yb:glass [2].

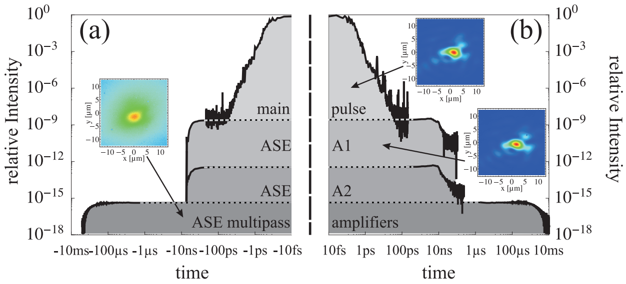

Figure 1: Combined log-log plot of the ASE from the different POLARIS amplifiers. The insets show the respective spatial distribution measured in the focal plane of the main pulse. The ASE measurements were carried out with a photo diode/oscilloscope combination while the main pulse was measured with a 3^{rd}-order cross-correlator.

In addition to the temporal characterization of the ASE energy in the POLARIS system, also the spatial distribution in the far field, which is determined by the FWHM area and the q-factor [1], was measured in the focal plane of the main pulse, cf. Fig. 1. For this purpose, the ASE was imaged to a high-dynamic CCD with the same setup as used to characterize the focal spot of the main pulse.

Finally, the average intensity within the spatial FWHM was calculated by $\overline{I} = q \cdot E/(\tau \cdot A)$ [2]. Here, it is obvious, that the main fraction of ASE of $\overline{I} = 3.2 \times 10^{10}\ \mathrm{W/cm^2}$ that will affect a laser-plasma interaction, is generated within the first regenerative amplifier A1. Bogeaerts *et al.* [3] found that a minimum intensity of $I_{\min} \approx 2 \times 10^{9}\ \mathrm{W/cm^2}$ is necessary to melt a Cu-target with a laser pulse comparable to the A1-ASE regarding wavelength and duration. Therefore an ASE improvement of 3 orders of magnitude to an intensity of less than $I_{\min}$ is necessary that the target conditions remain unchanged for laser-matter experiments using thin Cu-foils. This will in future be achieved using the principle of cross polarized wave generation (XPW) or optical parametric amplification (OPA) within a double-CPA setup in POLARIS.

References

[1] M. Hornung *et al.*, Opt. Lett. **38,** (2013) 718.

[2] S. Keppler *et al.*, submitted to Opt. Express.

[3] A. Bogeaerts *et al.*, Spectrochim. Acta, Part B **60** (2005).

* Work supported by the European commissions (EC) 7^{th} Framework Programme (LASERLAB-EUROPE, grant no. 228334) and the Bundesministerium für Bildung und Forschung (BMBF) (03ZIK445 and 03Z1H531).

† Sebastian.Keppler@uni-jena.de

POLARIS: Generation of ultra-high contrast laser pulses with a double-CPA frontend and crossed polarized wave generation

M. Hornung[*1,2], *H. Liebetrau*[2], *A. Seidel*[2], *S. Keppler*[2], *A. Kessler*[1], *M. Hellwing*[2], *F. Schorcht*[1], *J. Hein*[1,2], *and M.C. Kaluza*[1,2]

[1]Helmholtz Insitute Jena, Germany; [2]Institute of Optics and Quantum Electronics, Jena, Germany

While the fully diode-pumped POLARIS laser system [1] has continued its experimental program [2] with more than 16000 recorded shots on target during the last 1.5 years we have further optimized the laser performance in terms of temporal intensity contrast and pulse duration (spectral bandwidth). As the temporal intensity contrast has been shown to be one of the most important parameters for the laser's successful application in high-intensity experiments we have installed an additional stretcher-compressor system (double CPA [3]) in the frontend of POLARIS in order to generate a crossed polarized wave (XPW [4]) and improve the temporal contrast of POLARIS.

In the first CPA stage (cf. Fig. 1) the pulses are stretched to a pulse duration of 20 ps, amplified to 2 mJ pulse energy and finally recompressed to 130 fs FWHM pulse duration. These compressed pulses are focused by a lens shortly behind a BaF_2-crystal in order to generate a crossed polarized wave. This crystal is placed between two crossed polarizers with an extinction ratio of 2×10^{-6} each. The generated signal with crossed polarization is emitted in a TEM_{00}-mode with a maximum pulse energy of 140 μJ, a spectral bandwidth of 21 nm (FWHM) and used as the seed-source for the subsequent ns-stretcher. The signal has an improved temporal contrast and a broadened spectral bandwidth which allows for a shorter pulse duration after the final compression. For the full amplified laser pulses we have shortened the pulse duration from formerly 164 fs down to 144 fs (FWHM). The temporal contrast of the compressed laser pulses is displayed in Fig. 2. The measurements on different timescales were performed either with photodiodes or a third-order correlator. In contrast to the conventional frontend our new frontend is able to improve the ASE contrast by more than 4 orders of magnitude (cf. [1]).

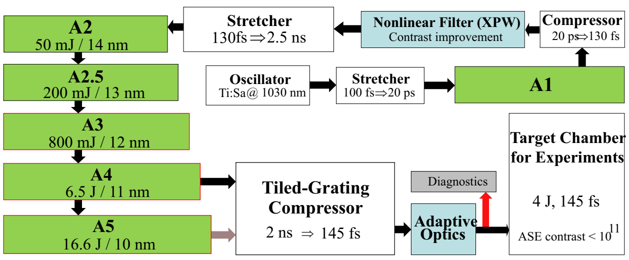

Figure 1: Schematic overview of POLARIS. A stretcher-compressor unit is placed around amplifier 1 (A1) to allow nonlinear filtering with XPW generation.

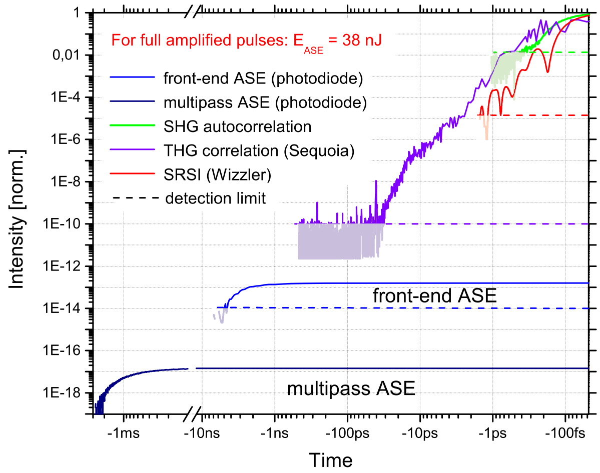

Figure 2: Measurements of the temporal intensity contrast at different timescales of the POLARIS laser pulses.

In conclusion, we have significantly improved the temporal contrast of POLARIS currently with an ASE energy of 38 nJ (from formerly 130 μJ) and a relative ASE-intensity compared to the main pulse of 2×10^{-13} (from formerly 2×10^{-9}).

References

[1] M. Hornung, S. Keppler, R. Bödefeld, A. Kessler, M. Hellwing, F. Schorcht, J. Hein, and M. C. Kaluza, "High intensity, high contrast laser pulses generated from the fully diode-pumped Yb:glass laser system POLARIS", Optics Letters, Vol. 38, Issue 5, 2013, pp. 718-720

[2] M. Hornung, S. Keppler, R. Bödefeld, A. Kessler, H. Liebetrau, M. Hellwing, F. Schorcht, J. Körner, O. Jäckel, A. Sävert, J. Polz, A.K. Arunachalam, J. Hein, M.C. Kaluza, "POLARIS – the high-intensity fully diode pumped laser system commences experimental operation", GSI Scientific Report 2012

[3] M.P. Kalashnikov, E. Risse, H. Schönnagel, A. Husakou, J. Herrmann, and W. Sandner, "Characterization of a nonlinear filter for the front-end of a high contrast double-CPA Ti:sapphire laser", Optics Express, Vol. 12, No. 21, 2004, pp. 5088-5097

[4] A. Jullien, O. Albert, G. Chériaux, J. Etchepare, S. Kourtev, N. Minkovski, and S.M. Saltiel, "Nonlinear polarization rotation of elliptical light in cubic crystals, with application to cross-polarized wave generation," JOSA B, Vol. 22, Issue 12, 2635-2641 (2005).

* M.Hornung@gsi.de

Highly efficient broadband amplification of laser pulse bursts

J. Körner[*1], *J. Hein*[1], *J. Reiter*[1], *R. Seifert*[2], *D. Klöpfel*[1], *and M.C. Kaluza*[1,2]
[1]Institute of Optics and Quantum Electronics, Friedrich-Schiller-University, Max-Wien-Platz 1, 07743 Jena, Germany;
[2]Helmholtz-Institute Jena, Fröbelstieg 3, 07743 Jena, Germany

Over the past years a significant effort has been made for the development of highly efficient laser-diode pulse-pumped laser amplifiers for nanosecond pulses with high energy and repetition rate. Such systems are typically based on Yb:YAG cooled down to the temperature of liquid nitrogen. At this temperature the overlap of absorption and emission bands, which is the main disadvantage of Yb^{3+}-doped gain media is suppressed [1].

However, when aiming at the amplification of pulses in the range of some picosconds or femtoseconds cryogenically cooled Yb:YAG is no longer an option since the amplification bandwidth is too narrow at low temperatures. The alternative material $Yb{:}CaF_2$ offers a large available bandwidth even at cryogenic temperatures because the broadening of the individual lines is mainly caused by inhomogeneity. In contrast to Yb:YAG this also leads to much smaller emission cross sections and a high saturation fluence of about 40 J/cm^2 even at cryogenic temperatures. Because this is much higher than the LIDT for pulse lengths of some nanoseconds, which is limited by the CPA laser scheme, saturating the amplifier with a single pulse becomes impossible.

To achieve an efficient extraction in such a scheme we developed a laser system using the so called burst mode. Here the extraction of energy is distributed over a number of pulses. Now the accumulated fluence of these pulses allows to saturate the laser material without reaching the LIDT.

The system consits of a frontend generating bursts of a total duration of 1 ms with up to 1000 single pulses with a duration of 350 fs and an energy of 3 μJ each. The pulses stretched within an Oeffner-type strecher to 150 ps. Then the bursts are amplified within two amplifier stages based on $Yb{:}CaF_2$ at 100 K.

Results of the first amplifier stage were allready published[2, 3]. Since then the performance of this amplfier has been increased by substituting the original 2.5 kW pump engine with a homogenized high brightness 4 kW setup. Due to these changes the amplifier now delivers a square tophat beam profile with a diameter of 2.5 mm. The average output power was ramped up to 760 W during a burst of 1000 pulses. A reduction of the number of pulses to 50 allows to increase the single pulse energy to 11 mJ.

To further boost the energy the second amplifier (cf. fig. 1) was installed. The amplifier utilizes a relay imaging scheme similar to the one of the first amplifier. Placing the whole amplifier into a vacuum environment allowed to significantly reduce the focal length of the optical elements used. This lowered the footprint of the amplifier on the optical table to about 1 m^2. Within this setup 16 imaged material passes are realized with a beam diameter of 8 mm. As the pump a homogenized 18 kW laser diode module is used(PM19.2, Lastronics GmbH), producing a square flat-top pump distribution matched with the profile of the incoming beam of the first amplifier.

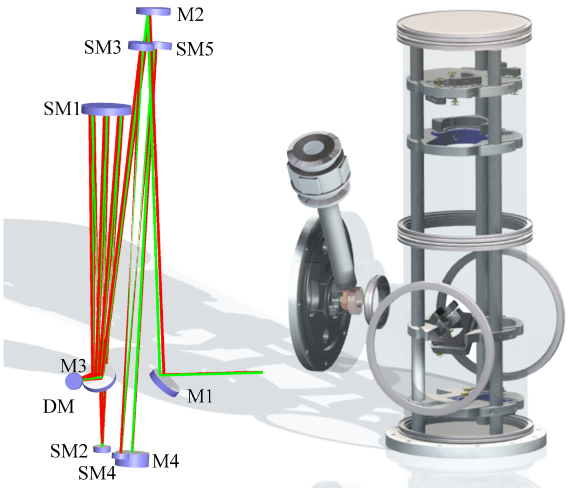

Figure 1: Layout of the second amplifer stage. Left: Ray tracing of the 16 pass relay imaging optics. Right: CAD of amplifier fitted into a vacuum tube

Seeded with pulses from the first amplifier, a maximum average output power of 7.4 kW within the burst duration was achieved (1000 pulses). With 50 pulses per burst the output power only reduced to 6.2 kW. This corresponds to a single pulse output energy of 125 mJ.

Continued development of the amplifier and the implementation of a compressor will result in TW-level output pulses at a kilohertz average repetition rate.

References

[1] J. Körner, et al. , “Spectroscopic characterization of Yb^{3+}-doped laser materials at cryogenic temperatures”, Appl.Phys.B (2013)

[2] J. Körner, et al. , “Amplifier development with cryogenically cooled $Yb{:}CaF_2$”, GSI Scientific Report 2012 (2013)

[3] J. Körner, et al., “Efficient burst mode amplifier for ultrashort pulses based on cryogenically cooled $Yb^{3+}{:}CaF_2$”, Opt.Expr. Vol.21 Issue 23 (2013) 29006-29012

* joerg.koerner@uni-jena.de

Temporal pulse combination for laser power scaling*

A. Klenke[1,2], *M. Kienel*[1,2], *T. Eidam*[1,2], *S. Hädrich*[1,2], *J. Rothhardt*[1,2], *J. Limpert*[† 1,2,3], *and A. Tünnermann*[1,2,3]

[1]Friedrich-Schiller-Universität Jena, Institute of Applied Physics, Abbe Center of Photonics, Albert-Einstein-Straße 15, 07745 Jena, Germany; [2]Helmholtz-Institute Jena, Fröbelstieg 3, 07743 Jena, Germany; [3]Fraunhofer Institute for Applied Optics and Precision Engineering, Albert-Einstein-Straße 7, 07745 Jena, Germany

The combination of multiple pulses into a single super-pulse has been proposed as a method to circumvent limitations of laser systems related to pulse energy and average power. There are different approaches for this technique, e.g. the parallel implementation of multiple amplifiers or amplifying multiple temporally separated pulses, followed by a spatial or temporal recombination. We have investigated the usage of the latter concept in a high power fiber CPA system, as well as using it for nonlinear compression.

Actively stabilized divided-pulse amplification (aDPA)

In the classic scheme of amplifying temporally separated pulses, called Divided-Pulse Amplification (DPA), the splitting and recombination of the pulses is done in the same stage and the amplifiers are working in a double-pass configuration. However, when approaching high-energy pulses, saturation effects occur. They result in a mismatch of the nonlinear effects and impact the pulse replicas [1].

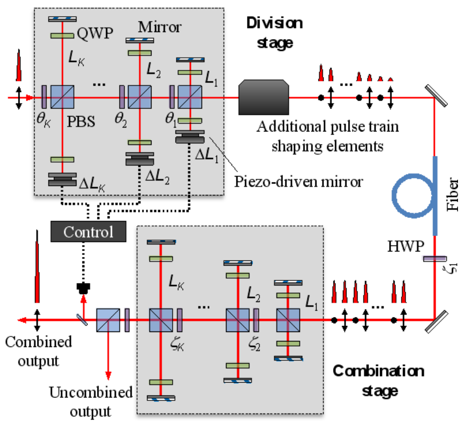

Figure 1: Schematic drawing of an actively controlled DPA setup with separated division and combination stage (PBS - polarizing beam splitter, HWP - half-wave plate, QWP - quarter-wave plate).

Therefore, recombination of the pulses is no longer possible with a high combination efficiency. To overcome this problem, we have realized a setup (see Figure 1 where the splitting- and combination stages were separated, leading to more possibilities of compensating for these issues. However, an additional active stabilization system has to be implemented for this scheme to work. We have demonstrated the viability of this concept in an experiment, showing the recombination of mJ-pulses with a high efficiency of 75% [2].

Divided-pulse nonlinear compression

To overcome bandwidth limitations in laser systems, non-linear compression can be used. However, the nonlinear medium (e.g. a solid-core fiber or a gas-filled capillary) can limit the achievable pulse energy for this approach due to self-focusing, ionization or damage. Again, the temporal pulse splitting/combination concept is a useful tool to overcome these limitations. In a first experiment [3], we split 320 fs femtosecond input pulses into four replicas each, therefore reducing the peak-power by a factor of four. These replicas were spectrally broadened in a solid-core fiber and temporally recombined into a single pulse. In contrast to the divided-pulse amplification case, there are no saturation effects. Therefore, the splitting and combination can be done in a single stage. Finally, the pulses were compressed to the sub 100fs-regime with a chirped-mirror compressor. We could demonstrate that a higher pulse energy than without this temporal division scheme was achievable, i.e. using a single pulse with the same peak-power would have resulted in the destruction of the fiber due to self-focusing. This concept will also be applicable to other use cases, e.g. with hollow-core fibers to create high energy few-cycle pulses in the near future.

Outlook The combination of the aDPA concept together with spatial combination of multiple amplifiers will allow to build laser systems with an unprecedented combination of pulse energy and average power. This opens up the possibility to make very demanding applications like laser particle acceleration work at high repetition rates.

References

[1] M. Kienel et. al. Opt. Express **21**, 29031-29042 (2013).

[2] M. Kienel et. al. accepted for publication in Opt. Letters

[3] A. Klenke et al. Opt. Lett. **38**, 4593-4596 (2013).

* This work has been partly supported by the German Federal Ministry of Education and Research (BMBF) and the European Research Council under the European Union's Seventh Framework Program (FP7/2007-2013)/ERC Grant agreement no [240460].

† jens.limpert@uni-jena.de

High average power nonlinear compression of coherently combined fiber chirped pulse amplifiers*

S. Hädrich[1,2], A. Klenke[1,2], J. Rothhardt[1,2], A. Hoffmann[1], M. Krebs[1], T. Eidam[1,2], T. Gottschall[1], J. Limpert†[1,2,3], and A. Tünnermann[1,2,3]

[1]Friedrich-Schiller-Universität Jena, Institute of Applied Physics, Abbe Center of Photonics, Albert-Einstein-Straße 15, 07745 Jena, Germany; [2]Helmholtz-Institute Jena, Fröbelstieg 3, 07743 Jena, Germany; [3]Fraunhofer Institute for Applied Optics and Precision Engineering, Albert-Einstein-Straße 7, 07745 Jena, Germany

Fiber chirped pulse amplifiers have lately seen significant improvements in their performance thanks to the develepement of the so-called large pitch fiber [1] and the implementation of coherent combination concepts [2]. The latter one means that multiple main amplifier stages are runnning in parallel, seeded by pulse replicas delivered by a common front-end. After amplification the replicas are interferometrically added leading to an improvement in the output parameters equal to the number of channels. By using a four-channel fiber CPA system up to 530 W, 1.3 mJ [2] or or 200 W, 2 mJ [3] pulses were generated, recently.

Nonlinear compression

The pulses that are delivered by the four-channel fiber CPA system have a pulse duration of $\sim$ 340 fs, which is too long for several applications, e.g. high harmonic generation. A well-known technique for post-compression of millijoule level pulses is based on propagation in noble gas filled hollow-core fibers [4] (Fig.1).

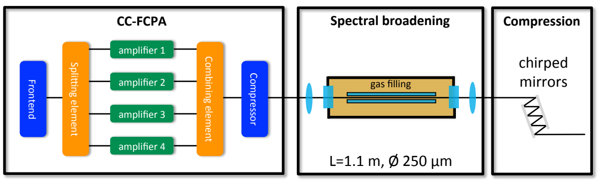

Figure 1: Experimental setup for nonlinear compression.

The pulses are coupled to a capillary with 250 μm inner diameter and a length of 1 m. After evacuation the capillary is statically filled with krypton or argon gas and the pressure is increased to achieve sufficient spectral broadening. Subsequently, the pulses are compressed in time by passing a chirped mirror compressor. The most critical point, however, for high average power operation are the inherently high propagation losses of the capillary. In our system the overall efficiency is better than 50 % with most of the losses coming from the propagation. Therefore, a specifically designed water-cooled setup has been developed to mitigate thermal load on the surrounding mechanical components.

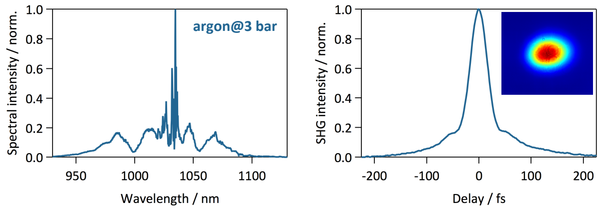

Figure 2: Spectrum (left) and autocorrelation (right) measured after the hollow-core fiber at 0.54 mJ, 26 fs and 250 kHz (135 W). The inset shows the collimated beam after the chirped mirror compressor.

The use of this system has allowed to achieve new record values for the performance of high energetic nonlinear compression. On the one hand the compression of 1.1 mJ, 340 fs pulses at 250 kHz (280 W) to 0.54 mJ (135 W), 26 fs (Fig.2) was demonstrated [5]. On the other hand it was possible to compress 2 mJ, 340 fs at 100 kHz (200 W) to 1 mJ, 45 fs [6], where the onset of ionization effects at the fiber entrance can be observed. Both of the aforementioned results are comparable to Ti:Sapphire laser system in terms of pulse energy and duration, but offer an order of magnitude higher repetition rate.

Outlook The experiments on nonlinear compression are the first experimental demonstration of the unique potential of coherent combination of fiber CPA systems. The sub-30 fs pulses with high average power have recently been used to generate more than 100 μW of average power in a single high harmonic [7]. This itself has the potential for a new generation of coherent extreme ultraviolet sources for various applications. A second compression stage will enable few-cycle pulses at high average power (repetition rate) in the near future.

References

[1] J. Limpert et. al. Light: Science & Applications **1**, e8 (2012)

[2] A. Klenke et al. Opt. Lett. **38**, 2283 (2013).

[3] A. Klenke et al., to be presented at Photonics West 2014

[4] M. Nisoli et al. IEEE JSTQE **4**, 414(1998).

[5] S. Hädrich et al. Opt. Lett. 38, 3866 (2013).

[6] S. Hädrich et al., to be presented at Photonics West 2014

[7] S.Hädrich et al., HIJ annual report 2013

* This work has been partly supported by the German Federal Ministry of Education and Research (BMBF) and the European Research Council under the European Union's Seventh Framework Program (FP7/2007-2013)/ERC Grant agreement no [240460].

† jens.limpert@uni-jena.de

Stimulated Raman Backscattering at JETI and PHELIX*

B. Landgraf[1,2], *D. Kartashov*[1], *B. Aurand*[3], *A. Hoffmann*[1], *T. Gangolf*[1], *F. Gärtner*[3], *P. Polynkin*[4], *T. Kühl*[3], *and C. Spielmann*[1,2]

[1]IOQ, FSU Jena, Germany; [2]HI Jena, Germany; [3]GSI, Darmstadt, Germany; [4]Optical Sciences, The University of Arizona, USA

Laser systems based on the Chirped Pulse Amplification Scheme (CPA) rely on laser pulses which can be first stretched, then amplified and subsequent re-compressed. Due to scaling issues High-Intensity Laser Systems need more expensive gratings each generation. Stimulated Raman Backscattering (SRBS) can circumvent pulse compression gratings and expensive broad band beam amplification by transferring energy from a narrow band picosecond to nano-second pulse into a broad band Ultrashort seed pulse. To achieve phase matched energy transfer wave vectors of pump pulse photons, plasma wave and seed pulse need to be aligned exactly. This entails a Redshift of the seed pulse in the range of $50 - 150nm$. Up to now most experiments use $Ba(NO_3)_2$ or similar crystals which can sustain good Redshift but insufficient conversion efficiency. Due to limiting instabilities competing with SRBS the usable parameter range is limited if the seed has low intensity and the process is in the linear transfer regime. To overcome these limitations we have done extensive studies and tested suitable Redshift processes supplying 10-100 times more intensity with outstanding temporal and spatial beam properties.

Broad Band Amplification

With the help of Self Phase Modulated (SPM) $sub - 20fs$ beams generated in a hollow core fiber [1] we were able to evaluate the amplification bandwidth of the SRBS process within a density gradient and compare results with the super radiant growth properties shown in [2]. The results estimated a bandwidth of $90nm$ theoretical supporting sub-20fs pulses. The measured energy in the seed beam before interaction in the wavelength region of $800 - 900nm$ was in the order of $100\mu J$. To overcome the linear regime in SRBS a pulse energy in the order of at least $1mJ$ is needed. This value needs to be scaled with the energy of the pump beam and the SPM method is limited to J-laser systems.

Scalable Seed

To develop a concept to be used at High Energy Lasers as the PHELIX laser facility we developed a scalable concept with the help of Axicon focusing. With this focus geometry up to 100 times more energy can be present in the focal region without generating filament channels. At the central axis of the Axicon geometry a Gaussian shaped beam (Fig. 1) generated by classical Raman scattering can be generated. Red-shift and conversion efficiency can be controlled by means of intensity either by variation of energy, pulse duration or focal length of the Axicon (Fig. 2). The process also generates near transform limited $100fs$ pulses out of ps-pump pulses.

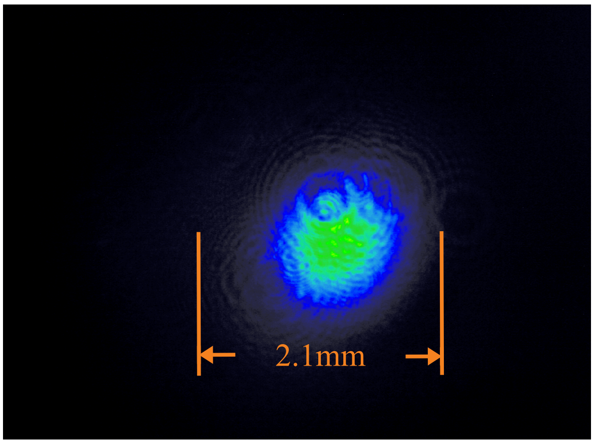

Figure 1: Measured Gaussian like beam profile.

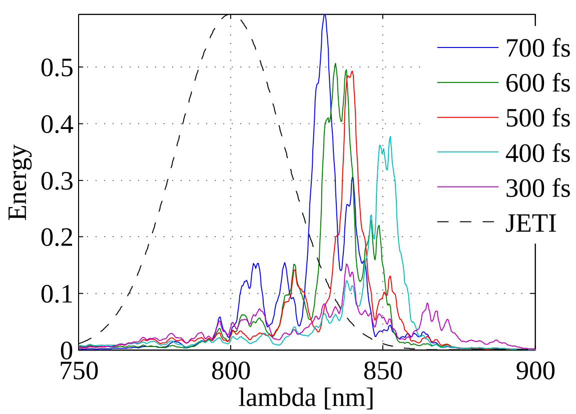

Figure 2: Measured Red-shifted spectra.

* bjoern.landgraf@uni-jena.de, Work supported by GSI(PHELIX)/HI Jena/U Arizona

References

[1] M. Nisoli "Compression of high-energy laser pulses below 5 fs" Opt. Lett. 22, 522-524 (1997)

[2] G. Vieux "Plasma density measurements using chirped pulse broad-band Raman amplification". Applied Physics Letters, Vol. 103, No. 12, 121106, 18.09.2013.

High harmonic generation achieving more than 100 μW average power in a single harmonic*

S. Hädrich[1,2], A. Klenke[1,2], J. Rothhardt[1,2], A. Hoffmann[1], M. Krebs[1], J. Limpert[† 1,2,3], and A. Tünnermann[1,2,3]

[1]Friedrich-Schiller-Universität Jena, Institute of Applied Physics, Abbe Center of Photonics, Albert-Einstein-Straße 15, 07745 Jena, Germany; [2]Helmholtz-Institute Jena, Fröbelstieg 3, 07743 Jena, Germany; [3]Fraunhofer Institute for Applied Optics and Precision Engineering, Albert-Einstein-Straße 7, 07745 Jena, Germany

Femtosecond laser pulses focused onto gas targets with intensities on the order of 10^{14} W/cm^2 generate extreme ultraviolet radiation via the process of high harmonic generation (HHG) [1]. Due to its spatial coherence and femtosecond-to-attosecond durations this radiation has found diverse applications. Currently, it is still mostly generated with kilohertz Ti:Sapphire lasers. However, applications in multidimensional surface science or coincidence detection would greatly benefit from both an increase in repetition rate and photon flux [2].

High harmonic generation with fiber lasers

For efficient HHG ultrashort laser pulses are required [3]. This is realized by post-compression of a fiber CPA system that incorporates four coherently combined main amplifier channels[4]. This system delivers sub-30fs pulses with a pulse energy of $\sim 140\,\mu$J, which are focused to a focal spot size of 90 μm (diameter) resulting in an intensity of $\sim 10^{14}$ W/cm^2. The harmonics are generated either in a 600 μm opening (krypton) or 1 mm opening (xenon) gas jet. The emerging harmonics and the fundamental pass a chicane of two SiO_2 substrates to reduce the average power of the infrared laser. The harmonics are filtered from the fundamental laser by two aluminum filters with a thickness of 1 μm each and are analyzed by a flat-field spectrometer. The generated photon flux is obtained by accounting for the known transmission properties of the spectrometer, the tabulated reflections coefficients of SiO_2 substrates and the measured transmision of the aluminum filters.

Figure 1 shows the spectrum of high harmonics generated in xenon (blue) and krypton (red). The laser system has been operated at 600 kHz repetition rate and > 80 W of average power. The gas jet position is optimized for the highest yield, which is the case for a position slightly behind the focus. This position favours the short trajectories resulting in a low divergent beam [5]. The beam profiles of the harmonics are well-behaved and Gaussian like with a divergence of less than 2 mrad. Together with the pressure-dependent behaviour of the harmonic yield it can be concluded that phase-matching has been achieved. This is further substantiated by a conversion efficiency of

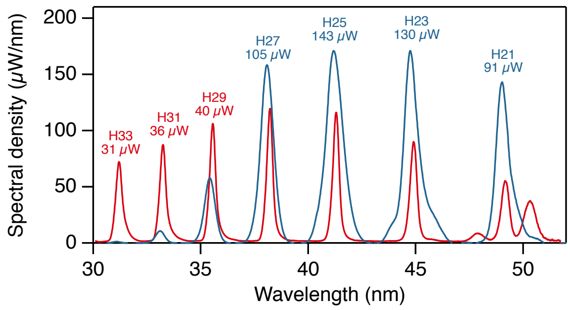

Figure 1: HHG spectrum generated in xenon (blue) and krypton (red) at 600 kHz repetition rate.

$\sim 2 \cdot 10^{-6}$ into the strongest harmonic (H25 at 41 nm), which has an average power of 143 μW ($> 10^{13}$ photons/s). Furthermore, all harmonics that are detected, i.e. H33-H21 (31 nm-49 nm), have an average power of more than 31 μW. So far only enhancement cavities have achieved similar power levels in HHG (200 μW at ~ 70 nm), but require an actively stabilized resonator and an out-coupling technique [6]. We extend the accessible parameter range to much shorter wavlengths, which is of interest, e.g. for coherent diffractive imaging [7].

Outlook A high average power ultrashort pulse fiber laser has been used to achieve phase-matched high harmonic generation resulting in more than 10^{13} photons/s in a single harmonic. This table-top setup allows for photon flux that is competitive, e.g. to synchrotron beamlines. A second compression stage will be implemented to achieve sub-10 fs pulses at very high average power allowing for high photon flux in the soft X-ray region potentially also covering the water-window, which is of particular importance for biological imaging.

References

[1] A. McPherson et. al. J. Opt. Soc. Am. B **4**, 595–601 (1987).

[2] G. Sansone et al. IEEE JSTQE **18**, 507–519 (2012).

[3] T. Popmintchev et al. Nat Phot. **4**, 822–832 (2010).

[4] S. Hädrich et al. Opt. Lett. **38**, 3866 (2013).

[5] P. Salières et al. PRL **74**, 3776 (1995).

[6] A. Cingöz et al. Nature **482**, 68–71 (2012).

[7] M. Zürch et al. HIJ annual report 2013

* This work has been partly supported by the German Federal Ministry of Education and Research (BMBF) and the European Research Council under the European Union's Seventh Framework Program (FP7/2007-2013)/ERC Grant agreement no [240460].

† jens.limpert@uni-jena.de

White light continuum seeded OPCPA for FEL applications*

M.J. Prandolini[1], *J. Zheng*[2], *R. Riedel*[1], *and F. Tavella*[1]
[1]HI-Jena, Jena, Germany; [2]DESY, Hamburg, Germany; [2]QUB, Belfast, Ireland

A white light seeded (WLS) OPCPA system is developed for pump-probe experiments at the FLASH-2 free-electron laser at Hamburg. The design parameters are a pulse duration of 20 fs and a pulse energy from several tens to hundreds of μJ, depending on the intra-burst repetition rate. FLASH operates in a 10 Hz burst mode with 800 μs duration and 0.1-1 MHz intra-burst repetition rate. The current OPCPA is pumped with a 500 W Innoslab amplifier and was tested at the highest repetition rate of 1 MHz. The entire amplifier is seeded with a 1030 nm Yb:fiber oscillator. A dedicated Yb:fiber amplifier generates a broadband white light used as an OPCPA seed. The advantage of this amplifier compared to laser amplifiers with Ti:sapphire oscillator is the higher long-term stability of 1030 nm oscillators. The challenge is to operate the white light continuum source stable on a long-term basis with high temporal and energy stability.

Pump-probe laser: overview and status

Fig. 1 shows an overview of the designed FLASH 2 pump-probe laser (PP-Laser). A commercial Yb:fiber oscillator seeds a pump CPA-system consisting of a fiber and 500 W Innoslab amplifier (see references in Ref. [1]) and a WLS consisting of a dedicated Yb:fiber amplifier that generates a white light continuum in a YAG crystal. The white light continuum is then stretched in a prism stretcher and is used to seed a two stage OPCPA operating at either 100 kHz or 1 MHz (these repetition rates are subject to revision). Presently, we have demonstrated this system at 1 MHz in burst mode. The resulting pulses had a pulse energy of 38 μJ with a pulse duration of 16.5 fs measured with a line autocorrelator. The pulses were close to the Fourier limit of $\sim$ 15 fs. The users have the possibility to change the energy and polarization of the pulses including the delay with respect to the XUV pulse of the FEL.

Timing jitter of WLS [1]

The OPCPA output power and the spectral bandwidth are sensitive to the temporal overlap between pump and signal pulses, which should be smaller than 50 fs. For a passive synchronization, the seed pulses are directly generated from a fraction of the compressed sub-ps OPCPA pump pulses. The 20 W Yb:fiber amplifier delivered pulse durations down to 433 fs at 1 MHz repetition rate. About 1.8 μJ pulse energy was used to achieve stable white-light continuum generation in a 5 mm YAG crystal. As shown

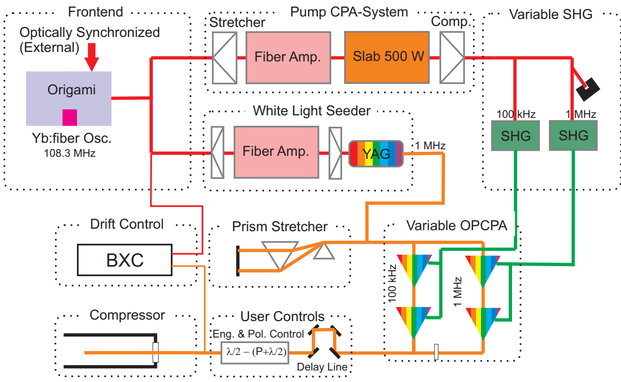

Figure 1: Overview of the FLASH Pump-probe laser.

in Fig. 2a, a long-term stable operation of the white-light operation could be achieved with a low instability of $<$ 0.85% rms over a period of 28 hours (WLS power, red). The fiber laser instability was $<$ 0.65% rms (fiber power, black). The pump-to-WLS time delay was measured using balanced cross-correlation between the 1030 nm fiber pulses and the 650 nm WLS pulses in dependence on the fiber pulse energy. A time delay variation of 0.66 fs nJ^{-1} was determined, yielding a timing jitter of 7 fs rms over the 28 hours period. In the future perspective, WLG-pumped OPCPAs will be tested with Innoslab amplifiers stable amplification of spectrally tunable sub-30 fs pulses at average power $>$ 10 W and repetition rates $>$ 1 MHz.

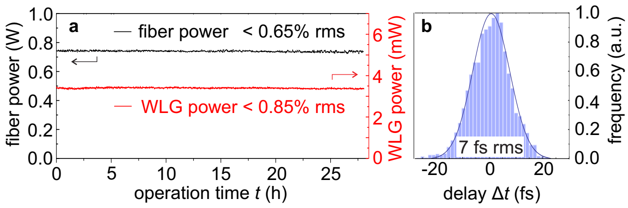

Figure 2: (a) Power stability of fiber laser (black) and white light generation (WLG, red). (b) Pump-to-WLG temporal jitter.

References

[1] R. Riedel, M. Schulz, M. J. Prandolini, A. Hage, H. Höppner, T. Gottschall, J. Limpert, M. Drescher, and F. Tavella, "Long-term stabilization of high power optical parametric chirped-pulse amplifiers", Optics Express 21, (2013), p.28987

* Work supported by HI Jena.

OPCPA and pump laser technologies for FEL seeding*

H. Höppner[2], M. Schulz[2], A. Hage[2,3], R. Riedel[1], A. Prandolini[1], and F. Tavella[1]
[1]HI-Jena, Jena, Germany; [2]DESY, Hamburg, Germany; [3]QUB, Belfast, Ireland

Laser amplifiers at the FLASH free electron laser operate in a 10 Hz burst mode with very high intra-burst repetition rate (0.1-1 MHz). The objective of this work is to increase the average output power of such lasers. One of the first application of burst mode laser based on OPCPA technology will be the laser amplifier for seeding FLASH-2. Currently, a prototype is tested on DESY site. This laser amplifier is designed to deliver a 10 Hz burst with 800 μs duration and an intra-burst repetition rate is 100 kHz. The design pulse duration is 30 fs and pulse energy of 1 mJ. The pump amplifier used for this development is a >1 kW Innoslab amplifier system with 1 ps pulse duration. Further increase in average power is possible for example with a thin-disk multipass amplifier. The scalability of this design has been investigated using two separate thin-disk units in series.

Seeding laser development: status

The current seeding laser OPCPA uses a pump amplifier chain, providing a total output of 1.5 kW in the burst. The streched 1030 nm part of a broadband Venteon oscillator is used to seed a fiber amplifiers system. The 10 W output of the fiber laser seeds two subsequent Innoslab amplifiers. The pump amplifier delivers compressed 14 mJ output pulse energy at 10 Hz burst operation with 800 μs burst duration and an intra-burst repetition rate of 100 kHz. A three-stage non-collinear OPCPA system has been tested using the frequency-doubled output of the pump amplifier with <1 ps pulse duration and 6.3 mJ at pulse energy. The output pulse energy of the OPCPA was 1.15 mJ with to an overall conversion efficiency of 18.2 %. The amplified bandwidth of the OPCPA system supports compression of the pulses to the design value of 30 fs (Fig. 1, t_{AC}=39 fs). A Similar design with a bandwidth support of sub-7 fs is descibed in [1].

Thin-disk multipass amplifier development

A schematic overview of the pump amplifier chain is shown in figure 2. The OPCPA pump amplifier is used as a frontend for the thin-disk amplifier chain. The Innoslab amplifier output is used to seed the first thin-disk amplifier after spatial filtering (improvement of spatial beam profile). We use a 7 pass setup with a 750 μm thin disk and amplify to an output power of 7 kW. The second amplifier uses 7 passes on a 360 μm thin disk, amplifying the seed of the first thin-disk amplifier stage to a total intra-burst output power of 14 kW. The output pulse energy is 140 mJ at an intra-burst repetition rate of 100 kHz, which marks a world record in output power for this type of amplifier.

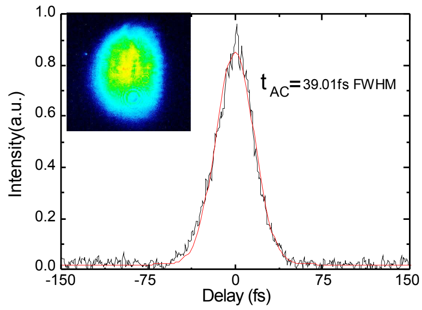

Figure 1: Autocorrelation measurement of compressed signal pulses (1.15 mJ/pulse) and beam profile measurement (inset).

For the implementation of the thin-disk amplifier in the OPCPA pump system, only one amplifier stage has been considered so far to achieve optimum stability. The first stage with 7 passes on the 750 μm disk was further characterized in more detail. The overall rms burst energy stability is 0.5 %. The spectral width of 1.7 nm FWHM yields a Fourier limited pulse duration of 917 fs. The output pulses could be compressed to a pulse duration of 970 fs FWHM. The beam quality of the output has been measured to $M^2 = 1.2$ in both x- and y-direction. The beam pointing stability at the amplifier output is 5 % rms. In summary, this is very promising for the implementation of thin-disk amplifier technology in our current pump amplifier setup.

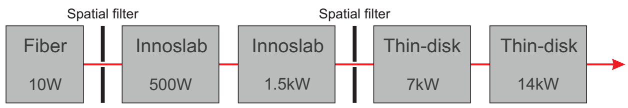

Figure 2: Schematic setup of the thin-disk amplifier chain. 1.5 kW (before spatial filtering) output from an Innoslab amplifier is used as seed for the two cascaded thin-disk amplifiers. The intra-burst output power from the two thin-disk multipass amplifiers is 14 kW.

References

[1] M. J. Prandolini, R. Riedel, M. Schulz, A. Hage, H. Höppner, and F. Tavella, "Design considerations for a high power, ultrabroadband optical parametric chirped-pulse amplifier", accepted in Opt. Express (22nd of Nov. 2013)

[2] M. Schulz, H. Hoeppner, M. Temme, R. Riedel, B. Faatz, M.J. Prandolini, M. Drescher, and F. Tavella, "14 kilowatt burst average power from 2-stage cascaded Yb:YAG thin-disk multipass amplifier", FIO conference proc., Oct. (2013), http://dx.doi.org/10.1364/FIO.2013.FTu4A.2

* Work supported by HI Jena.

Development and simulation for high resolution timing and pulse duration measurement device for free-electron lasers*

R. Riedel[1] *and F. Tavella*[1]

[1]Helmholtz-Institut Jena, Fröbelstieg 3, D-07743 Jena, Germany

The temporal pulse structure of extreme ultraviolet (XUV) and X-ray FELs, which rely on self-amplified spontaneous emission (SASE), is characterized by a number of spikes with varying pulse duration and intensity on a shot-to-shot basis. The presented single-shot cross-correlation method [1, 2, 3] is capable to provide accurate information about the intensity, for example, for studying nonlinear processes. The method can also be used to measure the arrival time jitter between FEL and optical laser pulses in parallel to a running experiment. We have further developed possible improvements of the temporal resolution to measure complex pulse structures using shorter optical probe pulses for the cross-correlation. These improvements will be tested at the FLASH and FERMI@ELETTRA FELs.

Simulation of complex FEL pulses

The method is based on probing the optical transmission change of a transparent solid material pumped by an FEL pulse. A comprehensive theoretical model allows the reconstruction of the pulse structure using a fitting algorithm. The performance of the fitting algorithm was tested for different pulse structures, such as, SASE spikes and seeded single and double pulses, as can be generated at the FERMI FEL. A simulated double pulse intensity is shown in Fig. 1a (dashed line). Due to an increasing carrier density within the target, the simulated optical transmission (cross-correlation rectangles) decreases accordingly. For the simulation, a 10 fs optical probe pulse was assumed. In the presented case, a signal-to-noise ratio of 13 dB was added. The fitting algorithm ensures a robust and accurate retrieval of the cross-correlation (blue) and thus the pulse structure (red). The deviation of the retrieved pulse parameters from the original parameters is smaller than 10%.

Compact OPA short probe pulses

Current lasers at the FLASH FEL (and other FELs such as FERMI at Elettra) use synchronized laser amplifiers with pulse durations around 70–120 fs for pump-probe experiments. A compact tunable OPA source was developed, which can be pumped by part of these available laser amplifiers. The OPA delivers dedicated probe pulses for our cross-correlation tool with pulse durations of 20 fs at 1.1 μJ pulse energy.

The available Ti:sapphire pump-probe laser at FLASH (pulse energy: about 0.5 mJ, pulse duration: 64 fs) was frequency doubled in a 1 mm BBO to pump the OPA at

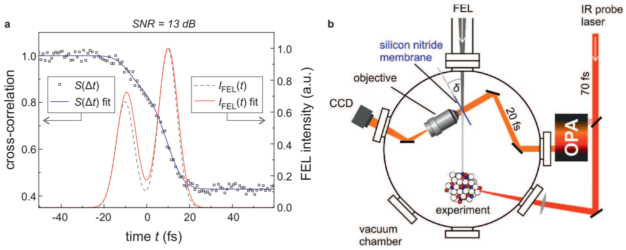

Figure 1: (a) Simulated cross-correlation with SNR=13 dB (rectangles), fitted cross-correlation (blue) of an FEL double pulse with 10 fs pulse separation (dashed). The retrieved pulse is also shown (red). (b) Planned experimental setup for cross-correlation measurements with 20 fs probe pulses and a silicon nitride membrane as target.

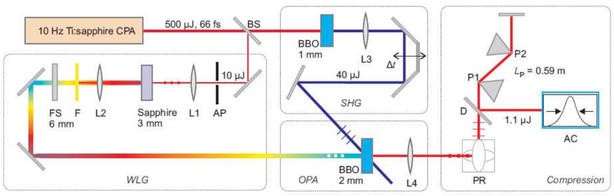

Figure 2: Schematic experimental setup of the compact OPA for the generation of 20 fs pulses for cross-correlation measurements at FEL beamline endstations.

400 nm, focused with a lens of $f = 300$ mm (L3). For the broadband signal seed generation, a fraction of the pulses was used for WLG in a 3 mm sapphire plate, focused by an $f = 100$ mm lens (L1) and an aperture (AP). After refocusing with $f = 100$ mm (L2), the pump was blocked by a notch filter (F). Additional material dispersion is added by a 6 mm fused silica glass plate. OPA is achieved in a BBO with type-I non-collinear phase-matching. After recollimation with an $f = 150$ mm lens, the pulses were compressed in a fused silica prism pair (apex distance $l_P = 0.59$ m, PR: polarization rotating periscope).

References

[1] R. Riedel *et al.*, "Single-shot pulse duration monitor for extreme ultraviolet and X-ray free-electron lasers", Nature Comm. **4**:1731 (2013).

[2] R. Riedel *et al.*, "Experiments at FLASH: temporal diagnostic tool", HI Jena Jahresbericht 2012.

[3] R. Riedel, "Pulse Metrology Tool and Burst-Mode Laser Amplifier for the Free-Electron Laser in Hamburg", Dissertation, Staats- und Universitätsbibliothek Hamburg (2013)

* Work supported by HI Jena.

PHELIX Pre-Amplifier High Repetition Rate Upgrade Project*

U. Eisenbarth[1], *S. Kunzer*[1], *D. Reemts*[1], *and V. Bagnoud*[1,2]
[1]GSI, Darmstadt, Germany; [2]HI-Jena, Jena, Germany

On the route to develop versatile laser solutions for FAIR, the increase of the repetition rate of high-energy lasers is a mandatory step. In order to develop the relevant diagnostics and tools to tackle this task, the pre-amplifier of the PHELIX laser system is being upgraded and serves as a testbed for this study. This system is based on flashlamp-pumped Nd:glass rods (2 x 19 mm + 1 x 45 mm diameter). The pulse repetition rate is currently limited to 1 shot every three minutes which exhibits a limit to several medium energy experiments.

For this purpose, a test bench for the investigation of upgrade possibilities of this system was set up 18 months ago. The main goal of this project is an increase of the shot repetition rate to 1 shot every 10 seconds. Furthermore it aims for an increase of the maximum output energy. In this regime, thermal wavefront aberration and stress-induced birefringence behaviour of the laser material seriously alter the beam quality and compromise experiments.

In order to achieve the higher repetition rate the existing electrical pulsed power system for driving the flashlamps with charge times of up to 45 s could no longer be used. Hence, a new commercial pulsed power system (Continuum PU-601K) has been installed and tested which allows for operating the flashlamps at repetition rates of up to 1 shot every 8 s.

When energy is pumped into a laser amplifier, some heat is inherently deposited in the active material and temperature gradients form because of the heat transfer with the environment. These radial gradients lead to both wavefront aberration as well as birefringence effects.

In the current pre-amplifier system used at PHELIX the time of three minutes between shots leads to a more or less complete cool-down of the rods. In this case only on-shot aberrations need to be considered. Higher repetition rates however lead to a pile-up effect of aberrations from shot to shot.

Wavefront measurements in the test setup however showed that a steady state of these aberrations is reached already after a few tens of shots. The main contribution to the thermal wavefront deformation is defocus, hence the laser rod acts as a positive or negative lens. This type of aberration can be easily compensated for by a movable lens as one component of the Kepler telescopes used in the amplifier system. In this case a motorized translation stage allows for a fine-grained control of the defocus term. At higher repetition rates additional higher order aberrations such as astigmatism, coma or spherical terms appear. These remaining aberrations can be compensated using adaptive optics. For this, a closed-loop systems consisting of a Shack-Hartman sensor (SHS) and a deformable mirror is used. In the frame of this work the diagnostic system (CamBox) was further improved. The SHS measurement software has been written from scratch based on the work of S. Brabetz. This new code developed with LabVIEW also seamlessly integrates with the existing PHELIX control system.

At higher repetition rates stress-induced birefringence effects start to occur. In this case, the initially linear polarized laser radiation is spatially altered across the beam profile with elliptical contributions. The use of polarization optics such as Pockels cells, Brewster surfaces as well as thin film polarizers in the beam path thus lead to significant energy losses and spatial intensity modulations (see fig. 1(a)). To overcome this behaviour, a well-established

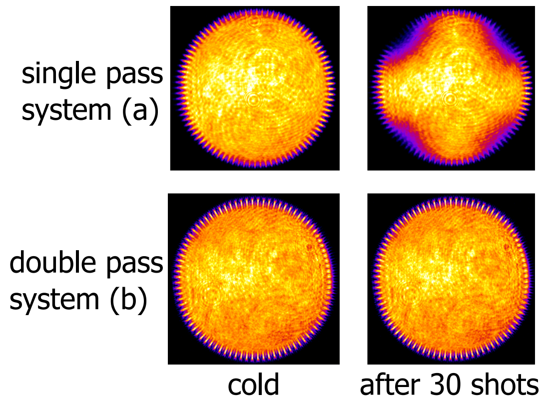

Figure 1: Beam profiles without (a) and with (b) birefringence compensation using a double-pass setup.

double-pass configuration in combination with a Faraday rotator is used. The Faraday rotator breaks the symmetry between the first an the second pass through the laser rod. The polarization alterations introduced in the first pass are perfectly compensated in the second pass(see fig. 1(b)). In addition, the double-pass configuration with one 19 mm and one 45 mm head allows for higher output energies in comparison to the existing setup (2x19 mm + 45 mm) while saving one pulsed power system.

The double-pass configuration of the two laser heads requires a complete change of the beam layout including an improved input section and diagnostic beam path. A new set of vacuum telescopes for beam magnification and image relay are currently being designed and will be tested in the near future, which is necessary for seamless upgrade with minimum down time of the laser facility.

* Work in collaboration with GSI (PHELIX)

Laser Particle Acceleration

Status of the JETi 200 laser system*

A. Sävert[1,2], G. Schäfer[1], B. Beleites[2], F. Ronneberger[2], M. B. Schwab[2], M.C. Kaluza[1,2], M.Zepf[1], V. Bagnoud[1,3], and T. Stöhlker[1,3]

[1]Helmholtz Institut Jena, Germany; [2]Friedrich-Schiller-Universität, Jena, Germany; [3]GSI, Darmstadt, Germany

The JETi 200 laser system

One of the Helmholtz Institut Jena's main research areas covers the field of laser accelerated particle beams, x-ray spectroscopy and experimental quantum electrodynamics in strong fields. For this purpose, a 200 TW Ti:sapphire laser is currently installed. The laser system will deliver laser pulses with 4 J energy and a duration of 17 fs. The pulses's intensity contrast, which is a critical factor in ion accleration experiments with ultra thin foils, is required to be better than 10^{-12} to avoid any pre-ionization of the target.

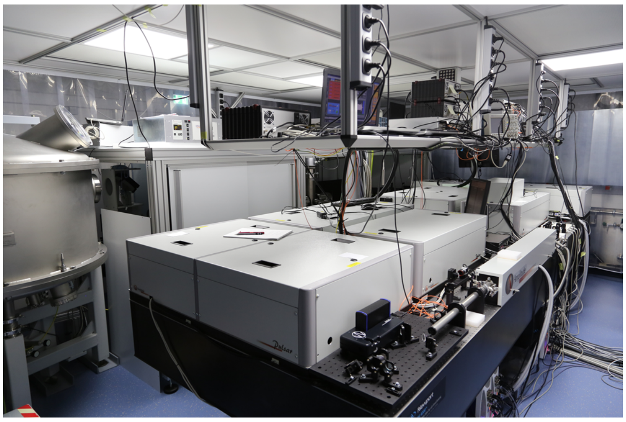

Figure 1: The JETi 200 front end with the super booster and XPW filtering stage.

The seed pulses with a bandwidth of > 100 nm (FWHM) for the laser chain are delivered by a femtolaser SYNERGY PRO. These pulses are amplified by a multipass to the μJ- level and the repetition rate is reduced to 10 Hz. After stretching and further amplification to 3 mJ, the pulses are compressed and sent into the temporal cleaning stage based on cross-polarized wave generation (XPW). Here, pulses with an energy of 1 mJ are focused into a BaF_2 crystal. The overall efficiency of the process is $> 10\%$. The XPW- process also spectrally broadens the laser pulse and allows for a Fourier-limited pulse duration $< 17fs$. Afterwards the pulses are stretched again and then amplified within a regenerative amplifier and a multi-pass to the 20 mJ level. The regenerative amplifier uses an Acousto-Optic Programmable Dispersive Filter (MAZZLER) which allows for compensation of the spectral gain narrowing and red shift during the amplification process. The next multi pass stage amplifies the pulses to 400 mJ level and then the last stage to 5.5 J. The crystal of this last power amplifier is cryogenically cooled to $120K$ and pumped with an energy of 15 J by three frequency doubled Nd:YAG lasers. After expanding the beam by means of two telescopes to 80 mm in diameter it is guided through the pulse compressor with an expected transmission of $> 75\%$. Currently, laser pulses with an energy of 5.5 J before compression with an energy stability of 0.6% rms can be produced. Pulses as short as 17 fs could be measured after the compressor.

Experimental target areas

After compression the beam is transported through a vacuum beamline to one of the two target areas. Target Area One is already completed with the entire vacuum system in place. A big target chamber which can support future two beam experiments has already been vacuum tested. A new few-cycle probe beamline is under construction and will provide $< 6fs$ probe pulses with > 1 mJ of energy synchronized to the 200 TW main beam. Target Area Two will be completed when the old target chamber, which is currently used with the JETi 40, is transfered to the Helmholtz Institut Jena building.

Figure 2: Target chamber and beam line in Target Area One.

* Work supported by HI Jena

Probing a laser wake field accelerator with few-cycle pulses

A. Sävert[1,2], M. Schnell[2], M. Nicolai[2], M. Reuter[1], O. Jäckel[1], M. B. Schwab[2], M. Möller[1], and M.C. Kaluza[1,2]

[1]Helmholtz Institut Jena, Germany; [2]Friedrich-Schiller-Universität, Jena, Germany

Experimental setup

With the 40 TW JETi laser system at the Institute of Optics and Quantum Electronics ultra short electron bunches with kinetic energies up to 200 MeV can be produced routinely. These electron bunches are generated during the interaction of a high intensity laser pulse with an under dense plasma. Here, the laser beam is focused by an off axis parabolic mirror to a spot size of 12 μm (FWHM) with a peak intensity of 8×10^{18} W/cm^2 into the leading edge of a super sonic gas jet to accelerate electron bunches by means of self injection into a plasma wave in the blow out regime. In our experiment helium is used as the target

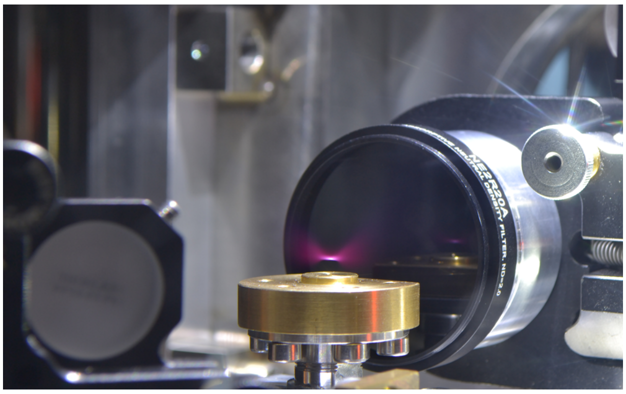

Figure 1: View of the laser plasma interaction. A high resolution microscope objective, protected from debris by a neutral density filter, is used for imaging.

gas. The electron density is optimized by varying the background pressure of the valve of the gas jet to produce well collimated electron bunches with a good shot-to-shot stability. Our newly developed few-cycle probe beam [1] was used to investigate the laser plasma interaction. The measured pulse duration was on the order of 6 fs. The probe pulses are synchronized to the main pulse and the relative delay can be scanned over a range of 2 ns. Due to the small dimensions of the plasma wave (on the order of the focal spot), a high resolution optical imaging system (Fig. 1) was installed to take shadowgraphic images of the evolution of the plasma wave, see Fig. 2.

Results

At the beginning of the interaction, before the laser pulse reaches the focal spot, a linear plasma wave can be identified (Fig. 2, top). The apparent tilt of the wave fronts is

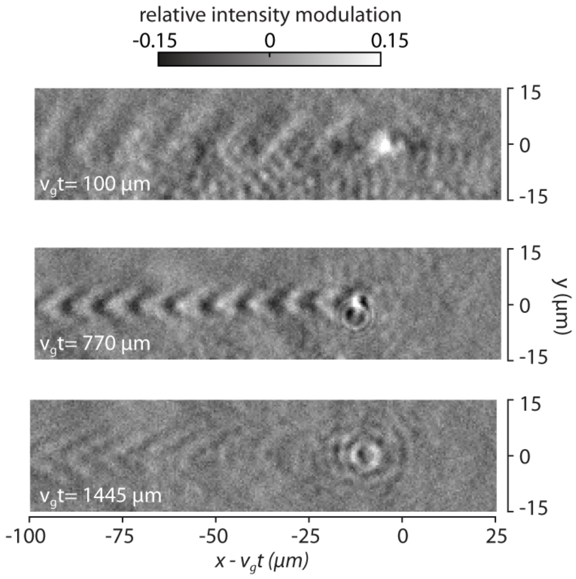

Figure 2: Snap shots of the evolution of the plasma wave at different positions in the gas jet at a plasma density of 1.7×10^{19}cm^{-3}. The laser pulse is propagating from the left to the right.[2]

a result of a spatio-temporal asymmetry of the laser pulse. However, after 600 μm of propagation, the plasma wave's shape is dominated by the relativistic motion of the electrons and shows a distinct curvature. The transverse extent is reduced to $\approx$ 10 μm as the laser pulse undergoes self-focusing (Fig. 2, center). More than ten oscillation periods are visible. After further propagation, the ampltitude of the plasma wave increases up to the point of transverse wave breaking and electrons are injected into the plasma wave and accelerated to energies up to 180 MeV. As the power of our driving laser pulses is sufficient to enter the so called "bubble regime", the wave structure is washed out after the first oscillation period (Fig. 2, bottom) leaving only a single-cycle plasma wave oscillation (the so-called plasma bubble).

References

[1] M. B. Schwab *et al*, "Few-cycle optical probe-pulse for investigation of relativistic laser-plasma interactions", Appl. Phys. Lett., 2013, 191118

[2] A. Sävert *et al*, "Direct imaging of the transient behavior of a laser wakefield through three-dimensional wave breaking", submitted

Relativistic plasma optics enabled by near-critical density nanomaterial

H. Y. Wang[*1], *J. H. Bin*[2,3], *W. J. Ma*[2,3], *M. Yeung*[1], *J. Schreiber*[2,3], *and M. Zepf*[1]

[1]Helmholtz-Institut-Jena, Fröbelstieg 3, 07743 Jena, Germany; [2]Max-Planck-Institute für Quantenoptik, D-85748 Garching, Germany ; [3]Fakultät für Physik, Ludwig-Maximilians-Universität München, D-85748 Garching, Germany

Introduction

The nonlinear optical properties of a plasma due to the relativistic electron motion in the intense laser field are of fundamental importance for current research and the generation of brilliant laser-driven sources of particles and photons. Yet, one of the most interesting regimes where the frequency of the laser becomes resonant with the plasma has remained experimentally hard to access. We overcome the difficulty of providing a target with uniform, near-critical density (NCD) by utilizing ultrathin carbon nanotube foam (UCNF) allowing the strong relativistic nonlinearities at NCD to be exploited for the first time. We report the experimental realization of relativistic plasma optics to spatio-temporally compress the laser pulse in a μm-scale NCD plasma[1]. The enhanced laser pulse results in a substantial improvement of the properties of an ion bunch accelerated from a secondary target.

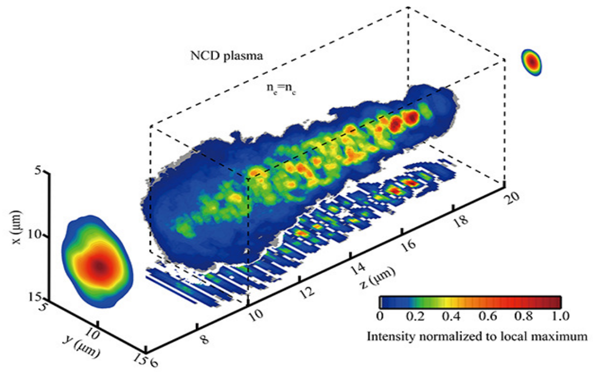

Figure 1: Perspective snapshot showing self-focusing laser pulse in the NCD plasma.

Simulation results

Three-dimensional simulations were carried out with the particle-in-cell code (KLAP3D)[2]. Fig.1 shows a 3D snapshot of the laser intensity distribution at the time when it reaches the maximum. The initial laser pulse has self-focused from initially 3.5 μm full-width half-maximum (FWHM) diameter to about 1μm, over a propagation length of only 8 μm, with its maximum intensity substantially increases by about a factor of 8. Furthermore, the temporal steepening of the pulse front is conspicuous at the position where the laser intensity peaks. It rises from almost zero to peak over two laser cycles only.

* Ho.Wang@gsi.de

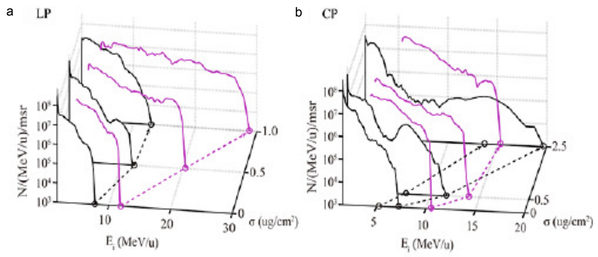

Figure 2: Experimental results of laser driven ion beams using plasma optics. a, Ion spectra for linear polarization in front of a 20 nm DLC foil, and b, for circular polarization in front of a 10 nm DLC foil with varying thickness of UCNF layer. The dashed lines in a and b are used to visualize the increase of the maximum and peak energy of protons (magenta) and C^{6+} (black).

Experiment results

The experiment was performed at the ASTRA Gemini facility at UK. UCNF layers with various thicknesses are directly deposited on nm-thin DLC foil to promote the pulse for following ion acceleration. For the linearly polarized laser pulses (fig2.(a)), the maximum energy of protons and carbons increases by a factor of 2.4 and 1.7, respectively. While for circular polarization (fig2.(b)), the maximum energy of protons increases only by a factor of 1.5, but the maximum energy of carbons are substantially increased by ratio of 2.7. Moreover, a distinct peak appears in all spectra of C^{6+}. Such features are often associated with a transition to radiation pressure dominant ion acceleration (RPA). The relativistic NCD plasma optics increases the laser intensity substantially and promotes a sharp rising edge; both conditions are favorable for RPA.

References

[1] Ma, W. et al. Directly synthesized strong, highly conducting, transparent single-walled carbon nanotube films. Nano Lett. 7, 2307 (2007).

[2] Wang, H. Y. et al. Laser shaping of a relativistic intense, short Gaussian pulse by a plasma lens. Phys. Rev. Lett. 107, 265002 (2011).

Theory And Numerical Simulations of Laser-Driven Ion Acceleration

T. Kiefer[1], *T. Schlegel*[1,2], *and M.C. Kaluza*[1,2]
[1]Friedrich-Schiller Universität Jena, Jena, Germany; [2]Helmholtz Institut Jena, Jena, Germany

In our theoretical and numerical studies we investigate the ion acceleration mechanism in the Target Normal Sheath Acceleration (TNSA) process. Since the mathematical models we are using are too complex to be solved purely analytically, one has to rely on estimates and computer simulations. The necessary simulations were performed using a self-developed computer code, which is based on a kinetic treatment of the particles. However, in contrast to a Particle In Cell (PIC) code, the electrons are assumed to remain in a stationary distribution which is in equilibrium with the electrical potential (see, e.g., Refs. [1, 2]).

In a recent theoretical study we have focused our investigations on the impact of a laser prepulse on the ion acceleration mechanism in the TNSA process. In the literature, there is a broad agreement that the existence of an optimal target thickness is connected to the presence of a laser prepulse and its impact on the ion acceleration process. To describe this effect analytically we have considered the influence of a finite initial density gradient on the target rear side on the ion acceleration mechanism. More precisely, we have used an analytic model similar to that of Mora [2], however, in contrast to Ref. [2] we start from a semi-infinite plasma slab with a linear density gradient. It is a well-known fact that a finite initial density gradient in the ion density distribution leads to wave breaking effects in the ions [3]. In general, this requires a complicated mathematical description of the expansion process. However, we could show that the wave breaking effects in case of a linear density gradient can be neglected with sufficient accuracy. As a result, we were able to describe the evolution of the ion front analytically using empiric expressions. Especially, we found a result for the maximum ion energy as a function of the normalized time τ ,

$$\varepsilon_{\mathrm{f}} = \frac{\alpha-\beta}{\sqrt{\beta\cdot(2\,\alpha-\beta)}}\cdot\left(\arctan\left[\frac{\alpha\,\beta\,\tau}{\sqrt{\beta\cdot(2\,\alpha-\beta)}}\right]+\right.$$
$$\left.\left.\arctan\left[\frac{\alpha-\beta}{\sqrt{\beta\cdot(2\,\alpha-\beta)}}\,\frac{\beta\,\tau}{\sqrt{1+\beta^2\,\tau^2}}\right]\right)\right\}^2 , \quad (1)$$

with some functions α and β which depend on the scale length l_{ss} of the initial density gradient only.

In the next step we have applied our model to experimental results [4] regarding the influence of the initial target thickness on the maximum ion energy. Here, one finds a good agreement between the analytical expression (1) and the experimental data (cf. Fig. 1a) by assuming an empirical relation between the initial scale length of the density gradient at the rear side of the target and the initial target thickness (cf. Fig. 1b). In a future work we will address the relation between the scale length of the initial density gradient and the initial target thickness in more detail by carrying out a series of hydrodynamic simulations.

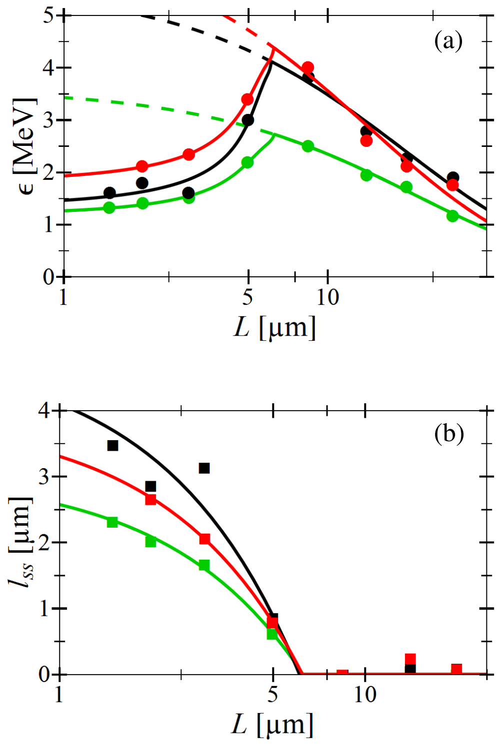

Figure 1: The experimental data (colored dots) shown in (a) corresponds to Fig. 2 in Ref. 4. Here, the prepulse duration is constant (2.5ns) and the ASE prepulse intensities are approximately $5\cdot10^{11}\,\mathrm{W/cm^2}$ (green), $6.5\cdot10^{11}\,\mathrm{W/cm^2}$ (black) and $7.5\cdot10^{11}\,\mathrm{W/cm^2}$ (red). The result (1) of our model is shown (solid lines) using a linear ansatz for the scale length of the initial density gradient as a function of the initial target thickness, $l_{\mathrm{ss}}(L)$. (b) shows the results for $l_{\mathrm{ss}}(L)$ for the three intensities. Here, the squares mark the values of l_{ss} which would exactly lead to the observed ion energies using Eq. (1).

References

[1] A. V. Gurevich, L. V. Pariiskaya, and L. P. Pitaevskii. *Sov. J. Exp. Theor. Phys.*, 22:449, February 1966.

[2] P. Mora. *Phys. Rev. Lett.*, 90(18):185002, May 2003.

[3] T. Grismayer and P. Mora. *Phys. Plasmas*, 13:032103, 2006.

[4] M. C. Kaluza and J. Schreiber and M. I. K. Santala and G. D. Tsakiris and K. Eidmann and J. Meyer-ter-Vehn and K. J. Witte. *Phys. Rev. Lett.*, 93(4):045003, 2004.

Enhanced radiation pressure-assisted acceleration by temporally tuned counter-propagating pulses*

B. Aurand†[1], *S. Kuschel*[2,4], *O. Jaeckel*[2,4], *C. Roedel*[2,4], *H.Y. Zhao*[7], *S. Herzer*[2,4], *A.E. Paz*[2,4], *J. Bierbach*[2,4], *J. Polz*[2,4], *E. Elkin*[8], *A. Karmakar*[9], *P. Gibbon*[5,10], *M.C. Kaluza*[2,4], *and T. Kuehl*[2,3,6]

[1]Department of Physics, Lund University, Lund, Sweden; [2]Helmholtz Institute Jena, Jena, Germany; [3]GSI Helmholtzzentrum für Schwerionenforschung GmbH, Darmstadt, Germany; [4]Institute of Optics and Quantum Electronics, Jena, Germany; [5]ExreMe Matter Institute; Darmstadt, Germany; [6]Department of Physics, Mainz University, Mainz, Germany; [7]Institute of Modern Physics, Lanzhou, PRC; [8]Fraunhofer IGB, Stuttgart, Germany; [9]Leibniz Center for Supercomputing;, Garching, Germany; [10]Institute for Advanced Simulation, Forschungszentrum Juelich GmbH, Juelich, Germany

Introduction

Recent results by our group on the acceleration of monoenergetic ions by radiation pressure assisted acceleration of a polymer foil show a first clear indication that those collective processes could be observed even at intensities of a 10^{19} W/cm^2 [1]. Nevertheless at those low intensities, the acceleration is dominated by the well known target normal sheath acceleration process (TNSA). In order to isolate the monoenergetic acceleration, we performed an experiment using a counter propagating laser pulse to create a well defined shock wave within the target, leading to an increase in density.

Setup

The experiment took place at the 27 fs, 1.1 J JETI laser system at Jena University, using a single plasma mirror [2] in order to enhance the laser-contrast to $>10^{11}$, enabling the use of few-nm thin target foils made from polymers [3, 4]. The pulses were splitted using a beamsplitter with an energy ratio of 90:10 and focused by two symmetrically arranged f/3 OAPs, onto the target front and back surface. Starting with precisely determining the spatial and temporal overlap of the counterpropagating pulses by plasma-probing, we could vary the timing of the pulses reaching the target – by moving the beamsplitter – within a precision of a few ten fs. For diagnostic we used a Thomson parabola to detect simultaneously the energy spectra of different ion charge states accelerated from the back side of the target.

Results

Performing a temporal scan by shifting the back pulse delay between -10 ps and +4 ps with respect to the front pulse, we could observe different behaviours for the collectively accelerated Ions. A positve backpulse delay in that case means that the back pulse interacts with the target before the – higher energetic – accelerating front pulse. For a negative delay, the cut-off energy (Fig 1a) is constant, which means the TNSA acceleration process is unperturbed. For a positive delay, the preplasma formation suppressed the generation of a stable electron sheath and therefore an efficient TNSA.

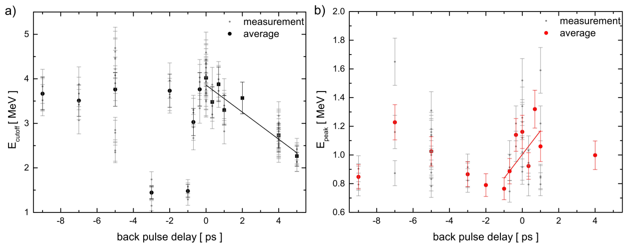

Figure 1: Influence of the back pulse timing on the TNSA dominated cut-off energy (left) and the energy of the collective modulations in the spectrum (right).

Studying the influence of the back pulse of the spectral modulations (Fig 1b), the break-off for a positive delay is much faster, which means that a slight perturbation due to a preplasma completely destroys the collective acceleration effect. A small energy increase within the range of-1 ps to +1 ps is observed. This could be due to a shock compression of the target foils, leading to a locally higher density. Another explanation could be a pre-compensation of instabilities due to the inhomogeneous laser profile. The foil is pre-expanded towards the front pulse and therefore matches better the Gaussian intensity profile. This seems to influence the collective acceleration process in a positive way. A more detailed description of the experiment and results can be found in [5]

References

[1] B. Aurand, *et al.*, New J. Phys. **15** (2013) 033031

[2] C. Roedel, *et al.*, Appl. Phys. B **103** (2011) 4329

[3] B. Aurand, *et al.*, J. Polym. Sci. Part B **51** (2013) 23340

[4] B. Aurand, *et al.*, J Radioanaly. Nucl. Chem. **299** 2 (2014)

[5] B. Aurand, *et al.*, NJP. *Enhanced radiation pressure-assisted acceleration by temporally tuned counter-propagating pulses* (2013, in press)

* Work supported by HI Jena, EMMI and Mainz University

† bastian.aurand@fysik.lth.se

Ion acceleration of ultrathin foils at the PHELIX Laser*

S. Kuschel[1,2], *D. Jung*[3], *B. Aurand*[4], *L. Senje*[4], *M. Yeung*[1,2], *C. Roedel*[1,2], *F. Wagner*[5], *B. Dromey*[3], *C.-G. Wahlstroem*[4], *T. Kuehl*[5], *and M. Zepf*[1,2,3]

[1]Helmholtzinstitute Jena; [2]Instute for optics and quantum electronics, Friedrich Schiller University Jena; [3]Queens University Belfast, UK; [4]Lund University, Sweden; [5]GSI

Monoenergetic ion acceleration using using table top laser systems has attracted strong interest and holds promise for numerous applications, such as hadron therapy, proton probing, ultrashort ion interaction physics or the fast ignitor concept. Numerical studies predict, that particularly ultrathin foils (10s of nm) are the theoretically optimal target thickness for entering the "leaky light sail" regime of radiation pressure acceleration (RPA) [1] leading to monoenergetic ion spectra in the multi MeV range.

Introduction

Since a photon carries momentum, reflecting a photon is a momentum change and thus exerts a pressure on the reflector. For an intense laser pulse focussed to the intensity I_L this pressure is given by $p = (1 + R) \cdot I_L/c$, where R is the reflectivity and c the speed of light. At current lasersystems like PHELIX this pressure can be in the order of some 10 Gbar and thus enables a uniform acceleration of a macroscopic target to a monoenergetic spectrum.

The radiation pressure of the laser will act mainly on the electrons in the target and thus induce a charge separation between electrons and ions until the radiation pressure and the elctrostatic pressure balance. This leads to an optimal target thickness d [1]:

$$a_0 \approx \sigma_\mathrm{n} = \frac{n_\mathrm{e}}{n_\mathrm{c}} \cdot \frac{d}{\lambda_L} \qquad (1)$$

with the normalised vector field amplitude of the driving laser $a_0 = \sqrt{I_L \lambda_L^2 / 1.37 \cdot 10^{18} \mathrm{W/cm^2} \mu\mathrm{m}^2}$ and the normalized areal density σ_n.

Competing acceleration mechanisms altering the monoenergetic ion spectrum of the RPA process are target normal sheath accelertion (TNSA) and volumentric acceleration int the relativistc transparency regime [4]. While TNSA is generally broadening the spectra, rel. transparency plays an important role using target thicknesses of some 100 nm and may also lead to spectral features as observed in the experiment (see below) [5].

Experiment

The experiment was performed at the PHELIX laser facility delivering pulses of 210 J in 550 fs with a contrast of 10^{-10} at -100 ps. This contrast was improved by almost 3 orders of magnitude by an additional plasma mirror [2] with more than 50% reflectivity. The laser pulse was focussed using a $f/2.5$ off-axis parabolic mirror to a theoretically maximal intensity of $I_\mathrm{max} = 5 \cdot 10^{20}$ W/cm^2. As primary diagnostics we were using an ion wide angle spectrometer [3] covering an off-axis angle up to 16°. The laser was aligned to normal incidence on the parylene foil target.

The integrated proton yield in the range between 6 and 30 MeV is shown in Figure 1 for different foil target thicknesses. The pronounced feature around 10° is consistant with recent observations at the Trident laser facility and is characteristic for volumetric acceleration in the rel. trasparency regime [4]. These features are consistent with particle-in-cell simulations and indentifying the relative contributions of competing acceleration mechanisms is part of the ongoing analysis.

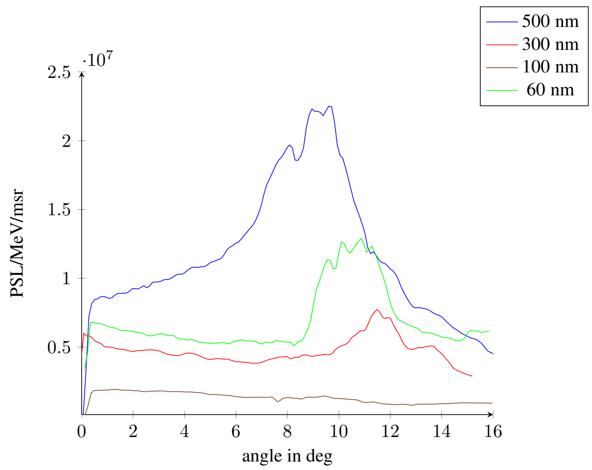

Figure 1: Angle dependent proton yield in the range of 6 to 30 MeV for different target thicknesses. The pronounced feature around 10° is spectrally located between 5 and 10 MeV.

* Work supported by HI Jena, GSI(PHELIX), Laserlab Europe

References

[1] B. Qiao et al. PRL, **105**, 155002 (2010)

[2] C. Rödel et al. Applied Physics B **103**, 2 (2011)

[3] D. Jung et al. RSI, **82**, 043301 (2011)

[4] D. Jung et al. NJP, **15**, 023007 (2013)

[5] B. Aurand et al. New J. Phys. **15**, 033031 (2013)

Influence of pre-plasma properties in laser proton acceleration with water micro droplets*

J. Polz[1], *A. Robinson*[2], *G. Becker*[1], *R. A. Costa Fraga*[3], *R. Grisenti*[3], *A. Kalinin*[3], *and M. C. Kaluza*[1,4]

[1]Institut für Optik und Quantenelektronik, Friedrich-Schiller-Universität, D-07743 Jena; [2]Central Laser Facility, Rutherford-Appleton Laboratory, Chilton, Oxon., OX11 0QX, UK; [3]Institut für Kernphysik, Goethe-Universität, D-60438 Frankfurt, Germany; [4]Helmholtz Institut Jena, D-07743 Jena

Introduction

In laser ion acceleration in the TNSA regime, the pulse contrast of the laser plays a crucial role for the achievable kinetic energy of the particles. If ASE and prepulses lead to the creation of a plasma at a rear surface of the target before the main pulse arrives, the acceleration process is disturbed, in particular by reducing the achievable ion energy. On the other hand the preplasma created prior to the arrival of the laser pulse, is important for the absorption of laser light and its underlying mechanisms to generate hot electrons. Here we present results showing the influence of tailoring the ASE preceding the main laser pulse in experiments with water micro droplets.

Setup

The experiment was performed at the JETI laser system, which was delivering 720 mJ on target within a pulse duration of 27 fs. The focal spot size was $A_{FWHM} = 5.3\mu\mathrm{m}^2$ leading to an averaged intensity of $I = 1.5 \cdot 10^{20}\,\frac{\mathrm{W}}{\mathrm{cm}^2}$. The JETI front end is equipped with a fast pockels cell, improving the nanosecond pulse contrast by 2 orders of magnitude. By changing the delay of the trigger edge of the pockels cell relative to the main pulse, we were able to change the duration of the ASE duration between 1.1 and 2.2 ns. The droplet source consisted of a piezo driven glas capillary with 10 μm orifice, delivering 19 μm diameter droplets with 20 μm separation at a repetition rate of 1.43 MHz. The synchronisation to the laser pulse was ensured by a triggerable piezo driver and an optical imaging system, looking perpendicular to the main pulse direction. The created ions have been detected by means of a Thomson parabola, equipped with a MCP online detection system.

Experimental Results

For each parameter set one hundred shots have been recorded. Due to filamentation of the created ion beam, the recorded proton spectra in the Thomson parabola show a large spread in cut-off energy over a single set. Figure 2 shows the average of the 20 most energetic shots per set. When applying the shortest ASE duration, we did not obtain the most energetic protons, while increasing the ASE duration by 150 to 350 ps, the cut-off energy increased.

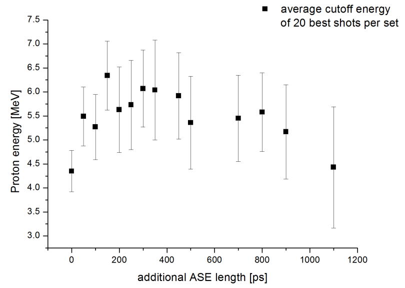

Figure 1: Averaged cut-off energies of the twenty most energetic proton spectra of every set, plottet against ASE pedastal duration.

When increasing the ASE pedestal duration even further, the maximum proton energy decreases again.

Numerical Simulations

To explain our experimental findings, we performed particle in cell simulations. The target consisted of a subcritical pre-plasma and an overcritical part, rendering the droplet itself. To reproduce the influence of the ASE, we changed the density of the pre-plasma shelf and studied its influence on the acceleration process (cf. figure 2). For values of 0.025 to 0.1 critical density no change in the resulting proton energies can be observed, but from 0.2 n_c onwards the proton cut-off energies increase. We are attributing this fact to a change of laser interaction with the pre-plasma. For the low density case, transverse ponderomotive acceleration is the dominant mechnism, while for higher densities direct laser acceleration sets in, generating more energetic electrons in a more efficient manner.

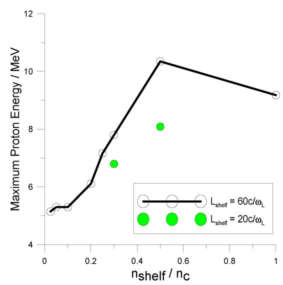

Figure 2: Maximum proton energy dependence on pre-plasma shelf densities determined with OSIRIS simulations

* Work supported by HI Jena

A laser-driven proton beamline at GSI*

S. Busold[1], D. Schumacher[4], O. Deppert[1], C. Brabetz[2], F. Kroll[3], A. Blazevic[4,5], V. Bagnoud[4,5], I. Hofmann[4], and M. Roth[1]

[1]TU Darmstadt, IKP, Germany; [2]JWG Universität Frankfurt, IAP, Germany; [3]Helmholtz - Zentrum Dresden-Rossendorf, Germany; [4]GSI, Darmstadt, Germany; [5]Helmholtz Institut Jena, Germany

The LIGHT beamline. Laser-based ion acceleration became an extensively investigated field of research during the last 15 years. Within several micrometers particles are accelerated to MeV energies. The main drawback for many applications is their continuous exponential energy spectrum and large envelope divergency from source. The exploration of proper beam shaping and transport is the major goal of the LIGHT collaboration [1] and an experimental test beamline has been built at GSI. This *LIGHT beamline* at GSI is located at the Z6 area within the experimental hall. The PHELIX 100 TW laser beamline is currently capable of delivering up to 15 J of laser energy in a 650 fs short pulse on target, focused to intensities exceeding 10^{19} W/cm^2 within the Z6 target chamber. Protons could be accelerated via the TNSA mechanism to maximum energies of 28.4 MeV and propagated through a pulsed high-field solenoid with a field strength up to 9 T, which is used to select a specific energy interval from the continuous initial spectrum via chromatic focusing. A large capture efficiency of 34% of the initial protons within a selected energy interval (ΔE=(10$\pm$0.5) MeV) was measured [2].

The protons are weakly focused to a 15×15 mm^2 spot at 3 m distance to the source, containing particle numbers $>10^9$ in a single 8 ns short bunch. The energy sprad of the bunch is (18$\pm$3)% and the central part of the bunch can be described by a Gaussian-like distribution:

$$\frac{dN}{dE} = \frac{N_0}{E} exp\left(-\frac{(E-E_0)^2}{2\sigma^2}\right) \qquad (1)$$

Figure 1 (upper graph) shows the experimental results (E_0=9.6 MeV, σ=(0.7$\pm$0.06) MeV) compared to simulations.

First experiments on phase rotation. The cavity is a three gap spiral resonator, inserted to the beamline between 2 and 2.55 m distance to the laser target and connected to the UNILAC rf system. Injection at -90 deg synchronous phase and 100 kW input power leads to energy compression of the bunch. The energy spread at FWHM ($\Delta E/E_0=2.35\sigma/E_0$) could be reduced to (2.7$\pm$1.7)% at a central proton energy of E_0=9.7 MeV (see lower graph in figure 1) and particle numbers of 1.2×10^9 ($\pm$15%) within the FWHM were measured. A detailed description will be published in [3].

Furthermore, the experimental setup allows for phase focusing. Simulations predict shortest possible bunch durations down to the sub nanosecond regime. Highest single bunch intensities of 10^{10} protons/ns are accessible. An experimental campaign is planned for 2014.

Thanks to the compact laser-driven source the whole beamline is only 3 m long in total and represents a currently unique combination of novel laser and conventional accelerator technology to generate highest single bunch intensities in the multi-MeV region.

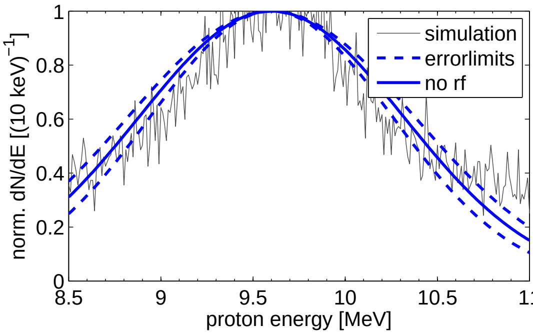

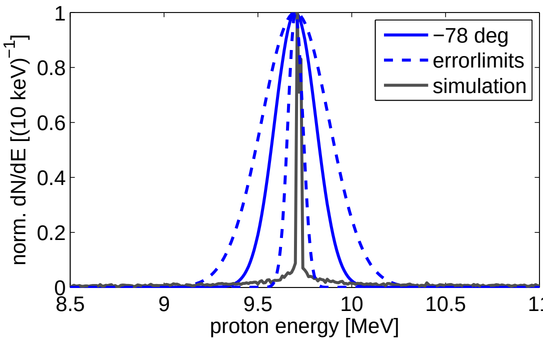

Figure 1: Simulated and measured proton spectra at a distance of 3 m to the source for solenoid focusing only (upper) and additional energy compression (lower figure) for a central bunch energy of E_0=(9.6$\pm$0.1) MeV.

References

[1] S. Busold *et al.*, *Shaping laser accelerated ion for future applications - the LIGHT collaboration*, NIMA **-**, - (2013)

[2] S. Busold *et al.*, *Focusing and transport of high-intensity multi-MeV proton bunches from a compact laser-driven source*, PRSTAB **16**, 101302 (2013)

[3] S. Busold *et al.*, *Commissioning of a compact laser-based proton beamline for high intensity bunches around 10MeV*, submitted to PRSTAB

* This work is supported by the Helmholtz Institute Jena and HIC for FAIR.

Photon and Particle Spectroscopy

High harmonic generation with multiple re-scattering of electrons

J. Seres[1,2], B. Landgraf[1,3], B. Ecker[3,4], B. Aurand[3,4], T. Kuehl[3,4], S. Namba[5], C. Spielmann[1,3]

[1]IOQ, Friedrich Schiller University, Jena, Germany; [2]Atominstitute, Vienna University of Technology, Vienna, Austria
[3]Helmholtz Institute Jena, Jena, Germany; [4]GSI, Darmstadt, Germany, [5]Hiroshima University, Japan

We observed high-order harmonic spectra consisting of only every fourth harmonic in the range 0.2 and 1 keV. The experimental findings can be explained by quantum path interference of two electron trajectories with multiple re-scattering.

Measurement results

To demonstrate experimentally that high-order harmonics in the few-100 eV range are generated by extended electron trajectories, experiencing multiple re-scattering, a series of measurements has been performed using the JETI laser system (Jena, Germany). It delivers 30-fs-long pulses with energies up to 1 J at 800 nm central wavelength and 10 Hz repetition rate. The high laser pulse energy allowed a loose focusing geometry (f/100) and peak intensity up to 8×10^{15} W/cm² in a Helium gas target was realized. The target consisted of Ni-tube with interaction length of 1 mm backed with Helium in pressure range of 0.1 to 1.2 bar. To reduce the gas load and the reabsorption, the target was operated with a pulsed valve at 10 Hz. After blocking the fundamental laser light with thin Al (200 nm) and Ti (100 nm) foils, the spectra were measured with an x-ray scanning monochromator (McPherson 248/310G) equipped with a 1200 grooves/mm grating and a photomultiplier (Channeltron 4751G). The photomultiplier was operated with supply voltage of -2.5 kV (SRS PS350) and read out with a lock-in amplifier (Signal Recovery 5209) with integration time of 0.1 ms. With this equipment we were able to record harmonic spectra in the spectral range of 0.2-2 keV with a resolution sufficient to detect single harmonic lines below 1 keV.

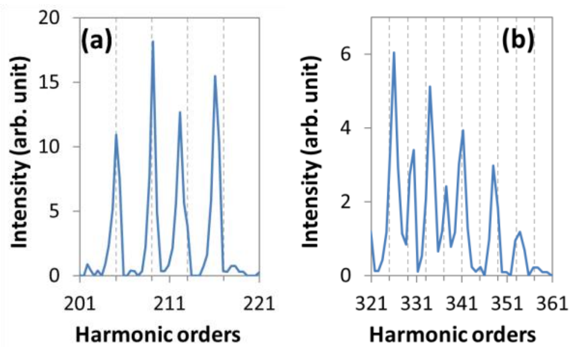

Figure 1: Harmonic lines in the measured spectra are sitting in the 4i+1 harmonic position, which is the consequence of the quantum path interference of two dominating electron trajectories.

Part of the recorded spectrum at 0.3 bar is highlighted in Fig. 1. for the range of the 200th to 360th harmonic corresponding to energy range of about 300 to 560 eV, respectively. In this range we found a reasonable agreement between the position of the measured harmonic lines and the expected 4i+1 harmonic orders. The harmonic lines are especially very well resolved in the range of harmonic order 201 and 221 (Fig. 1(a)). Above harmonic order 321 (Fig. 1(b)) the visibility of the harmonic lines gets weaker as a consequence of the decreasing spectral resolution of the spectrograph and the limited sampling rate.

Discussion

At moderate laser intensities, at 5×10^{14} W/cm², the kinetic energy of the electrons is sufficient for generating HHG radiation in the spectral range below ~150 eV. In this range high-order harmonics are generated if the released electron returns to the atom for the first time, which happens about ¾ optical cycles after the ionization. If the electron does not recombine, it moves further away from the ion as a consequence of the strong perturbation of the Coulomb potential and never returns again.

With a much higher probability (~5×10^{14} W/cm²), the electron is accelerated further within the next optical cycles and has the chance for recombination about one or more optical cycles later. These trajectories are extended trajectories and two possible electron trajectories exist in every half optical cycle separated by ~¼ optical cycle, which are linked to an impact parameter suitably small for XPA [1], and a kinetic energy in the few-100 eV regime. Consequently the generated harmonic spectrum will only consist of harmonics of the order 4i+1, in contradiction to the conventional high harmonic spectrum [2].

From the presented measurements we can draw the following major conclusions. For laser intensities in the range of 10^{15}-10^{16} W/cm², high order harmonics can be generated and stimulated emission of x-rays can be realized from extended long electron trajectories. For these extended trajectories, the time between ionization and recombination is about two optical cycles and in every optical cycle four x-ray pulses are generated.

The authors acknowledge for the contributions of the JETI laser team.

References

[1] J. Seres, E. Seres, C. Spielmann, Phys. Rev. A **86**, 013822 (2012).

[2] J. Seres, E. Seres, B. Landgraf, B. Ecker, B. Aurand, T. Kuehl, C. Spielmann, Nature Sci. Rep. (2014) to be publisehd

Dependence of laser-driven coherent synchrotron emission efficiency on pulse ellipticity and implications for polarization gating

M.Yeung[1] B. Dromey[2], S. Cousens[2], D. Kiefer[3], J.Schreiber,[3] J. H. Bin[3], W. Ma[3]C. Kreuzer,[3] J. Meyer-ter-Vehn,[3] S. Rykovanov[4] and M. Zepf[1,2]

[1]HI-Jena, Jena; [2]Queens University, Belfast, United Kingdom; [3]MPQ, Garching; [4]LBL Berkeley, USA

We investigate the polarisation dependence of Coherent Synchrotron Emission (CSE) in laser plasma interactions and observe the almost complete suppression of the harmonic emission for circular polarization during a relativistic laser-plasma interaction. This is the first time polarisation controlled suppression of a HHG process has been observed for high energy laser pulses with relativistic intensities - key to producing bright, energetic attosecond pulses. Our particle-in-cell (PIC) simulations demonstrate that the observed ellipticity scaling is sufficient to allow the production of a single attosecond pulse by implementing polarisation-gating techniques on currently available laser systems.

In common with other HHG techniques, the temporal substructure of CSE is characterised by a train of attosecond pulses. This temporal sub-structure has given rise to generation of isolated attosecond pulse for applications in attoscience, where low energy attosecond pulses are generated at moderate intensities when a femtosecond laser interacts with a gaseous medium. Isolating a single attosecond pulse can be achieved either with extremely short laser pulses which exhibit a single dominant laser cycle and hence a single dominant attosecond pulse in the temporal structure. Alternatively, the strong ellipticity dependence of HHG in gaseous media is frequently exploited to achieve the generation of a single, isolated attosecond pulse. This is achieved by generating pulses with a complex polarisation state, which exhibits strong ellipticity throughout the pulse apart from for one linearly polarised cycle at peak intensity where the pulse switches from left to right-circular (or vice versa). For all optical cycles with significant ellipticity the generation of XUV harmonics is suppressed and hence only a single attosecond pulse is emitted. The transmitted harmonic radiation was detected on an XUV spectrometer consisting of vertical slit placed 30cm from the laser focus followed by a 1000 lines/mm freestanding gold transmission grating. A quarter waveplate was used to generate a circularly polarized pulse and the targets were 300nm Parylene-N foils. Harmonic orders up to the 15th were clearly observed while the spectral resolution of the diagnostic limited the observation of higher orders. Figure 1 shows the background subtracted and spatially integrated harmonic signal against the pulse ellipticity. It can be seen that for circular polarization the transmitted harmonic signal is almost reduced to the noise floor of the spectrometer, which is determined by integrating the signal for a shot with no target, providing ideal conditions for applying polarisation gating to CSE. The energy contained in the 9th harmonic can be estimated to be on the order of several µJ with most uncertainty arising the beam divergence, which was not measured on this occasion. This is comparable with efficiencies from previous measurements of this transmitted harmonic emission [1] but considerably lower than that expected for ideal cases of CSE in reflection [2]. A possible explanation for the discrepancy is the fact that the nanobunch density depends sensitively on the precise interaction parameters, particularly the laser contrast and preplasma scalelength, which were not scanned systematically on this occasion.

In terms of the interaction physics, the substantial reduction in efficiency can be understood from considering the forces acting upon the target. At normal incidence the only oscillatory component of the force normal to the interaction surface is the vxB term. For circular polarisation both magnitude and direction of the force become constant over a laser cycle for sufficiently slowly varying intensity envelope, hence preventing the formation of nano-bunches and the emission of CSE.

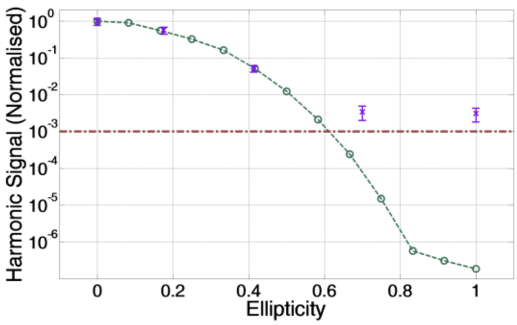

Figure 1: Comparison of simulation and experiment – Harmonic efficiency for orders 8-25 as obtained from PICWIG simulations (circles) plotted alongside the integrated harmonic signal for orders 7 – 15 from the experimental data (crosses). The dashed-dotted line shows the detector noise floor.

In conclusion, experimental studies of the CSE process in transmission of thin foils have shown that the process can be heavily suppressed by increasing the pulse ellipticity. The possibility of exploiting this ellipticity dependence using the polarization gating technique was explored using 1-D PIC simulations and the results show that isolated, intense attosecond pulses can be generated from ultra-high intensity interactions with thin foils.

References

[1] B.Dromey et al, Nature Physics 8, 804(2012)
[2] D. an der Brugge et al, Phys. Plasmas 17, 033110 (2010)

Coherent Diffraction Imaging with a Narrow-band High Average Power XUV Source

M. Zuerch[1], J. Rothhardt[2,3], S. Haedrich[2,3], S. Demmler[2], M. Krebs[2], J. Limpert[2,3], A. Tuennermann[2,3,4], A. Guggenmos[5,6], U. Kleineberg[5,6], and C. Spielmann[1,3]*

[1]IOQ, FSU Jena, Germany; [2]IAP, FSU Jena, Germany; [3]HI Jena, Germany; [4]Fraunhofer IOF, Jena, Germany; [5]LMU Munich, Garching, Germany; [6]MPQ, Garching, Germany

FELs and synchrotrons are used since a decade as sources to provide insight into matter at the nanoscale [1]. The key requirements for imaging at the nanoscale are: i) a short illumination wavelength, ii) a high photon flux, and iii) a narrow bandwidth. High Harmonic Generation sources are a promising alternative and were successfully used for coherent diffraction imaging (CDI) before [2]. Typically Ti:Sa laser driven HHG sources feature a high relative bandwidth ($\triangle\lambda/\lambda \sim 3 \times 10^{-2}$) and thus prevent CDI at the Abbe limit by violating condition iii).

To overcome this limitation we used a XUV source based on a high repetition rate fiber CPA system (λ = 1030 nm, f_{rep} = 100 kHz, E_p = 250 μJ, P_{avg} = 25 W) with subsequent nonlinear compression in a noble gas filled hollow core fiber [3]. The long pulse duration of $\tau \sim 60$ fs causes harmonic lines having a small relative bandwidth of $\triangle\lambda_{\text{FWHM}}/\lambda = 5 \times 10^{-3}$. Hence, requirement iii) is fulfilled much better. In addition our system provides a high XUV photon flux in a compact and robust architechture. The CDI setup contains specially designed XUV mirrors for selecting a single narrow-bandwidth harmonic line (31$^{\text{st}}$ harmonic @ 37.3 eV or 33.2 nm) out of the harmonic frequency comb. Two curved XUV mirrors are used to enhance the spectral selectivity (overall reflectivity $\sim 7\%$), while the first mirror collimates the XUV beam and the second focuses it down onto the sample. The focal spot size was determined to $d \sim 3\,\mu$m (FWHM), which is well suited for high resolution imaging of e. g. single cells.

With this optimized setup we conducted a first proof-of-principle experiment. The simple structure, that was imaged, consisted of a pinhole (2 μm diameter) that was milled into a gold-coated silicon nitride membrane. The measured diffraction pattern is depicted in Fig. 1a and features the expected Airy disc. The bright central speckle was blocked by a beam stop. Fig. 1b shows the reconstructed complex-value object. The pinhole is resolved with a flat phase in good detail. A profile (Fig. 1c) allows to determine the achieved spatial resolution to $\sim$ 100 nm. The structure was successfully reconstructed with a resolution of approximately three times the XUV wavelength. The numerical aperture in the experiment was 0.3, hence the achieved resolution corresponds approximately to the Abbe limit for this configuration.

The integration time is currently in the order of several 10s. However, the scalability of FCPA systems, unlike standard Ti:Sa CPA systems, allows to increase the photon flux easily. With an increased photon flux we could take advantage of an even higher NA and thus increase the resolution. Due to the excellent spatial beam quality and narrow bandwidth of the generated harmonics it seems feasible to achieve sub-wavelength resolution in the near future.

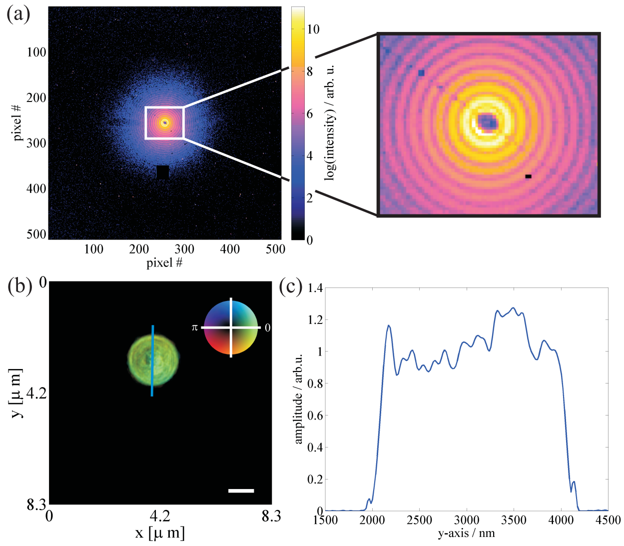

Figure 1: (a) Measured diffraction pattern of the two micron aperture. (b) Reconstructed real-space image of the sample, the brightness and hue encode the amplitude and phase respectively (see colorwheel). The scale bar is one micron. (c) From the profile (blue line in (b)) a resolution of $\sim$ 100 nm can be estimated.

References

[1] S. Boutet, et al., "High-Resolution Protein Structure Determination by Serial Femtosecond Crystallography", Science 337 (2012), pp. 362-364

[2] M. Zuerch, C. Kern, and C. Spielmann, "XUV coherent diffraction imaging in reflection geometry with low numerical aperture", Opt. Express 21 (2013), pp. 21131-21147

[3] J. Rothhardt, S. Haedrich, H. Carstens, N. Herrick, S. Demmler, J. Limpert, and A. Tuennermann, "1 MHz repetition rate hollow fiber pulse compression to sub-100-fs duration at 100 W average power", Opt. Lett. 36 (2011), pp. 4605-4607

* michael.zuerch@uni-jena.de

A gigawatt class T rays source*

A. Gopal[1,2], D. Brömmel[4], P. Gibbon[4], S. Herzer[1], A. Karmakar[4], T. May[3], H.-G. Meyer[3], G. G. Paulus[1,2], A. Reinhard[1], A. Schmidt[1], P. Singh[1], and W. Ziegler[1]

[1]Institute of Optics and Quantum Electronics, Friedrich-Schiller University, Jena; [2]Helmholtz Institute Jena; [3]Quantum detection group, Institute of Photonic Technologies, Jena; [4]Jülich Super Computing Center, Institute of Advanced Simulations, Jülich

Introduction

Terahertz radiation (T rays) are known to be a next generation light source due to their unique properties, finds many applications in material science, non-linear optics and next generation particle accelerators[1, 2, 3]. We report here the efficient generation of gigawatt (GW) class T rays during laser-matter interaction.

T rays are generated during the interaction of a multi terawatt (TW) laser pulse with a thin metal foil. The generation mechanism of T ray is based on the well known particle acceleration mechanism, target normal sheath acceleration. The transient nature of the accelerating field is responsible for the emission of radiation perpendicular to the direction of acceleration in the non-relativistic regime. The field is expected to last few times the laser pulse duration, thus emitting radiation in the millimeter/sub-millimeter range, i.e. in the THz frequency band. The power of the radiation emitted by the particles is given by the dipole formula, $P = \frac{2}{3c^3}\ddot{d}^2$ where $\ddot{d} = \sum e\ddot{x}$. i.e. the power of the emitted radiation is a function of the number density of the dipoles and the magnitude of acceleration which in turn is directly proportional to the strength of the electrostatic sheath field.

The Experiment

The experiments were performed at the multi TW JETI (Jena Ti-Saph) laser at the Institute of Optics and Quantum Electronics (IOQ) at the University of Jena. 5 μm thick Titanium foils were irradiated with tight focused JETI beam generating intensities above 10^{19}W/cm^2. The radiation was collected from the rear of the target, mainly in the non-collinear direction with respect to the target normal[4]. The collected T-rays were relayed out of the experimental chamber using THz optics. To measure the space-time integrated energy a calibrated broadband pyroelectric detector was employed. The temporal profile of the THz pulse was measured using a non-collinear single shot pump-probe diagnostic [5].

Results

By calibrating the beam relay system, we measured THz pulses of minimum 700 microjoules for incident laser energies of 600 mJ, thus giving a conversion efficiency greater than 10^{-3}[6]. The analysis of the pump-probe measurements showed sub-pico second THz pulses of 570 fs duration, thus rendering peak powers of the order of GW[5]. Fourier analysis of the measurements revealed that most of the energy is localized in the low frequency regime (below 3 THz). However, further analysis with band pass filters showed spectral components upto 133 THz.

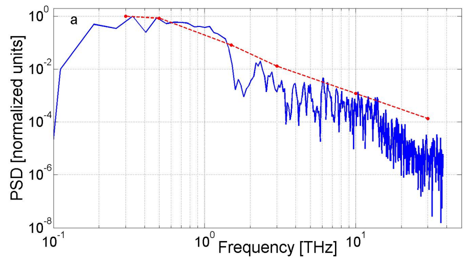

Figure 1: Results of the power spectral density measurements (blue: pump-probe measurements, red: using band pass filters).

Summary

We observed sub-millijoule T rays with gigawatt peak power. Simultaneous measurement of the T rays and particle spectra showed strong correlation between the power of the T-rays and the particle energy and number.

References

[1] Jones, R.R. *et al.* Ionization of Rydberg atoms by subpicosecond half-cycle electromagnetic pulses, *Phys. Rev. Lett.* **70**,1236 (1993).

[2] Cole, B. E. *et al.* Coherent manipulation of semiconductor quantum bits with terahertz radiation. *Nature* **410**, 60 (2001).

[3] Gopal, A. and Herzer, S. Verfahren und Vorrichtung zur Erzeugung einer laserangeregten Teilchenstrahlung im MeV-Bereich, 10-2012-012-492.9, German patent pending.

[4] Gopal, A. *et al.* Observation of energetic terahertz pulses from relativistic solid density plasmas *New Journal of Physics***14**, 083012 (2012).

[5] Gopal, A. *et al.* Gigawatt class THz pulses from a compact laser-driven particle accelerator *Phys.Rev.Lett.* **111** 074802 (2013).

[6] Gopal, A. *et al.* Characterization of 700 μJ T rays generated during high-power laser solid interaction *Opt.Lett.* **38**,4705 (2013).

* Work supported by DFG

High-resolution energy-angle correlation measurement of hard x-rays from Laser-Thomson-Backscattering source at HZDR

A.Irman[1], A.Jochmann[1], S.Trotsenko[2,3], U.Lehnert[1], J.P.Couperus[1], M.Kuntzsch[1], A.Wagner[1], A.Debus[1], H.P.Schlenvoigt[1], K.D.Ledingham[4], T.E.Cowan[1], R.Sauerbrey[1] , Th. Stöhlker[2,3,5], and U.Schramm[1]
[1]HZDR, Dresden, Germany; [2]GSI, Darmstadt, Germany; [3]Helmholtz Institute Jena, Jena, Germany;
[4]University of Stratclyde, Glasgow, Scotland; [5]Friedrich-Schiller-Universität Jena, Jena, Germany

A finite bandwidth of a Thomson scattering x-ray source is the result from the complex interplay between electron energy spread, electron beam emittance, laser focusing geometry, laser bandwidth and detector solid angle. An ensemble of electrons in a bunch crosses the interaction plane at multiple angles relative to the beam axis due to the beam transverse emittance. The Electron direction deviation has to be added to the observation angle and therefore causes an observation angle spread. Due to superposition of the emitted x-ray photons, the detected x-ray spectrum is broadened. For a detector placed on the electron propagation beam axis the photons can only contribute to the low-energy tail of the spectral distribution. This effect caused by the θ dependence in the eq. (1) results in a skewed x-ray spectrum assuming symmetry distributions of the electron beam energy and the laser bandwidth. In this case, the x-ray bandwidth scales with the laser bandwidth, the electron energy spread and the electron beam emittance. Due to the finite size of the detector it collects scattered x-ray photons emitted in a certain solid angle, so increasing the detected x-ray bandwidth.

$$\omega_{sc} = \frac{2\gamma^2\,(1-\cos\varphi)}{1+\left(\frac{a_0{}^2}{2}\right)+\gamma^2\theta^2}\,\omega_0 \qquad (1)$$

In previous experiments the spectral characteristics of Thomson scattering were deduced from indirect filter-pack measurements or with single element semiconductor detection systems. Both methods suffer from limited detector resolution and a low signal-to-noise ratio.

We report the influence of the electron beam emittance, the laser bandwidth, and the energy-angle correlation on the bandwidth of the scattered x-rays [1]. We suppress the influence of laser focusing by using a long focal length parabola (f/30) which makes the interaction length longer than each beam’s pulse length. The spectra were collected by a pixelated detector (CCD camera) at various observation angles and analyzed by a single photon counting technique.

The experiment based on the head-on collision was carried out at HZDR with the DRACO Ti:sapphire laser system and the ELBE linear accelerator facility. For details of the experiment we refer to [1]. X-ray spectra were obtained by counting single-pixel

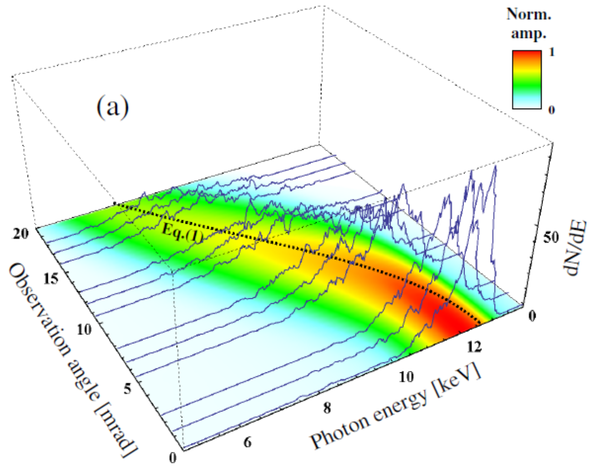

Fig 1. Full data set (QE corrected) combined with CLARA simulation results and Eq. (1) (dotted line).

absorption events (SPAE) from a 50x50 pixel area on the CCD chip. This size corresponds to an angular resolution of 0.6 mrad, which guaranteed the detection of the intrinsic bandwidth inhibiting any broadening effects due to the finite detector size.

Fig. 1 shows recorded x-ray spectra (blue curves) at increasing observation angles (from 0 to 18 mrad in the y-z plane) in the plane perpendicular to the laser polarization. The simulated angle-dependent spectra are presented as a color code distribution underlying the experimental data. It is clearly visible that the measured x-ray spectrum shifts to lower photon energies for larger emission angles. The trend follows the prediction from the simulation.

The measured maximum cutoff energy is about 13.1keV, which agrees well with Eq. (1) taking the laser energy of 1.61eV and the electron energy of 22.5 MeV. The spectrum peaks at 12.3 keV on the axis and shifts to 8.2 keV at θ=18.0 mrad. The positions of the x-ray peaks are found to deviate from Eq. (1), particularly near the electron beam propagation axis. This is an effect due to the angular spread of the incoming electrons, which modifies the simple correlation between the scattered photon energy and the observation direction in Eq. (1).

References

[1] A. Jochmann et.al, PRL, 111, 114803 (2013)

High Purity X-Ray Polarimetry

K. S. Schulze[1,2], I. Uschmann[1,2], B. Marx[2], R. Röhlsberger[3], K.P. Heeg[4], J. Evers[4], E. Förster[1], and G.G. Paulus[1,2]

[1]Helmholtz-Institut Jena, Germany; [2]Friedrich-Schiller-Universität Jena, Germany; [3]Deutsches Elektronen Synchrotron DESY, Germany; [4]Max-Planck-Institut für Kernphysik, Heidelberg, Germany.

X-ray polarimetry is a versatile tool in many applications at synchrotron sources [1]. The Jena X-ray polarimeter offers new perspectives in polarization analysis at synchrotrons due to its unique precision which is enabled by a polarization purity of 2.4 x 10^{-10} [2].

Recently, we successfully combined high purity X-ray polarimetry with resonant nuclear scattering leading to new opportunities in quantum optics with X-rays and the discovery of spontaneously generated coherence [3].

Furthermore, we have transferred our experience with precision X-ray polarimetry to laboratory X-ray sources. Using the Borrmann effect, we measured a polarization purity in the order of 10^{-5}.

X-ray Quantum Optics

The great success of high purity X-ray polarimetry in combination with nuclear resonant scattering leads to the discovery of spontaneously generated coherence in the X-ray range recently [3]. This quantum optical effect occurs in a nanometer sized multilayer system which forms a cavity for X-rays. A trace of ^{57}Fe atoms inside this cavity leads to a quantum electrodynamical coupling of the cavity modes and the nuclear transition of ^{57}Fe. This interaction can be probed with 14.4 keV X-rays, the energy of the transition, and reveals insights into different quantum optical effects, like spontaneously generated coherence, energetic shifts of the transitions and slow light. These effects are being investigated in detail in collaboration with the nuclear scattering group from DESY and theorists from the MPI Heidelberg.

Particular knowledge about the phenomenons inside the cavity could improve future developments in quantum simulation and quantum control.

Polarimetry Using the Borrmann Effect

The brilliant parallel beam of the new microfocus rotating anode X-ray system at HI-Jena enables the application of precision X-ray polarimetry in our laboratory. Because of the small size of the X-ray source and the performance of the Confocal Max-Flux® optics, the system delivers 4x10^9 copper K-alpha photons per second in an almost parallel beam (divergence of about 0.4 mrad).

The determination of the wavelength at X-ray tubes demands new methods in precision X-ray polarimetry. Therefore, we investigated anomalous transmission, also called Borrmann effect [4]. If the incident beam fulfils Bragg's law, the transmission through a crystal increases by many orders of magnitude depending on the thickness of the crystal. Since this is just the case for one polarization component, a high polarization purity can be reached by this method. We have measured purities down to almost 10^{-5} for silicon plates with a thickness of 4 mm. This is just the detection limit due to the low count rate behind the polarimeter in the crossed position of polarizer and analyzer. Nevertheless, such a small value cannot be measured with a conventional X-ray tube and available X-ray polarizers.

In addition, the Bormann effect enables the analysis of the polarization state of X-rays in one single scan. Turning the azimuth of the crystal in such a way that multiple reflections occur, different polarization planes can be analyzed in one angular scan. Thus, the three first Stoke's parameters can be determined and therefore it is possible to distinguish between circularly, elliptically or linearly polarized light.

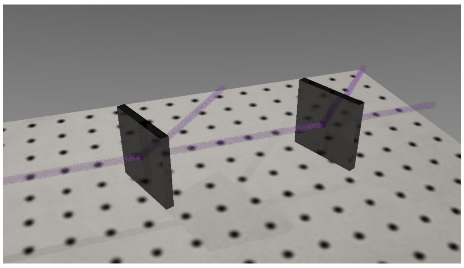

Figure 2: Setup of the Borrmann polarimeter consisting of two plane silicon crystals in transmission geometry.

References

[1] C. Detlefs, M. Sanchez del Rio, and C. Mazzoli. "X-ray polarization: General formalism and polarization analysis." The European Physical Journal Special Topics 208.1 (2012): 359-371.

[2] B. Marx, K. S. Schulze, I. Uschmann, T. Kämpfer, R. Lötzsch, O. Wehrhan, W. Wagner, C. Detlefs, T. Roth, J. Härtwig, E. Förster, T. Stöhlker, G. G. Paulus, "High-precision x-ray polarimetry", Physical Review Letters 06/2013; 110(25):254801.

[3] K. P. Heeg, H.-C. Wille, K. Schlage, T. Guryeva, D. Schumacher, I. Uschmann, K. S. Schulze, B. Marx, T. Kämpfer, G. G. Paulus, R. Röhlsberger, J. Evers, "Vacuum-assisted generation and control of atomic coherences at x-ray energies", Physical Review Letters 08/2013; 111(7):073601.

[4] Cole, H., FW T. Chambers, and C. G. Wood. "X-Ray Polarizer." Journal of Applied Physics 32.10 (1961): 1942

Angular differential measurement of linear polarization of elastically scattered hard x-rays.*

M. Schwemlein[1,2,3], *K.-H. Blumenhagen*[4,5], *T. Gassner*[4,6], *T. Groß*[7], *A. Gumberidze*[1,2], *R. Märtin*[4,6], *N. Schell*[8], *U. Spillmann*[4,6], *S. Trotsenko*[4,6], *G. Weber*[4,6], *and Th. Stöhlker*[4,5,6]

[1]ExtreMe Matter Institute EMMI, Darmstadt, Germany, ; [2]FIAS, Frankfurt a.M., Germany;
[3]PI, Univ. Heidelberg, Germany; [4]HI-Jena, Jena, Germany; [5]IOQ, Univ. Jena, Germany; [6]GSI, Darmstadt, Germany;
[7]IGVP, Univ. Stuttgart, Germany; [8]HZG, Geesthacht, Germany

Elastic scattering of photons from atoms and molecules, also known as Rayleigh scattering, is one of the fundamental processes in the interaction of light with matter. Understanding of this scattering process, in particular in the hard X-ray regime, is important for various applications such as medical imaging, material research and it also provides information about the inner structure of atomic and molecular systems [1,2]. Also from theoretical point of view, there is ongoing interest at present [3,4].

Former experimental studies of this scattering process have used either unpolarized or linearly polarized photon sources to investigate the angular distribution and absolute peak intensities of the scattered radiation. However, the polarization properties of the elastically scattered photons have not been resolved up to now. Due to recent development in coherent light sources on one side and highly-segmented semiconductor based detection systems [5,6] on the other, it became feasible to control both, the polarization of the incident as well as the scattered photons.

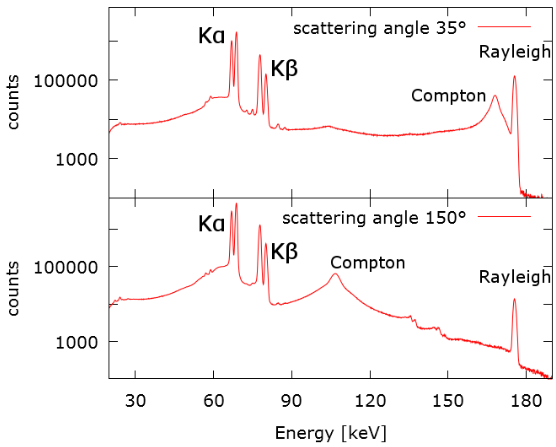

Figure 1: Ge(i) detector response to synchrotron radiation that is scattered at a Au target under 35° and 150°. The characteristic target radiation $K\alpha_2$ (67 keV), $K\alpha_1$ (68.8 keV), $K\beta_1$ (77.9 keV) and $K\beta_2$ (80.1 keV) is clearly visible. The 175 keV line correspond to elastic Rayleigh-scattering. The broader structure, shifting with the scattering angle, correspond to inelastic Compton scattering.

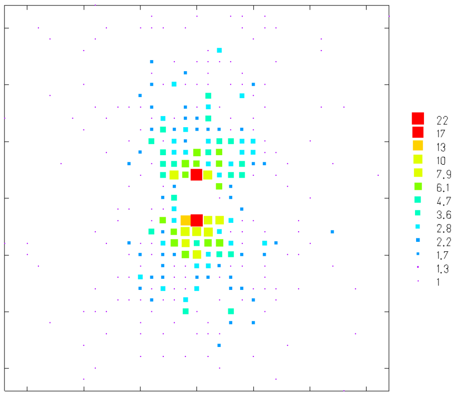

Figure 2: 175 keV X-rays are elastically scattered in the Au target at a scattering angle of 120°. These Rayleigh photons are again Compton-scattered in the Si(Li) detector crystal. The figure shows their position distribution inside the Si(Li) detector with respect to the scattering position.

The present experiment aims to measure the angular distribution and polarization of the initially linearly polarized hard x-rays, scattered off a high-Z target. Therefore, a Si(Li) Compton polarimeter, developed for experiments at the international FAIR facility, as well as standard Ge(i) detectors have been used. The experiment took place at the DESY PETRA III beamline P07-EH3, where nearly 100% linearly polarized photons in the hard X-ray regime can be produced.

Fig. 1 shows the Ge(i) detector response to the radiation, coming from the target. A thin Au foil was used as the target. The synchrotron radiation energy was set to 175 keV. Fig. 2 shows the position distribution of Compton scattered photons (elastically scattered in the target) inside the Si(Li) detector crystal. The anisotropy indicates a high degree of linear polarization of the Rayleigh-scattered photons from the Au target. The data are currently being evaluated.

References

[1] S. C. Roy, Radiat. Phys. Chem. **41**, 725 (1993).
[2] M. Y. Sfeir et al., Science **306**, 1540 (2004).
[3] A. Surzhykov, Phys. Rev. A **88**, 062515 (2013).
[4] L. Safari, Phys. Rev. A **85**, 043406 (2012).
[5] U. Spillmann et al., Rev. Sci. Instr. **79**, 083101 (2008).
[6] G. Weber et al., JINST **5**, C07010 (2010).

* Work supported by HGS-Hire / Helmholtz Alliance EMMI / DESY and HZG support at beamline P07.

Forward-angle electron spectroscopy in ion-atom collisions studied at the ESR*

P.-M. Hillenbrand[1,2], *S. Hagmann*[1,3], *D. Banaś*[4], *C. Brandau*[2,5], *K.-H. Blumenhagen*[6,7], *W. Chen*[1], *R. Dörner*[3], *E. De Filippo*[8], *A. Gumberidze*[5], *D. L. Guo*[9], *O. Kovtun*[10], *C. Kozhuharov*[1], *M. Lestinsky*[1], *Y. A. Litvinov*[1], *A. Müller*[2], *H. Rothard*[11], *S. Schippers*[2], *M. S. Schöffler*[3], *U. Spillmann*[1], *S. Trotsenko*[1,6], *N. Winckler*[1], *X. L. Yan*[9], *X. L. Zhu*[9], *and Th. Stöhlker*[1,6,7]

[1]GSI Darmstadt; [2]Univ. Giessen; [3]Univ. Frankfurt; [4]Univ. Kielce, Poland; [5]EMMI Darmstadt; [6]HI Jena; [7]Univ. Jena; [8]INFN Catania, Italy; [9]IMP Lanzhou, China; [10]Univ. Heidelberg; [11]CIRIL-GANIL, Caen, France

The spectroscopy of electrons emitted in low-energetic ion-atom collisions, in particular in forward direction parallel to the projectile ion beam, has been in the focus of research in atomic physics since several decades. These electrons populate low-energetic continuum states of the projectile and, due to Lorentz transformation, are observed in the laboratory frame as electrons emitted under $\vartheta_e \approx 0°$ with a velocity v_e similar to the projectile velocity $v_e \approx v_p$. Experimentally the spectroscopy of these so-called "cusp-electrons" benefits from enhanced energy resolution due to a reduced Doppler broadening.

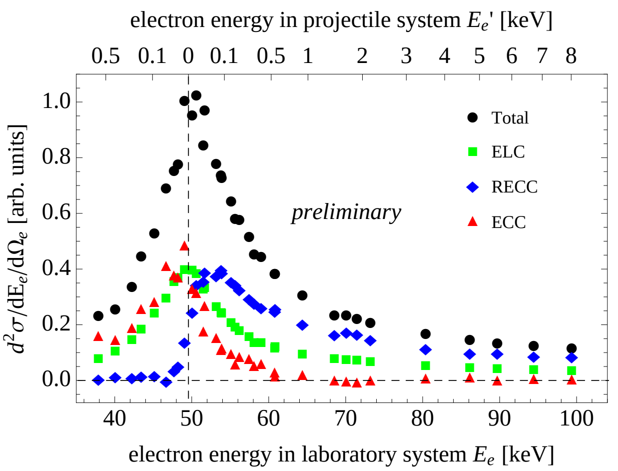

Figure 1: Electron energy distribution of forward emitted electrons originating in processes (a) – (c).

At GSI this field of research was extended to high-energetic heavy-ion atom collisions. For this purpose collisions of beryllium-like U^{88+}-projectile ions at 90 MeV/u colliding with a molecular gas-jet target of N_2 were studied at the ESR in a beam time in 2012. The energy distribution of cusp electrons emitted in these collisions was measured with a dedicated magnetic electron spectrometer located downstream the gas-jet target. Additionally five X-ray detectors were positioned around the target, and two particle detectors were used to detect projectile ions which had lost or captured one electron during a collision with the target (or the rest gas). Applying coincidence conditions between the electrons observed in the spectrometer and signals of one of the X-ray or particle detectors three different collision processes could be observed, which each resulted in an electron populating a low-energetic continuum of the projectile:

(a) The **electron loss to continuum** (ELC) corresponds to the ionization of a projectile electron into the projectile continuum during the collision with the target:

$$U^{88+} + N_2 \to U^{89+} + [N_2]^* + e^-.$$

(b) The **electron capture to continuum** (ECC) corresponds to the capture of a target electron into the projectile continuum, while the excess energy is carried away by the recoil of the generated target ion:

$$U^{88+} + N_2 \to U^{88+} + \left[N_2^+\right]^* + e^-.$$

(c) The **radiative electron capture to continuum** (RECC) corresponds to the capture of a target electron into the projectile continuum, while the excess energy is carried away by a photon:

$$U^{88+} + N_2 \to U^{88+} + \left[N_2^+\right]^* + e^- + \gamma.$$

Previously the RECC process (c) was for the first time observed unambiguously at GSI and experimentally proven to be equivalent to the high-energy endpoint of electron-nucleus bremsstrahlung studied in inverse kinematics [1]. Succeeding this pioneering experiment a high-resolution measurement of the processes (a) – (c) was performed in 2012, with a significantly improved experimental setup [2]. Whereas for low-energetic projectiles used in former times the cusp electron spectrum was dominated by ECC or ELC, it was proven within this experiment that at 90 MeV/u the cross sections of the three processes are comparably large, while the shape of the electron energy distribution shows significant variations (Fig. 1). Notably the opposite asymmetry of ECC and RECC gives a clear signature of the different underlying collision mechanisms. Comparison of the experimental results with various theoretical calculation is currently under way and soon to be published.

References

[1] M. Nofal *et al.*, Phys. Rev. Lett. **99**, 163201 (2007)

[2] P.-M. Hillenbrand, *Elektronenspektroskopie im Fundamentalprozess der Elektron-Kern-Bremsstrahlung*, Doktorarbeit Universität Giessen (2013)

* Work supported by HIC-for-FAIR through HGS-HIRe and Helmholtz-CAS Joint Research Group HCJRG-108.

Retrieval of Multiple Ionization Dynamics in Strong-field Ionization of Atomic Ions

P. Wustelt[1,2], M.Möller[1,2], T. Rathje[1,2], A.M. Sayler[1,2], S. Trotsenko[1], T. Stöhlker[2,3], and G.G. Paulus[1,2]

[1]Helmholtz Institute Jena, Germany, [2]Institute of Optics and Quantum Electronics, Jena, Germany, [3]GSI, Darmstadt, Germany

When pushing towards relativistic intensities, strong-field ionization processes of atomic ions becomes increasingly important. The highly nonlinear multi-photon multi-electron ionization dynamics is a particularly challenging problem for the present understanding of laser matter interaction. Results from this field of research are not only of fundamental interest, rather these investigations are also relevant for laser based schemes of electron and ion acceleration. However, most of the existing strong-field ionization experiments have been performed at relatively moderate intensities and starting from neutral atomic or molecular targets. Investigating strong-field interaction with atomic or molecular ions enters an experimentally largely unknown territory.

In the experiments performed here, the recently developed ion beam apparatus is used together with a high-power high-repetition rate laser system that delivers 10-mJ, 35-fs laser pulses. The ion beam is produced by a duoplasmatron ion source or an EBIT (electron beam ion trap). The duoplasmatron produces a dense ion beam with ion currents up to several μA and low charge states. The EBIT provides the option to start from different initial charge states of the same atom. In order to produce a dense and collimated beam at the interaction point with the laser, the ion beam is accelerated to several keV and guided through a series of Einzel lenses, a Wien filter, deflectors and pinholes. After the laser matter interaction, the full three dimensional momentum distribution of the resulting fragments are measured with a position- and time-sensitive detector.

Status of the project: The ion beam setup is routinely operated during dedicated beam times of the laser system. The momentum and charge state distributions of ions resulting from the ionization of singly charged Xenon, Neon and Helium are studied as a function of intensity and ellipticity of the laser pulses. Peak intensities up to $4{\cdot}10^{16}$ W/cm² allow the observation of highly charged ions up to Xe^{8+}, Ne^{5+} and He^{2+}, see Figure 1 for an example.

In contrast to linear polarization, for elliptically polarized many-cycle pulses, the final ion momentum distribution in single ionization provides direct and complete information on the ionizing field strength as well as the ionization time. Furthermore, using a deconvolution method we are able to reconstruct the electron momenta from the ion momentum distributions after multiple ionization and, therefore, gain information on the ionization field strength as well as on the release times during the laser pulse for subsequent ionization steps (see Fig. 2). In addition, the subtle effects of the Coulomb interaction on the electron trajectory lead to a tilt in the observed momentum distribution. These effects can be used to study the kinematics and the initial conditions of the electron following tunnel ionization. The results are compared to predictions from classical Monte-Carlo simulations based on quasistatic ionization rates.

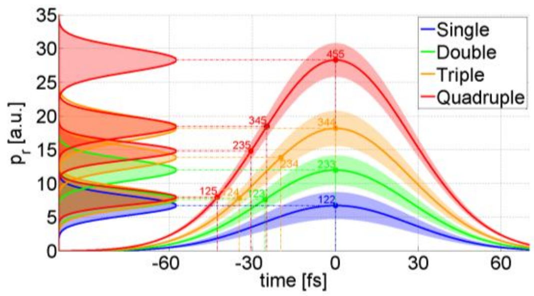

Figure 2: Retrieved ionization dynamics of single up to quadruple ionization of Ne^{+}-ions during the envelope of an elliptically polarized laser pulse. The retrieval is based on the measured momentum distributions shown in Fig. 1. The numbers mark transitions between different charge states. For example, the step '123' means ionization step from Ne^{+} to Ne^{2+} from all ions ending in the final charge state of Ne^{3+}. Different envelopes (red, orange, green, and blue) are related to different regions within the focal volume.

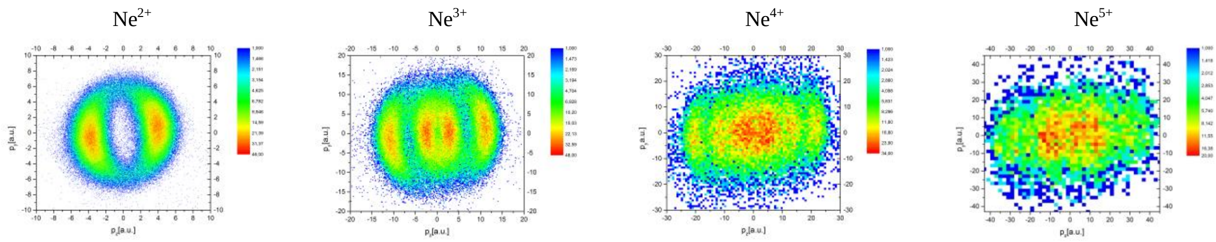

Figure 1: Measured ion momentum distributions in the polarization plane for single, double, triple and quadruple ionization of Ne^{+}-ions. The major polarization axis is y axis (e = 0.74). The different final charge states of the ions are created in different areas of the focal volume. The peak intensity of the laser pulse was $4 \cdot 10^{16}$ W/cm^2.

The Effect of the Breit-Interaction Studied for the Emission Characteristics of $1s2s^22p_{1/2}$ Decay in Be-like Uranium *

S. Trotsenko[1,2], A. Gumberidze[3,4], Y. Gao[2,5], C. Kozhuharov[2], S. Fritzsche[1,6], A. Surzhykov[1,2,6], N. Petridis[2,7], D. B. Thorn[3,4], H.F. Beyer[2], R.E. Grisenti[2,7], S. Hagmann[2,7], P.-M. Hillenbrand[2], U. Spillmann[2], G. Weber[1], and Th. Stöhlker[1,2,3,6]

[1]Helmholtz-Institut Jena, D-07743 Jena, Germany; [2]GSI Helmholtzzentrum für Schwerionenforschung, D-64291 Darmstadt, Germany; [3]ExtreMe Matter Institute EMMI, D-64291 Darmstadt, Germany; [4]FIAS, Frankfurt a. M., Germany; [5]Institute of Modern Physics, Chinese Academy of Sciences, Lanzhou, China; [6]Friedrich-Schiller-Universität Jena, D-07743 Jena, Germany; [7]Institut für Kernphysik, Universität Frankfurt, Germany

The well-known Breit interaction was first worked out by Gregory Breit in order to calculate the fine-structure of atomic helium [1]. Nowadays, the Breit interaction is described as quantum electrodynamics (QED) effect. It includes magnetic interactions and retardation in the exchange of a single virtual photon between the electrons, and affects not only the energy level structure but also the dynamics of atomic processes. The interaction has aroused great interest in further exploration and analysis of relativistic contributions to the electron-electron interaction, and its importance has already been confirmed for several processes in the collisions between electrons and highly charged ions (HCI) [2, 3, 4, 5, 6, 7, 8, 9].

More often than not the influence of the Breit interaction is small, so it is treated as a minor correction to the Coulomb interaction. However, in certain cases it can even dominate dynamics involving highly charged ions. Nakamura et al. [10] found that the Breit interaction can enhance dielectronic recombination (DR) resonant strengths by almost 100%. Soon afterwards, Fritzsche et al. [11] predicted that the Breit interaction could dominate the Coulomb interaction in the x-ray emission of Li-like heavy ions following dielectronic recombination and could even qualitatively change the angular distribution of x-rays for heavy ions with nuclear charge $Z \geq 73$. Three years later, Hu et al. [12] obtained experimental evidence for the prediction of Fritzsche et al. by measuring the angular distribution of the $[1s2s^22p_{1/2}]_1 \rightarrow [1s^22s^2]_0$ transition in dielectronic recombination of Li-like Au with free electrons in an electron beam ion trap (EBIT).

In this report, we present the experimental results for angular distribution of characteristic x-rays following the resonant transfer and excitation (RTE) in U^{89+} collisions with H_2 target at the experimental storage ring ESR of GSI. The RTE is equivalent to the DR processes, but with the difference that the electron is initially in a bound state of target. The experiment performed by colliding Li-like uranium (U^{89+}) ions with H_2 at the resonance energy (116.15 MeV/u) for the $U^{89+}[1s^22s] \xrightarrow{H_2} U^{88+}[1s2s^22p_{1/2}\,]_1$ process. The accurate and stable value of the ion beam energy was guaranteed by the electron cooler of the ESR. The layout of the experimental arrangement at the gas-jet target is shown in Fig. 1. We measured the angular distribution of the $[1s2s^22p_{1/2}]_1 \rightarrow [1s^22s^2]_0$ x-ray transition following the resonant transfer and excitation.

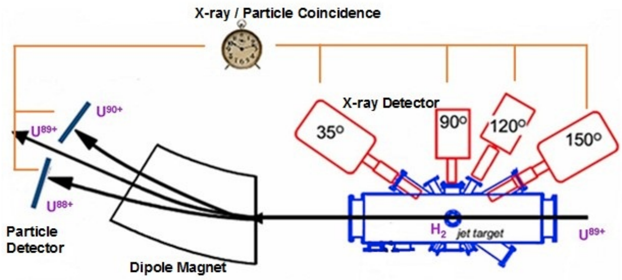

Figure 1: The experimental setup at the internal gas-jet target of the ESR.

The x-ray emission from the collisions was recorded with four high purity intrinsic germanium (HPGe(i)) detectors placed at 35^0, 90^0, 120^0 and 150^0 angles with regard to the direction of the ion beam. Exploiting time coincidences between the x-ray detectors and a particle detector mounted after the ESR dipole magnet, we were able to obtain the x-ray spectra corresponding only to the events of U^{89+} capturing an electron into singly or doubly excited states.

Four x-ray spectra have been obtained in the experiment at 35^0, 90^0, 120^0 and 150^0 observation angles corresponding to one-electron-capture events. As an example, Fig. 2 shows the spectrum recorded at 35^0 angle. In the spectrum, several radiative electron capture (REC) lines are present. They are denoted according to the shell where the target electron is captured into, i.e. L-REC stands for the capture into the L-shell (n=2), M-REC stands for the capture into the M-shell (n=3), etc. In addition, the RTE induced peak ($[1s2s^22p_{1/2}]_1 \rightarrow [1s^22s^2]_0$ transition) very close to the radiative electron capture into the $2s_{j=1/2}$ and $2p_{j=1/2}$ states (L-REC$_{1/2}$) is found. The REC peaks are significantly broader than the RTE-induced characteristic transition, due to the Compton profile of the target. This allows us to fit the RTE and REC lines separately and obtain the corresponding intensities. This is also possible for x-ray spectrum recorded at 150^0. However, at 90^0 and 120^0, the large Doppler broadening and a poorer energy resolution

* Work supported by HI Jena/EMMI/GSI(ESR)

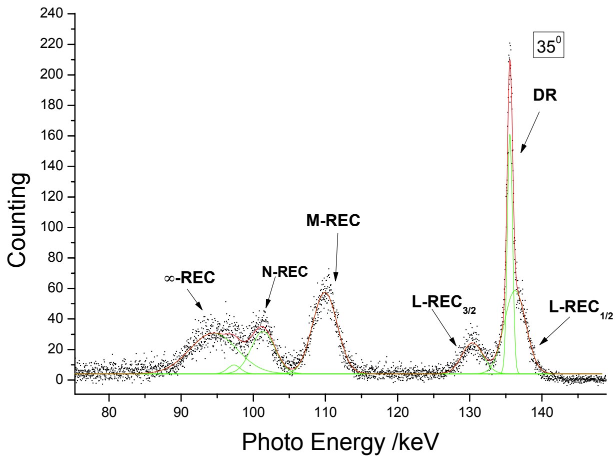

Figure 2: X-ray spectrum obtained at the ESR corresponding to one-electron-capture events in 116.15 MeV/u U^{89+} collisions with the H_2 gas target, obtained at 35^0 observation angle.

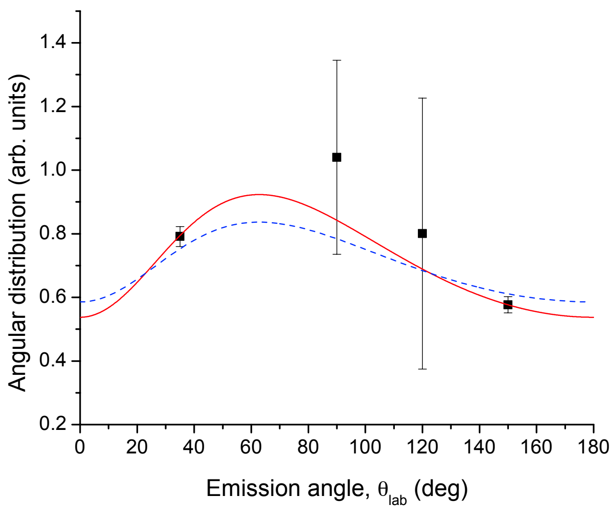

Figure 3: Experimental angular distribution for the $[1s2s^22p_{1/2}]_1 \rightarrow [1s^22s^2]_0$ transition following the RTE into initially Li-like uranium. The dashed line is a theoretical angular distribution from [11], with the alignment parameter A_2= -0.314. The solid line is from fitting the equation of the electric dipole emission [11] to our experimental data, having A_2 as a free fit parameter.

of the corresponding detectors smear out the difference between the RTE and L-REC$_{1/2}$ peaks, making it impossible to fit them separately and obtain directly their intensities. Therefore, we have to rely on the relativistic REC theory which has been extensively tested in many different experiments [13] and is currently known to provide accurate description of the process. Namely, we used the angular differential cross sections for L-REC$_{3/2}$, L-REC$_{1/2}$ and M-REC [14] together with our experimental data for obtaining the intensity of the L-REC$_{1/2}$. As a cross check of theory, we also compared the theoretical values with our experimental results for L-REC$_{1/2}$: L-REC$_{3/2}$ and L-REC : M-REC ratios at 35^0 and 150^0 where we could obtain the experimental values independently from the theory. We found a fair agreement between the theoretical and experimental results, however, in couple of cases a deviation of about 10% has been observed. The reason of this deviation is currently unclear. Therefore, we included the uncertainty of 10% for obtaining the experimental RTE intensity values at 90^0 and 120^0 angles. Furthermore, in order to obtain the angular distribution of the RTE induced $[1s2s^22p_{1/2}]_1 \rightarrow [1s^22s^2]_0$ transition, we normalized its intensity to the one of the closely spaced L-REC$_{3/2}$ peak and used the theoretical angular differential cross-section for the latter. In this way, uncertainties related to different solid angles and efficiencies of the x-ray detectors are almost completely cancelled out.

Our experimental and theoretical angular distributions [11] of the $[1s2s^22p_{1/2}]_1 \rightarrow [1s^22s^2]_0$ transition are shown in Fig. 3. From the figure, a good qualitative agreement between the experiment and theory agreement can be observed. By fitting the equation for angular distribution of the electric dipole emission [11] to the experimental angular distribution, we received the experimental value for alignment parameter $A_2 = -0.46 \pm 0.07$. Our result is definitely closer to the prediction from [11] with Breit interaction included (-0.314) than to the one without the Breit interaction (0.47). This can be considered as a proof for the high importance of the Breit interaction for this case. The reason for the relatively small ($\sim 2\sigma$) quantitative deviation between our experimental and theoretical results for the alignment parameter (A_2) has still to be clarified.

References

[1] G. Breit, *Phys. Rev.* **36**, 383 (1930).

[2] G. Breit, *Phys. Rev.* **39**, 616 (1932).

[3] C. Fontes, D. Sampson, and H. Zhang, *Phys. Rev. A* **59**,1329 (1999).

[4] R. E. Marrs, S. R. Elliott, and D. A. Knapp, *Phys. Rev.* **72**, 4082 (1994).

[5] W. R. Johnson, Springer, New York (2007).

[6] I. P. Grant, Springer, New York (2007).

[7] R. W. Childers, *Phys. Lett. B* **126**, 485-488 (1983), ISSN 0370-2693.

[8] C.-Y. Wong and R. Becker, *Phys. Rev. B* **182**, 251 (1986), ISSN 0370-2693.

[9] I. P. Grant and H. M. Quiney, *Int. J. Quantum Chem.* **182**, 283 (2000).

[10] Nobuyuki Nakamura *et al.*, *Phys. Rev. Lett.* **100**, 073203 (2008).

[11] Stephan Fritzsche *et al.*, *Phys. Rev. Lett.* **103**, 113001 (2009).

[12] Zhimin Hu *et al.*, *Phys. Rev. Lett.* **108**, 073002 (2012).

[13] J. Eichler, Th. Stöhlker, *Physics Reports* **439**, (2007) 1-99.

[14] A. Surzykov, (private communication).

FOCAL – PRECISION X-RAY SPECTROSCOPY FOR EXTREME FIELDS IN HIGH-Z IONS *

H.F. Beyer[1], D. Banaś[2], K.-H. Blumenhagen[8], F. Bosch[1], C. Brandau[4], W. Chen[1], Chr. Dimopoulou[1], E. Förster[3,8], T. Gaßner[1,8], A. Gumberidze[4], S. Hagmann[1,5], R. Heß[1], P.-M. Hillenbrand[1], P. Indelicato[6], P. Jagodzinski[2], T. Kämpfer[8], Chr. Kozhuharov[1], M. Lestinsky[1], D. Liesen[1], Yu.A. Litvinov[1], R. Loetzsch[8], B. Manil[7], R. Märtin[8], F. Nolden[1], N. Petridis[4,5], M.S. Sanjari[1,4], K.S. Schulze[8], M. Schwemlein[1], A. Simionovici[10], U. Spillmann[1], M. Steck[1], Th. Stöhlker[1,8], C.I. Szabo[6], M. Trassinelli[10], S. Trotsenko[8], I. Uschmann[3,8], G. Weber[8], O. Wehrhan[3,8], N. Winckler[1], D. Winters[1], N. Winters[1], and E. Ziegler[11]

[1]GSI Helmholtzzentrum, Darmstadt, Germany; [2]Institute of Physics, Swietokrzyska Academy, Kielce, Poland; [3]Inst. für Optik und Quantenelektronik, Friedrich-Schiller-Universität, Jena, Germany; [4]Extreme Matter Institute, EMMI, GSI Helmholtzzentrum, Darmstadt, Germany; [5]Institut für Kernphysik, Goethe-Universität, Frankfurt am Main, Germany; [6]Lab. Kastler Brossel, Université P. et M. Curie, Paris, France; [7]Laboratoire de Physique des Lasers (LPL) UMR 7538 CNRS - Université Paris 13, Villetaneuse, France; [8]Helmholtz-Institut Jena, Jena, Germany; [9]LGIT, Observatoire des Sciences de l'Univers de Grenoble, Grenoble, France; [10]Institut des Nanosciences de Paris, Université Pierre et Marie Curie-Paris 6 and CNRS-UMR 7588, Paris, France; [11]ESRF, Grenoble, France

Introduction and Motivation The extraordinarily strong electric field provided by the nucleus of a very heavy one-electron ion exposed to its inner electrons is the testing ground for bound-state quantum electrodynamics (QED) in a largely unexplored domain. Experimentally the QED contribution to the 1s binding energy is accessible via a direct measurement of the K-shell transitions with sufficient accuracy. The corresponding Lyman transitions in high-Z ions lie in the hard x-ray region. Previously the x-ray energy has been measured with the aid of germanium x-ray detectors of limited resolution [1]. The present experiment marks the leap to wavelength-dispersive spectroscopy of substantially higher spectral resolving power simultaneously coping with the low x-ray intensity.

Experiment Figure 1 schematically shows the twin crystal-spectrometer assembly, Bi-FOCAL, operated in the **FO**cusing **C**ompensated **A**symmetric **L**aue [2] geometry which has been arranged at the ESR gas jet. The spectrometer system [3, 4] equipped with two 2D position-sensitive Ge strip detectors [5, 6], F1 and F2, was used in an experiment with one-electron Au^{78+} ions at a velocity corresponding to $\beta = 0.4711$. The twin spectrometers were deliberately arranged symmetrically around the ion-beam at observation angles of $\pm 90^{\circ}$ in an angular-sensitive geometry where the usual Doppler broadening and angular Doppler uncertainties are near their maximum. The imaging properties of the FOCAL crystal optics are turned to advantage retaining nearly full spectral resolution also for the fast moving source.

Complementary to the crystal spectrometer an array of low-temperature micro calorimeters were mounted in

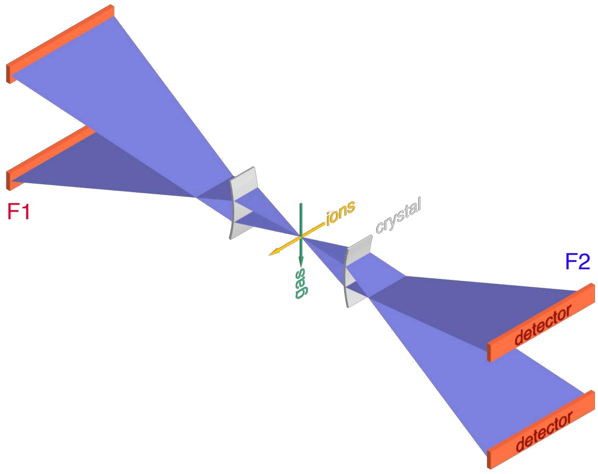

Figure 1: Two crystal-spectrometers, Bi-FOCAL, symmetrically arranged around the ion beam at the ESR gas jet. Wavelength dispersion occurs in the vertical direction and the spectra are recorded by two position-sensitive x-ray detectors F1 and F2 mounted at two of the possible four locations as indicated.

a velocity-sensitive geometry at an observation angle of 145°, where angular uncertainties are reduced. That experiment, run in parallel, is described in another report [7].

Besides the high background-suppression capabilities of FOCAL figure 2 demonstrates its slanted Lyman-α and -β lines of Au^{78+} in accordance with the underlying x-ray-optical design. Without crystal optics Doppler broadening would blur the whole spectral range displayed. The spectrum shown in figure 3 was obtained by projecting the intensity along the slanted lines. In the experiment the Lyman-α_1 line was Doppler tuned to the position of the 63.1-keV gamma-ray line emitted from a radioactive sample of ^{169}Yb used as a calibration source rendering dispersion uncertainties unimportant.

* This work has been supported by the European Community FP7 Capacities, contract ENSAR No. 262010. D. Banas acknowledges the support by the Polish Ministry of Science and Higher Education under Grant No. N N202 46353. P.-M. Hillenbrand acknowledges support by HIC-for-FAIR through HGS-HIRe and the Helmholtz-CAS Joint Research Group HCJRG-108.

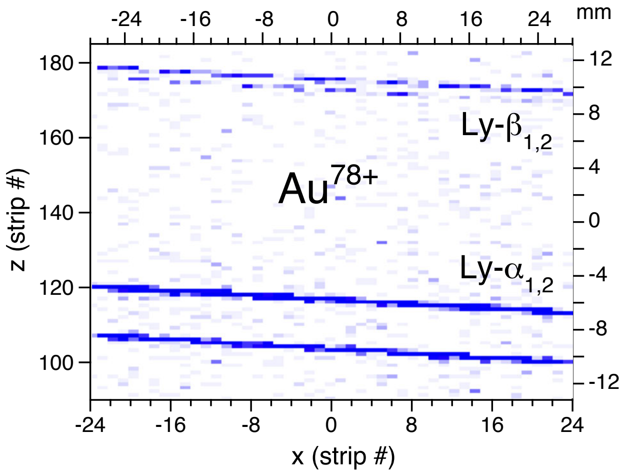

Figure 2: The spectrum of hydrogen-like Au^{78+} revealed as a position spectrum taken by F2. The Lyman-α and -β doublets appear as slanted lines caused by the Doppler effect in counterplay with the crystal optics employed.

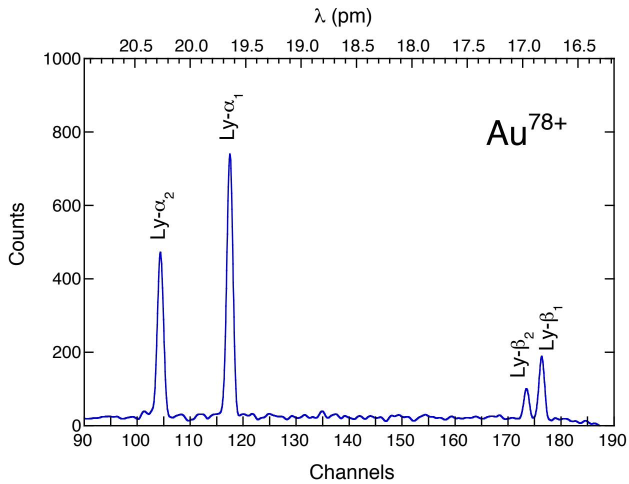

Figure 3: The Lyman-α and -β doublets of Au^{78+} obtained by a projection of the two-dimensional intensity distribution of figure 2.

Systematic Effects At an observation angle of exactly 90° the required transition wavelength λ_{ion} in the emitter frame is simply related to the laboratory wavelength by $\lambda_{lab} = \gamma\, \lambda_{ion}$ where γ denotes the relativistic Lorentz parameter. The two arms of the spectrometer assembly are mounted accurately inline resulting in observation angles $\lambda_{\rm lab}(\vartheta)$ and $\lambda_{\rm lab}(\pi - \vartheta)$, respectively. However missalignment of the ion beam relative to the spectrometer axis might still persist. This class of uncertainties are well canceled by averaging the two laboratory wavelengths as $\lambda_{\rm ion} = (\lambda_{\rm lab}(\vartheta) + \lambda_{\rm lab}(\pi - \vartheta))/(2\gamma)$.

In addition there are a number of systematic influences on the measured wavelength that do not simply cancel and which need to be carefully identified and analyzed. We are currently in the process of assessing systematic corrections and their corresponding uncertainties referring to the procedures and mathematical algorithms by which the spectral lines are located including long-term drifts plus all the geometrical effects due to the positions and angular orientations of the x-ray source, of the curved silicon crystals and of the x-ray detectors. A particularly important example is the position of the gas-jet target in the horizontal plane spanned by the ion-beam and the spectrometer axis. This was investigated in a separate experiment by scanning a thin wire across the gas jet [8].

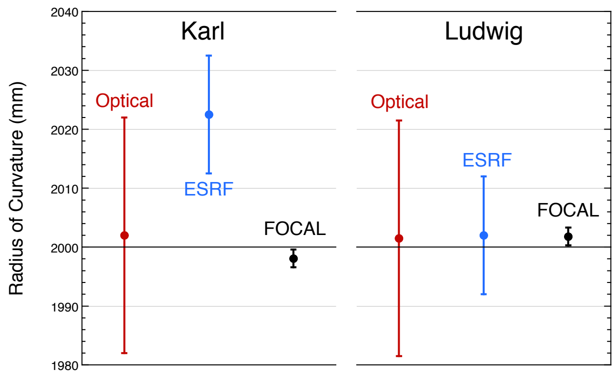

Figure 4: The radius of curvature of the two silicon crystals *K*arl and *L*udwig determined by three different methods: optical reflections on the polished crystal surfaces, mapping with synchrotron radiation at the ESRF and by operating FOCAL as a scanner.

Here we mention two other examples of the crystal optics which need to be understood: *(i)* the radius of curvature of the two crystals named *Karl* and *Ludwig* was measured by three different methods which gave consistent results as summarized in figure 4. *(ii)* the observed slope of the spectral lines along with the calculated prediction is summarized in Table 1. Although the slanting effect is generally confirmed the measured slopes tend to be slightly lower than predicted.

Table 1: Doppler slanting: predicted and observed slopes of the Lyman-$\alpha_{1,2}$ and Lyman-β spectral lines of Au^{78+} at a velocity of $\beta \equiv v/c = 0.4711$.

	Lyman-α_2	Lyman-α_1	Lyman-β
predicted	0.01922	0.01862	0.01597
observed			
FOCAL-1	0.0184(2)	0.0183(2)	
FOCAL-2	0.0188(3)	0.0179(2)	0.0165(4)

We thank K. Eberhard from the Institut für Kernchemie of the Johannes Gutenberg-Universität, Mainz, for the preparation of our calibration sources.

References

[1] A. Gumberidze *et al.*, Phys. Rev. Lett. **94** (2005) 223001.
[2] H. F. Beyer, Nucl. Instrum. Methods. A**400** (1997) 137.
[3] H.F. Beyer *et al.*, Spectrochimica Acta **B 59** (2004) 1535.
[4] H.F. Beyer *et al.*, Spectrochimica Acta **B 64** (2009) 736.
[5] D. Protić *et al.* IEEE Trans. Nucl. Sc. **52** (2005) 3194.
[6] U. Spillmann *et al.*, Rev. Sc. Instr. **79** (2008) 083101.
[7] S. Kraft-Bermuth *et al.*, GSI scientific report 2013.
[8] T. Gaßner *et al.*, GSI scientific report 2013.

Spatial Characterisation of the Internal Gas Target at the ESR for the FOCAL Experiment

T. Gassner[1,2], *H. F. Beyer*[2], *and the FOCAL Collaboration*[1]

[1]GSI, Darmstadt, Germany; [2]Helmholtz-Institute Jena, Germany

The FOCAL experiment involves a highly accurate twin crystal spectrometer, designed to measure the Lamb shift of stored highly charged ions, like hydrogen-like Au^{78+}, with an accuracy down to the few-eV level where higher-order QED contributions become accessible [1]. Since the geometrical configuration of the whole apparatus is of crucial importance, all parameters influencing the final value have to be known as accurately as possible. In this annual report we present our efforts to characterise the internal gas target [2, 3] at the ESR at GSI Darmstadt were in 2012 the FOCAL experiment was conducted.

In the accurate spectroscopy of fast moving ions a recurring task is the transformation of the measured wavelength in the laboratory frame back to the wavelength in the emitter frame. The according relation between the laboratory wavelength λ_{lab} and the emitter wavelength $\lambda_{\mathrm{emitter}}$ is the relativistic Doppler formula

$$\lambda_{\mathrm{lab}} = \lambda_{\mathrm{emitter}}\,\gamma\,(1 - \beta\cos(\theta_{\mathrm{lab}})) \qquad (1)$$

with two main unknown: The first unknown is the velocity of the ions hidden in the Lorentz parameters β and γ, the second one is the observation angle θ_{lab} under which the x-ray emission is measured. The velocity can be determined (in case of the ESR) with very high accuracy with the electron-cooler voltage. For determining the observation angle θ_{lab} one has to know the position of (i) the detector and (ii) the position of the emitter. In the FOCAL experiment conducted in 2012 as in many other experiments the position of the x-ray emitter is the volume defined by the intersection of the stored ion beam and the internal gas-jet target of the ESR. Since the detectors where accurately aligned with the help of optical telescopes just before the beam time the remaining unknown is the position and the density distribution of the gas target. Therefore the experiment presented in this report was conducted.

To measure the position, the diameter and the density distribution of the internal gas target of the ESR we decided to use a mechanical gas-scatter approach. At the low particle density of the gas target of only 10^{11} particles/cm^3 encountered other methods considered such as photon scattering or photo absorption/re-emission suffer from prohibitively low event rates. The probe used consisted of an aluminium body on which a Constantan wire of 0.6 mm diameter is tensed. If the gas jet hits the wire the pressure in the target chamber will rise which can easily be detected by standard methods. In order to scan the frame over a suitable position range it was mount on a linear actuator installed under 35° with respect to the ion-beam direction. All anchors for the wire are placed in a way that the wire runs parallel or perpendicular with respect to the ion-beam axis. Therefore it is possible to measure the density profile of the gas target in north-south (longitudinal) and east-west (transversal) direction and to determine a position centroid. In addition to the wire anchors there are also three fiducial marks used by the telescopes located left and right of the ion axis and in-line with the vertical gas-jet, respectively. This alignment is needed to relate our probe and hence the measured gas target position with the reference frame of the ESR.

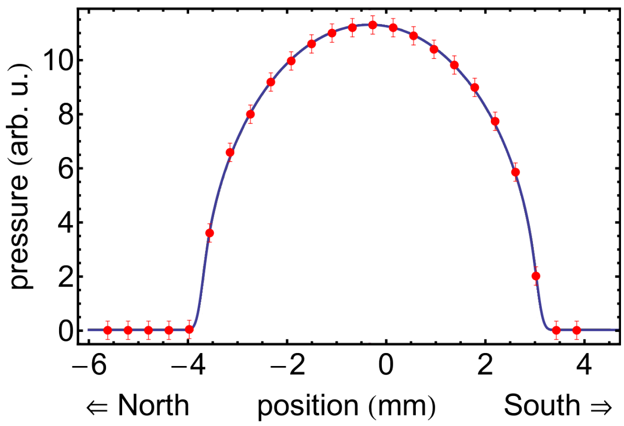

Figure 1: Measured pressure in the target chamber (red dots) as a function of the wire position. The blue curve is the best fit of our model which assumes a round gas-jet, with constant particle density in the center.

Figures 1 shows the measured pressure rise in the target chamber (red dots) and the best fit of our model (blue curve) assuming constant density in the central region of the round gas target. The measurement values are in good agreement with the model enabling us to determine the position and the diameter with an estimated uncertainty of ± 0.3 mm dominated by small telescope imperfections leading to a significant reduction of systematic uncertainties.

References

[1] H. F. Beyer *et al.*, Spectrochimica Acta B64, 736 (2009)

[2] A. Gruber *et al.*, Nuclear Instruments and Methods in Physics Research A 282, 87 (1989)

[3] M. Kühnel *et al.*, Nuclear Instruments and Methods in Physics Research A 602, 311 (2009)

Detector tests of a Si(Li) Compton polarimeter*

K.-H. Blumenhagen† [1,2,3], *A. Gumberidze* [4,5], *R. Märtin* [1], *M. Schwemlein* [4], *U. Spillmann* [3], *G. Weber* [1], *and Th. Stöhlker* [1,2,3]

[1]HI-Jena, Germany; [2]IOQ, University of Jena, Germany; [3]GSI, Darmstadt, Germany; [4]EMMI, Darmstadt, Germany; [5]FIAS, Frankfurt, Germany

Compton polarimetry is a powerful method to measure the linear polarization of hard x-rays as it has been demonstrated in recent experiments at e.g. the experimental storage ring ESR at GSI. In these experiments double-sided 2D segmented Ge(i) and Si(Li) detectors were applied [1,2,3,4,5,6,7]. In order to perform a comprehensive characterization of such a device – in this case a Si(Li) detector – it has been investigated at a dedicated detector test beam time at the synchrotron PETRA III at DESY. The used photon beam was – after attenuation – impinging directly on the detector. The beam size was limited to 0.01 mm using collimators and its position on the detector could be defined with a $\mu m-$precision by the movable support platform. Several scans over the detector were performed, this report describes the one that investigated effects of the gaps between adjacent detector strips (gap width $\approx\ 50\ \mu m$ at a pitch width of 2 mm). The scanning positions on the detector are indicated by the dashed arrow in figure 1. A closer spacing between positions was chosen near the gaps between x-strips 16/17 and 17/18. The beam energy was 53 keV. The described scan was repeated for the y-strips in a corresponding way. In the following we restrict the discussion to the scan across the x-strips.

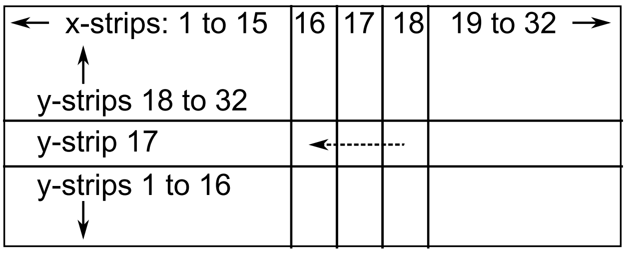

Figure 1: Strip pattern (detail) of the Si(Li) polarimeter. The dashed arrow indicates the scan over the gaps between x-strips.

In Fig. 2 the results of a preliminary analysis are shown. Fig. 2a displays the fraction of single hits, whereas the double hit fraction is shown in Fig. 2b. Note, in order to avoid possible crosstalk contributions, events where two adjacent strips have triggered were rejected. In order to elucidate the role of crosstalk including charge-sharing between neighbouring strips, we depict in Fig. 2c those events, where neighbouring strips showed a valid signal. The origin of the asymmetry of the peaks around the beam positions ± 0.1 cm (gap positions) is not yet understood, one pos-

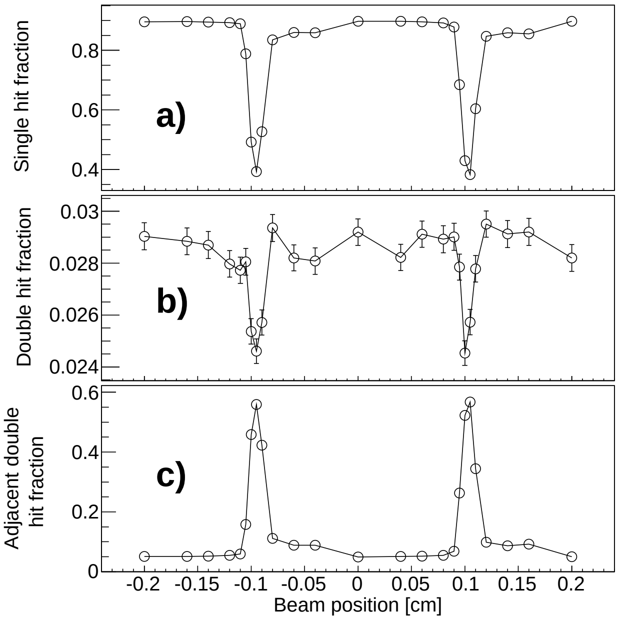

Figure 2: Preliminary results for the x-strips scan: fractions of a) single hits, b) double hits, c) double hits in adjacent strips. Normalization was the number of valid events. Strip centers are at 0 and ± 0.2 cm. Statistical errors are shown, but they are smaller than the point size in a) and c).

sibility is a tilt of the detector with respect to the beam axis. Another observation was, that the proportion of valid events that are single- or double hits does not vary significantly with the beam position (always between ≈97.5 and 98 %). On the other hand the proportion of all recorded events that are valid does vary between ≈98 % at strip centers and ≈94 % at gaps.

References

[1] H. Bräuning et al., AIP Conference Proceedings, 1099, 117 (2009).

[2] G. Weber et al., PRL 105, 243002 (2010).

[3] G. Weber et al., JINST 5, C07010 (2010).

[4] R. Märtin et al., PRL 108, 264801 (2012).

[5] R. Märtin et al., Phys Scr 2013 014070 (2013).

[6] K.-H. Blumenhagen et al. Phys Scr 2013 014102 (2013)

[7] U. Spillmann et al., Phys Scr 2013 014103 (2013)

* Work supported by HDRI, http://www.pni-hdri.de

† k.-h.blumenhagen@gsi.de

Demonstrator: Electronic Readout for a Si(Li) – Compton – Polarimeter

U. Spillmann[1,2], E. Badura[1], K.H. Blumenhagen[2], H. Bräuning[1], J. Hoffmann[1], K. Koch[1], N. Kurz[1], R. Märtin[2], S. Minami[1], W. Ott [1], I. Rusanov[1], Th. Stöhlker[1,2,3], G. Weber[2], M. Weber[4]

[1]GSI, Darmstadt, Germany; [2]HI Jena, Germany; [3]IOQ, Friedrich-Schiller-Universität Jena, Germany, [4]IPE, KIT, Karlsruhe, Germany

Within the portfolio process of the Helmholtz Association Detector Technology and System Platform (DTS) [1] KIT, GSI, and HI Jena collaborate closely bringing together the expertise of the partners in the development of advanced detector readout systems. As one of the first common projects we develop a self-triggering 2-dimensional position-, time-, and energy sensitive Si(Li)-strip detector read out with modern custom designed FPGA-based signal digitizer hardware as a demonstrator system. This project is of great importance for future x-ray spectroscopy and polarimetry experiments of the SPARC collaboration [2] at GSI and FAIR.

As detector platform we have chosen an already existing Si(Li)-strip detector [3] that has worked reliable in several beam times at the ESR as well as external places, e.g. TU Darmstadt and DESY, Hamburg, and has produced excellent results [4]. Up to now it was equipped with standard NIM and VME electronic. The outcome of this project using custom designed FPGA-based signal digitizer hardware will serve as a blue print for the next generation of compact and cost efficient readout electronics of thick planar strip detectors within the collaboration.

The concept is based on the fast digitizing of the preamplifier signals coming from the detector to acquire the small signals directly. The consecutive employment of pulse shape analysis techniques will show the energy and timing information of an event.

For this first demonstrator we profit from recent developments of the Experiment Electronics department of GSI. They provided us with a set of 8 FEBEX2 – ADC boards [5] with 8 input channels each. Sampling the data is performed with a frequency of 65 Ms/s and a resolution of 12 bit at an input range of +/-1V. A 1.6 Gbit fibre link connects the digitizer board with the PLEXOR3-PCIe Interface hosted by a commercial PC that manages the event building and data transport by ethernet. In addition a TRIXOR-PCIe board takes over the trigger handling and the dead time locking. The PC runs a LYNX RT-operating system and as DAQ we employ MBS [6] to take advantage of the GSI data acquisition and storage environment. With this system we studied the electronic response of the strip detector system for offline testing of appropriate pulse shape analysis algorithms.

Meanwhile we moved to the next FEBEX generation (version 3a) which is a 16 channel ADC-board with differential inputs. The FEBEX3a boards are mounted in a crate with PCIe backplane together with a fibre link interface to fit into the existing DAQ environment. The digitizer cards host enough on-board FPGA resources to perform online self-triggering, double hit detection and trapezoidal filters for energy and timing applications.

To adapt the signal output of the preamplifier to the input of the FEBEX3a board the fast linear amplifier SiLiVer was developed. At a later stage the small form factor of the amplifier boards will allow us to mount them inside the preamplifier housing to avoid losses on the signal cables.

The main goal of this first step is to rebuild the functionality of the NIM and VME hardware and to be able to handle photo effect and Compton events. From this point on we can make use out of the system in atomic physics experiments. In collaboration with the KIT we will refine the algorithms for the digital pulse shape analysis with the aim to manage more complex event histories like two or three Compton events for one incident photon. We plan to meet the demand of increased computing power by dedicated hardware solutions designed by KIT.

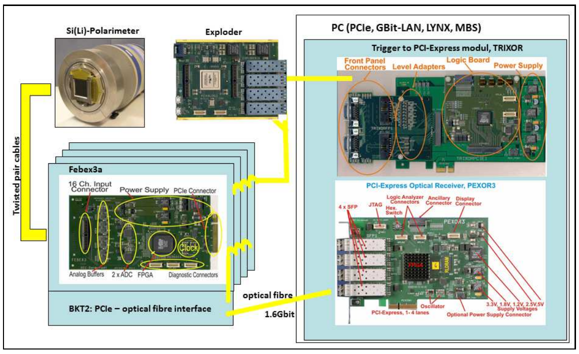

Figure 1: Sketch of the new readout chain of the Si(Li)-Polarimeter Demonstrator

References

[1] http://www.helmholtz-detectors.de

[2] Technical Report of the SPARC collaboration http://www.gsi.de/fair/experiments/sparc/index_e.html

[3] G. Weber et al., “Performance of a position sensitive Si(Li) x-ray detector dedicated to Compton polarimetry of stored and trapped highly-charged ions”, JINST 5,C07010 (2010)

[4] Th. Stöhlker et al., “Polarization and angular correlation studies of X-rays emitted in relativistic ion-atom collisions”, EPJ-ST 169, 5-14 (2009)

[5] https://www.gsi.de/fileadmin/EE/Module/FEBEX/febex2.pdf

[6] http://www-win.gsi.de/daq/

Hard X-ray Compton polarimetry with a two-detector Timepix setup

C. Hahn[*1,2], *G. Weber*[1,3], *S. Höfer*[1,2], *and T. Kämpfer*[1,2]
[1]Helmholtz Institute Jena, Germany; [2]FSU, Jena, Germany; [3]GSI, Darmstadt, Germany

The interaction of high-intensity laser pulses with matter typically leads to the creation of an X-ray-emitting plasma. Various processes occurring in such plasmas exhibit anisotropic features, leading to an anisotropic emission pattern and causing the generated radiation to be polarized. Thus, angular distribution measurements as well as polarimetry of this radiation constitute important techniques to investigate the plasma's anisotropic properties, including, notably, its electron dynamics.

At photon energies below 20 keV, X-ray CCD cameras are an efficient tool, but decreasing quantum efficiency at energies above that threshold renders them impractical for experiments involving hard X-ray radiation, making unsegmented large-volume detectors of high-Z material the equipment of choice in this energy regime. However, in high-flux, low-repetition-rate modes of operation, the latter systems often suffer from photon pile-up or would require unreasonably long acquisition times to obtain single-photon spectra. An attractive alternative to such detectors is provided through the recently developed combination of pixelated CdTe sensors and the Timepix readout chip, offering an energy-resolving detector system which merges the high granularity of X-ray CCDs with the excellent stopping power of high-Z detector materials [1].

As first described in [2], we have constructed a combined Compton spectroscopy/polarimetry setup comprising two CdTe sensors, each having 1 mm thickness and up to 256×256 pixels, positioned to record X-ray radiation which is Compton-scattered at a polar angle of about $90°$ within a low-Z target. The setup grants the possibility to reconstruct the spectrum of the primary, incident radiation, as well as to deduce its degree of linear polarization through Compton polarimetry. This method relies on the spatial asymmetry of the scattered photons' emission direction with respect to the azimuthal scattering angle ϕ, as defined relative to the electric field vector of the incident photons. Assuming that detectors are located at positions corresponding to angles of $\phi = 0°$ and $\phi = 90°$, respectively, the degree of linear polarization P_L is given by the scattered radiation's intensity contrast $M\frac{I_{0°}-I_{90°}}{I_{0°}+I_{90°}}$, where the modulation factor M accounts for the photon energy and various properties of the experimental setup [3].

Using this polarimeter setup, a test experiment was conducted in 2013 at the PETRA III synchrotron facility at DESY. The measured contrast of about 85% is remarkably close to the theoretical value of 90% expected for the specific experimental setup that was used.

In a first attempt to employ the assembly at a laser-generated plasma source, 3 mJ, 60 fs-pulses generated by a Ti:sapphire kHz-repetition rate laser system, operated by IOQ, FSU Jena, were focused on titanium band targets with a focal spot intensity of some $10^{17}\ \mathrm{W/cm^2}$. Unfortunately, the low photon flux at high X-ray energies, caused by the unstable laser-target interaction, severely limited the setup's ability to pick up possible spatial variations of the scattered intensity, compared to the significant background contributed by cosmic radiation and natural radioactivity. It was not until the laser pulses' polarization direction was rotated by $90°$ that an asymmetry could be observed, as illustrated by Figure 1: With both detectors remaining at a fixed position, the switch from p- to s-polarized laser radiation entails a 20% increase in the intensity of detected photons for one detector, while the intensity recorded by the other sensor is reduced by about 7%. This might point to a change in the preferential direction of the high-energy electrons inside the plasma, possibly linked to different heating mechanisms that depend on the laser pulses' polarization. A more detailed evaluation of the experiment is hampered by the small amount of data acquired.

In summary, the presented setup has been successfully tested at PETRA III's polarized X-ray source. Additionally, it has been able to obtain indications of the radiation emitted by the studied laser-generated plasma being – at least partially – linearly polarized.

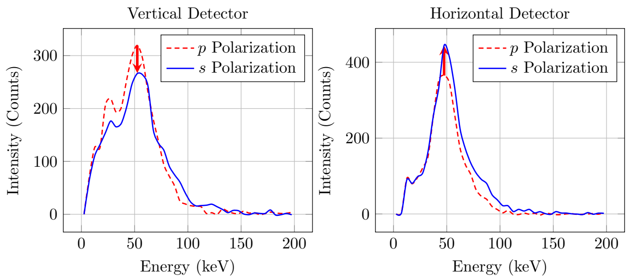

Figure 1: Spectra of X-ray photons, generated by focusing laser pulses of p- and s-polarization, respectively, onto a titanium band target and subsequently scattered within a PMMA cylinder, as recorded by two Timepix sensors covering different azimuthal scattering angles. Switching the laser polarization causes the detected intensity to increase for one detector and decline for the other, indicating a linearly polarized component of the studied X-ray radiation.

References

[1] D. Greiffenberg et al., JINST 6 (2011) C01058
[2] G. Weber et al., GSI Scientific Report 2012 (2013) 323
[3] F. Lei et al., Space Sci. Rev. 82 (1997) 309

* christoph.hahn@uni-jena.de

Cryogenic Micro-Calorimeter Arrays for Future X-Ray Spectroscopy Experiments at FAIR

R. Märtin[1,2], K.-H. Blumenhagen[1,2,3], A. Fleischmann[4], T. Gassner[1,2,3], D. Hengstler[4], C. Pies[4], and Th. Stöhlker[1,2,3]

[1]HI-Jena, Jena, Germany; [2]GSI, Darmstadt, Germany; [3]IOQ, University Jena, Jena, Germany; [4]KIP, University Heidelberg, Heidelberg, Germany

The recent developments of cryogenic magnetic calorimetric detectors offer the ideal tool for the precision study of x-rays arising in various collision processes involving charged particles. This is due to the fact that the micro-calorimeters provide a stopping power and spectral acceptance range comparable to standard solid state x-ray detectors combined with an energy resolution competitive to crystal spectrometers at the same time [1,2]. Therefore such detector systems are likely to become a key instrument for the atomic physics program as it is planned at the FAIR facility which is currently in the construction phase [3].

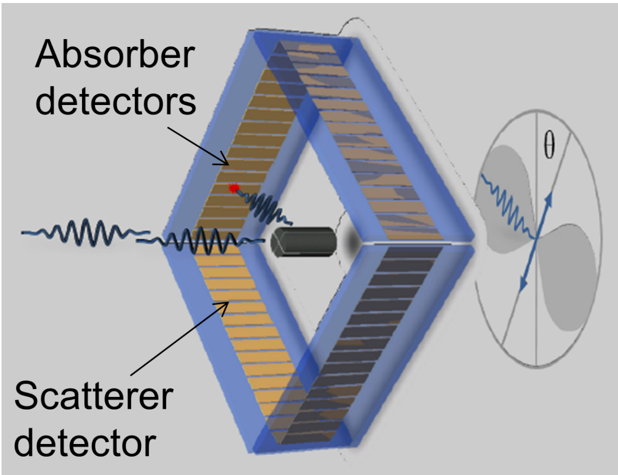

Figure 1: Example for a possible realization of a micro-calorimeter array. Here the detector array serves as a high resolution Compton polarimeter with one active scatterer in the center and surrounded by a ring of absorber pixels.

The maXs (cryogenic micro-calorimeter arrays for high-resolution X-ray spectroscopy) detector design was developed within the SPARC collaboration and its assembly was mostly completed through the delivery of a pulse-tube cooled ^{3}He/^{4}He-dilution refrigerators in 2013. The cryostat serves as a common cryogenic platform for different types of calorimeter arrays adapted to the specific needs of various experiment. The flexible detector array made of gold absorber pixels is one of the great advantages of maXs. Besides the low and high energy prototypes maXs-20 and maXs-200 [4] there are many possible array designs for x-ray spectroscopy applications. One array consists of 64 individual pixelswhich can partly compensate the low solid-angle coverage due to the small single pixel size. The detector array pixels are designed and arranged according to the relevant x-ray energy range and the corresponding energy resolution needed. Currently a combined array maXs-30 with two different kind of pixels is in development. Medium sized pixels with an approx. resolution of 10 eV will serve for efficient x-ray detection up to 30 keV, while pixels comparable to the maXs-20 will offer a resolution better than 2 eV especially for energies below 10 keV. Note that the energy resolution of an individual pixel roughly scales with the square root of its volume. This array is planned to be used for initially feasible experiment at the first stages of FAIR e.g. for the study of Balmer transitions in highly charged one-electron-systems [5] at the CRYRING storage ring [6]. Besides CRYRING, the installation of the S-EBIT on the HITRAP platform at GSI is at an advanced stage [7], consequently we expect that the maXs-detector can be possible used at both facilities soon. However, as a first step test experiments using the micro-calorimeter in a ion storage ring will be performed. For this purpose the 64-pixel array and the new cryogenic platform will be employed in parasitic mode during two different x-ray spectroscopy experiments at the ESR storage ring at GSI in 2014. But the micro-calorimeter can not only be used for x-ray spectroscopy applications but also for x-ray precision Compton polarimetry. Here the so called polar-maXs consists of dedicated active low-Z scatterer and high-Z absorber pixels and can be used in the energy range from 20 to approx. 80 keV (see Fig.1). This novel kind of polarimeter is subject of a recently approved BMBF project for experiments at PETRAIII at DESY.

References

[1] L. Fleischmann et al., IEEEm European Supercond. News Forum 7 (2008).

[2] A. Fleischmann et al., AIP Conf. Proc. 1185, 571 (2009).

[3] Th. Stöhlker et al., AIP Conf. Proc. 1336, 132-7 (2011).

[4] C. Pies et al., AIP Conf. Proc. 1185, 603 (2009).

[5] E. Silver et al., Nucl. Inst. Meth. Phys. Res. A 520, 60-62 (2004).

[6] M. Lestinsky et al., CRYRING@ESR: A study group report (2012).

[7] R. Schuch et al., JINST 5, C12018 (2010).

Particle diagnostics for FAIR based on a Cryogenic Current Comparator*

R. Geithner[1,2]*, J. Vodel*[1]*, W. Vodel*[1]*, R. Neubert*[2]*, and P. Seidel*[2]

[1]Helmholtz-Institut Jena, Germany; [2]Institur fuer Festkoerperphysik, Friedrich-Schiller Universitaet Jena

Monitoring of ion beam intensities in particle accelerators without affecting the beam guiding elements, interrupting the beam current or influencing its profile is a major challenge in accelerator technology. A solution of this issue is the detection of the magnetic field generated by the moving charged particles. In a joint effort of Institute of Solid State Physics at FSU Jena and HI-Jena a non-destructive beam monitoring system for particle beams in accelerators based on the Cryogenic Current Comparator (CCC) principle was recently developed [1].

The CCC consists of a high-performance, low-temperature DC superconducting quantum interference device system, a superconducting toroidal pick-up coil, and an extremely effective meander-shaped superconducting niobium shield. This device allows the measurement of continuous as well as pulsed beam currents in the nA-range. The resolution and the frequency response of the detector strongly depend on the toroidal pick-up coil and its embedded ferromagnetic core [2].

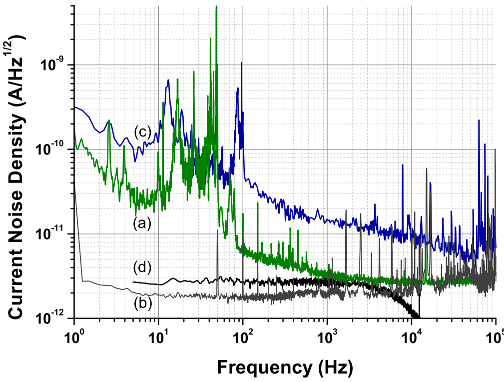

Figure 1: Measured current noise density of the improved FAIR-CCC with Nanoperm M764 core (a) whereas plot (b) represents the intrinsic current noise density of the Supracon SQUID sensor CP2 blue. For comparison the measured current noise density of the DESY-CCC pick-up coil including a Vitrovac 6025F core is shown (c) whereas plot (d) represents the intrinsic current noise density of the SQUID sensor UJ111 from Jena University.

The current noise of the CCC could be decreased by a factor of five compared to previous systems [3] (see figure 1). This results from the usage of iron-based nanocrystalline Nanoperm as core material for the pick-up coil. With this optimized CCC, a noise limited current resolution of 1 nA should be achievable in the disturbed environment of an accelerator [3].

Figure 2 shows the full-bandwidth response of the FAIR-CCC to a rectangular current signal of 1.438 μA (a), 185 nA (b), and 42.5 nA (c) applied to the additional calibrating loop. There is no low pass filter or time-averaging used.

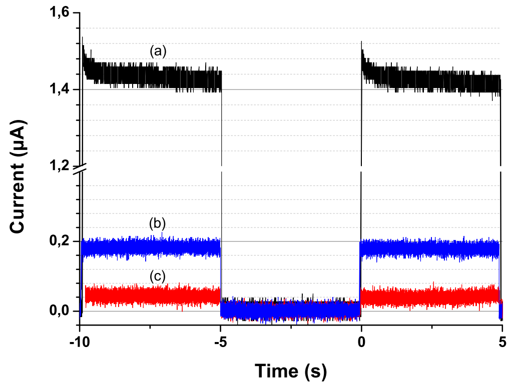

Figure 2: Full-bandwidth response of the FAIR-CCC to a rectangular current signal of 1.438 μA (a), 185 nA (b), and 42.5 nA (c) applied to the additional calibrating loop.

For the international FAIR project at Darmstadt it is foreseen to install several CCC detectors at the high-energy transport beam lines. Here, beam currents in the range between 10^{-4} and 10^{-2} mA are to be expected. In addition the installation of a CCC system at CRYRING is planned for highly accurate absolute current measurements at low beam energies and small particle numbers for ions as well as for antiprotons.

References

[1] Geithner R, Neubert R, Vodel W, Schwickert M, Reeg H, von Hahn R, Seidel P. “A Non-Destructive Beam Monitoring System Based on an LTS-SQUID”. Applied Superconductivity, IEEE Transactions on 2011;21(3):444-447

[2] Geithner R, Heinert D, Neubert R, Vodel W, Seidel P, “Low temperature permeability and current noise of ferromagnetic pickup coils”. Cryogenics; 54:16-19, 2013

[3] Geithner R, Vodel W, Neubert R, Seidel P, Kurian F, Reeg H, Schwickert M. “A Cryogenic Current Comparator for FAIR with Improved Resolution”, Proceedings of International Beam Instrumentation Conference 2013, Oxford, UK, TUPF32, 545, 2013

* Work supported by GSI (LOBI).

Many-electron projectile stripping cross section studies at the ESR gas target*

G. Weber[1,2], *M. O. Herdrich*[2,3], *R. D. DuBois*[4], *P.-M. Hillenbrand*[1,5], *S. Sanjari*[1,7], *D. F. A. Winters*[1], *N. Petridis*[1,6], *and Th. Stöhlker*[1,2,3]

[1]GSI, Darmstadt, Germany; [2]HI-Jena, Germany; [3]IOQ, Univ. Jena, Germany; [4]Missouri S&T, Rolla, MO, USA; [5]IAMP, Univ. Giessen, Germany; [6]IKF, Univ. Frankfurt, Germany; [7]EMMI, Darmstadt, Germany

Charge-changing processes, i. e. loss or capture of electrons, occurring in ion-atom and ion-ion collisions belong to the most basic interactions in all types of plasmas. Moreover, in accelerators interactions between projectile ions and the residual gas can lead to a change of the projectile charge state. In the presence of dispersive ion optical elements, the trajectories of up- or down-charged ions do not match the one of the reference charge state, resulting in a successive defocussing and, as a consequence, loss of beam intensity. Moreover, ions impinging on the beam line walls give rise to several unwanted effects, such as increased radiation levels and significant degraded vacuum conditions due to ion-impact induced desorption. For the FAIR project, in order to reach highest beam intensities, while minimizing the limitations induced by space charge, and avoiding losses in stripper targets, the use of low- to medium-charged, many-electron ions is planned [1]. However, in the relevant energy region from 10 MeV/u up to a few GeV/u the number of bound electrons of these ions is far above that of the corresponding equilibrium charge state, making projectile stripping, sometimes also referred to as electron loss, the dominant beam loss process. Thus, for the planning of future accelerators and ion beam experiments, precise knowledge of the stripping cross sections of many-electron projectiles is necessary. As the theoretical treatment of such many-body atomic physics problems is quite challenging, experimental benchmarks are needed to test the various predictions of different theory models.

Recently, a first electron loss study in the ESR covering beam energies up to 50 MeV/u for U^{28+} ions was presented [2]. We now report on a follow-up experiment using again U^{28+} but also U^{73+} projectiles which was performed under improved experimental conditions at the ESR gas target and covering a broader range of the target atomic number Z. After injecting the ion beams with energies between 30 and 150 MeV/u into the ESR the ions were stored and electron cooling was applied. After a few seconds, when stable beam conditions were reached, the shutter of the internal gas target was opened and a gas jet being perpendicular to the ion beam axis was formed inside the interaction chamber of the ESR. Up- or down-charged ions produced in interactions with the target were subsequently lost due to collisions with the beam line walls or dedicated scrapers after passing the bending magnets. Besides H_2 and N_2 also Ne, Ar, Kr and Xe were used as target gases with densities between a few times 10^9 and a few times 10^{11} particles/cm^3.

The beam lifetime, which is dominated by the electron loss cross section (i. e. projectile ionization), was deduced from measuring the ion beam intensity as a function of time using a DC current transformer (DCCT) and the integrated Schottky signal of the new resonant pickup. Note that both instruments are complementary to each other as the current transformer is limited to ion currents above a few times 10^{-3} mA, whereas the Schottky diagnosis can detect very low beam intensities down to a few ions while at the same time exhibiting non-linearities at beam currents above 0.01 mA. The ability to follow the decay of the ion beam intensity over several orders of magnitude was a significant improvement compared to our previous study at the gas target.

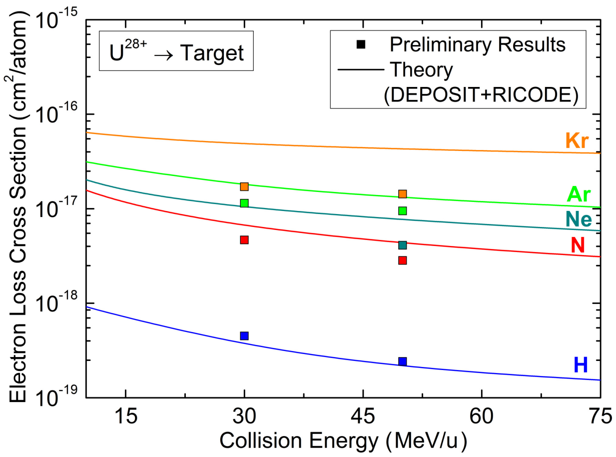

Figure 1: Preliminary: Compilation of the total electron-loss cross section for U^{28+} ions in collisions with various target gases.

A detailed analysis of the obtained data in order to extract the projectile electron loss cross section for different beam energies and various target gases has been performed. Preliminary results are shown in Fig. 1.

References

[1] FAIR - Baseline Technical Report (2006)

[2] V. P. Shevelko et al., *Electron Loss and Capture Processes in Collisions of Heavy Many-Electron Ions with Neutral Atoms*, in: Atomic Processes in Basic and Applied Physics **68**, 125-152, Springer (2012)

[3] G. Weber et al., Phys. Rev. ST AB **12**, 084201 (2009)

* Work supported by the Alliance Program of the Helmholtz Association (HA216/EMMI) and by HIC-for-FAIR through HGS-HIRe and Helmholtz-CAS Joint Research Group HCJRG-108.

The HILITE Penning trap and first tests at the HILITE setup

M. Vogel[1,2], *W. Quint*[2,3], *G. Paulus*[4], *and Th. Stöhlker*[2,4,5]
[1]TU Darmstadt; [2]GSI, Darmstadt; [3]Ruprecht Karls-Universität Heidelberg; [4]Universität Jena; [5]Helmholtz-Institut Jena

We have built a dedicated Penning trap for preparation and control of suitable ion targets for irradiation with high-intensity laser light and study of subsequent reactions, depicted in figure 1. Of particular interest is the detailed investigation of multiphoton-ionisation of confined particles by highly intense laser light. One important aspect is control over the confined particles' mass, charge, density, localization and optimized overlap with the laser light by Penning trap techniques like the use of trap electrodes as 'electrostatic tweezers' and by application of a 'rotating wall', respectively [1]. Also, the non-destructive detection of reaction products is a central property. The Penning trap setup is designed in a portable fashion, such that it can be attached to existing laser systems easily, see figure 2.

The interaction of highly intense radiation with matter and the corresponding non-linear effects have been subject of lively research, both theoretical and experimental, especially in the infrared and visible photon energy regimes. Laser systems capable of producing high intensities also at photon energies in the extreme ultra-violet (EUV) and (soft) X-ray regime open access to novel effects like non-linear Compton effects or simultaneous elastic and inelastic photon scattering, and allow multiphoton-ionisation experiments in a new domain. However, experiments have so far not been able to prepare and investigate well-defined particle ensembles and to non-destructively analyse the reaction products with high accuracy, nor were they able to select or prepare products for further studies in a well-defined way.

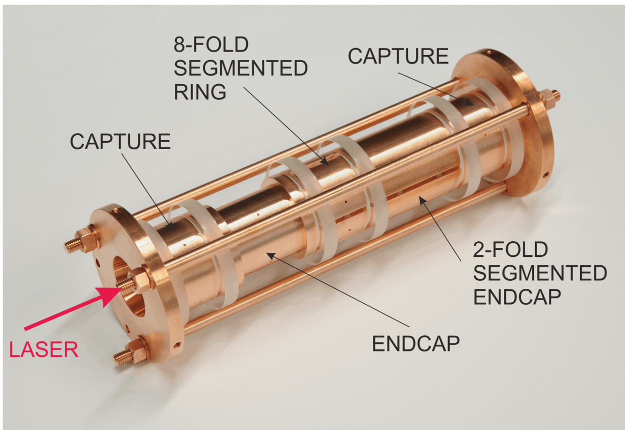

Figure 1: Photography of the HILITE Penning trap. The function of the individual electrodes is indicated, separation between electrodes is achieved by Sapphire rings (milky white).

The particles (atomic or molecular ions) are confined in the Penning trap following in-trap production or capture of externally produced ions. Confined ions can be cooled, compressed, positioned and selected with respect to their mass and charge prior to laser irradiation. The reaction products are analysed by non-destructive methods and hence remain confined for further studies. Such measurements are, for example, able to determine cross sections for multiphoton-ionisation in an energy- and intensity- regime so far not or not sufficiently examined. Additionally, the created electrons may be extracted from the trap and analysed externally. Hence, the reaction energetics may be reconstructed as completely as possible.

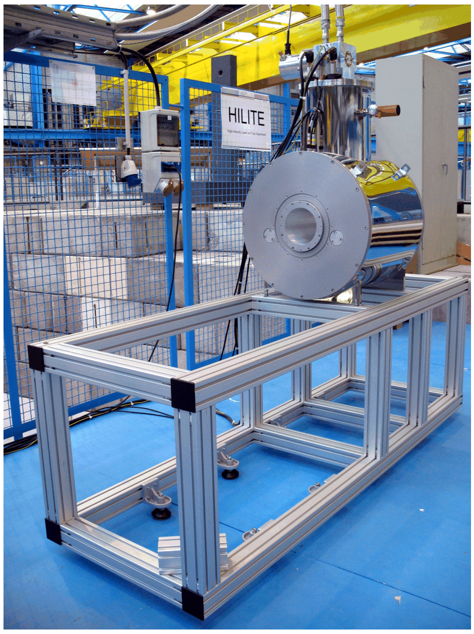

Figure 2: Photography of the HILITE superconducting magnet setup. The Penning trap from figure 1 will be installed in the centre of the magnet bore.

By now, we have completed the vacuum system which will host the Penning trap inside the magnet bore and cool it to cryogenic temperatures using a two-stage cryocooler. The magnet has been operated at fields up to 6 T and the vacuum system has successfully been tested to leak rates below the 10^{-10} mbar l/s scale. We will now focus on the operation and detection electronics as well as on connectivity to an external (EBIT) ion source for highly-charged ions.

References

[1] M. Vogel, W. Quint, Th. Stöhlker and G.G. Paulus, Nucl. Inst. Meth. B **285**, 65 (2012).

The status of the CRYRING@ESR project*

F. Herfurth†1, *M. Lestinsky*1, *R. Bär*1, *A. Bräuning-Demian*1, *S. Litvinov*1, *O. Dolinskii*1, *W. Enders*1, *M. Engström*1, *B. Franzke*1, *O. Gorda*1, *A. Källberg*2, *Y. Litvinov*1, *I. Pschorn*1, *A. Reiter*1, *A. Simonsson*2, *T. Sieber*1, *J. Sjöholm*2, *M. Steck*1, *Th. Stöhlker*1, *G. Vorobjev*1, *and N. Winckler*1

1GSI, Darmstadt, Germany; 2MSL, Stockholm University, Stockholm, Sweden

The low energy storage ring LSR [1] shall provide highly charged ions and antiprotons at low energy for two collaborations at FAIR, SPARC and FLAIR. Those collaborations intend to perform precision experiments pursuing atomic and nuclear physics questions. The LSR is a Swedish in-kind contribution to the FAIR facility in Darmstadt.

The LSR is the swedisch low energy storage ring CRYRING modernized and adapted to the additional needs for injection and ejection of antiprotons and highly charged ions at about 10 MeV per nucleon. CRYRING has been operated at the Manne Siegbahn Laboratory in Stockholm until 2010, was dismantled in 2012 and transported to GSI in the first months of 2013. At GSI it will be installed behind the ESR, as proposed and described in detail in 2012 by a swedish-german working group [2]. This proposal has been accepted end of 2012 by the relevant committees.

CRYRING can decelerate, cool and store heavy, highly charged ions down to a few 100 keV/nucleon. It provides a high performance electron cooler and a straight section for flexible experiment installations as for instance a gas jet target. It is equipped with it's own injector and ion source, to allow for standalone commissioning.

The storage ring accelerates ions with mass to charge ratio below two injected at only 300 keV/nucleon from the off-line ion source to the maximum rigidity of 1.44 Tm. It also decelerates ions injected at the maximal rigidity down to the lower rigidity limit of 0.054 Tm. The magnets are conceived for fast ramping, such that the whole deceleration (acceleration) can be as short as 150 ms.

After dismantling the ring in Stockholm under the supervision and with the help of the Transport and Installations department the components where transported to GSI in spring 2013. Close to twenty lorries arrived over several weeks at GSI.

The concerned specialist departments for power converters, radio frequency supplies, magnets, survey and alignment, control system as well as beam diagnostics and electron cooling, scheduled the required work for getting the ring back into operation. This included detailed tests as well as modifications to meet the GSI and FAIR standards.

A detailed survey has been completed to prepare for the precise alignment of all components in the refurbished cave. The positions of the components have been indicated on the floor to prepare for installation. Dipoles, quadrupoles and sextupoles, have been equipped with measurement points for the foreseen laser tracking alignment and the position of those references have been transferred to the beam axis for each devices.

Beam diagnostic devices like the in ring transformer and the ionization profile monitors have been tested. The ionization profile monitor was set for this under vacuum on the HITRAP experiment installation and tested with an alpha source.

The 3D models of the ring and the two injection lines, from the ESR and the local ion source, are basically completed. The cable planning is ongoing as well as the installation of the required infrastructure like lighting, cooling water and miscellaneous supplies.

Much time, effort and resources went into the preparation of the cave that should house CRYRING@ESR. The former experimental installation, FOPI, has been removed with the help of the FOPI collaboration and the cave has been reconstructed. Fig. 1 shows the recently completed cave. On the roof the area for the power converters has been prepared and the containers for the more fragile electronic equipment were installed.

Figure 1: The completed cave for the installation of CRYRING@ESR. The light spots on the floor indicate the position of the bending dipoles and straight sections. The future beam path is marked with the blue line.

* Work supported by GSI/HI Jena/FAIR@GSI PSP code:1.3.4.2./The SPARC collaboration/Uni Krakov/KVI Groningen

† F.Herfurth@gsi.de

References

[1] H. Danared, et al. (2011) "LSR - Low-energy Storage Ring, Technical design report", Manne-Siegbahn Laboratory, Stockholm University, version 1.3.

[2] M. Lestinsky, et al. (2012) "CRYRING@ESR: A study group report", Project study, GSI, Darmstadt,

SPARC at Storage Rings of FAIR*

Yu. A. Litvinov[†1,2], *Th. Stöhlker*[‡1,3,4], *and the SPARC Collaboration*[5]

[1]GSI Helmholtzzentrum für Schwerionenforschung; [2]Ruprecht-Karls-Universität Heidelberg; [3]Helmholtz Institut Jena; [4]Friedrich-Schiller-Universtät Jena; [5]http://www.gsi.de/sparc

The FAIR project will be realized in stages as determined by the Modularized Start Version (MSV) [1]. Since the New Experimental Storage Ring (NESR), which is the main instrument for SPARC experiments in FAIR [3], is not within the first stage of the MSV, its realization will inevitably be delayed. Therefore, the MSV has triggered substantial efforts to investigate alternatives enabling unique experiments in the realm of atomic physics using stored and cooled ion-beams already within the MSV. Apart from the MSV program at a dedicated fix-target experimental hall, APPA-Cave, and laser-cooling experiments in SIS-100, these plans include the installation of the CRYRING at the presently operating ESR [2] and the realization of an experimental program with relativistic ions beams in the High-Energy Storage Ring (HESR) [4].

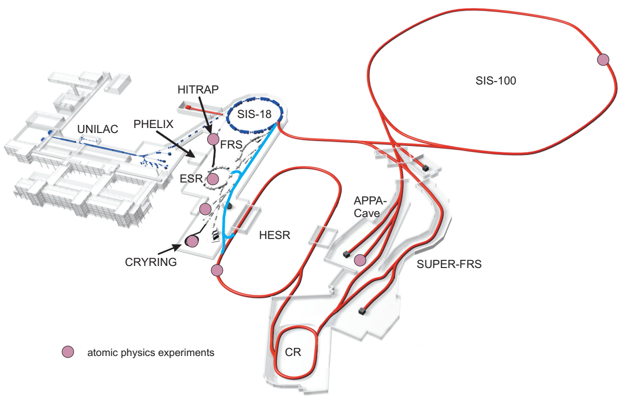

Figure 1: Schematic view of the presently operational accelerator facility at GSI (gray) and the initial phase of the future FAIR facility (red). The main locations of SPARC experiments are indicated, including the HITRAP, which is being commissioned at the ESR, and CRYRING, which is presently under construction. Possible beam lines for transport of protons and ions from SIS-18 directly to the HESR and of antiprotons and ions from HESR to the ESR are shown with light-blue color. These beam lines are currently subject of detailed investigations.

The latter was described in a dedicated feasibility study [5]. Since then the conditions for SPARC experiments were further investigated in a close collaboration with researchers from FZ Jülich. Stochastic and electron cooling of heavy ions has been studied in very detail. It was shown that – by using the available system [6] – stochastic cooling of ion beams will be possible at the injection energy of 740 MeV/u [7] as well as at the highest energies of a few GeV/u [8]. Furthermore, adding an available barrier bucket voltage will allow for a sufficient cooling of the ions also with dense internal targets [9]. The simulation of the full cycle SIS-100 → CR → HESR including bunching, cooling and acceleration has been performed [10]. These studies have shown that the SPARC experiments even with highest target densities can be performed in the HESR without any additional modifications of the HESR stochastic cooling and RF systems.

To facilitate the commissioning of the various machines of the FAIR facility, a direct beam line connecting SIS-18 and HESR could be imagined [11]. This would allow for an easier commissioning of the HESR on the one side. On the other side, since the HESR is capable to efficiently accelerate the stored beams, this would enable the exciting SPARC physics program [12] at a very early stage of FAIR, even before the commissioning of the complex accelerator chain SIS18-SIS100-CR-HESR is completed. A possible location of such a beam line is indicated in Figure 1.

With CRYRING@ESR two fully commissioned storage rings will be available, and, by installing an anti-proton transfer line, the physics program of the FLAIR collaboration could be realized at a very early stage. A possible beam line could connect the HESR with the ESR as, e.g., indicated in Figure 1. In such a case the cooled and slowed-down antiprotons would be extracted from the HESR at 9.5 Tm towards the ESR, where they would further be cooled and slowed-down to about 1.4 Tm, the injection rigidity of the CRYRING, and transferred to CRYRING.

Fruitful collaboration with T. Katayama, E. Mahner, R. Maier, D. Prasuhn, R. Stassen, M. Steck, H. Stockhorst on the SPARC@HESR issues is greatly acknowledged.

References

[1] FAIR Green Paper: The Modularized Start Version (2009).
[2] M. Lestinsky *et al.*: CRYRING@ESR: A Study Group Rep.
[3] R. Schuch *et al.*: SPARC Technical Proposal (2005)
[4] R. Maier *et al*: HESR Technical Design Report (2008)
[5] T. Stöhlker *et al*: SPARC Exp. at HESR: A Feasibility Study
[6] R. Stassen *et al.*, Proc. IPAC2013, Shanghai, China.
[7] H. Stockhorst *et al.*, Proc. IPAC2013, Shanghai, China.
[8] H. Stockhorst *et al.*, Proc. IPAC2012, New Orleans, USA.
[9] T. Katayama *et al.*, Proc. IPAC2013, Shanghai, China.
[10] T. Katajama and H. Stockhorst, in preparation (2014).
[11] T. Stöhlker *et al.*: Hyperfine Interactions, in press (2014).
[12] T. Stöhlker *et al.*: Phys. Scripta T **156**, 014085 (2013).

* Work supported by Helmholtz Institute Jena, and the Helmholtz-CAS Joint Research Group HCJRG-108
† Y. Litvinov@gsi.de
‡ T.Stoehlker@gsi.de

Theory

Two-photon inner-shell decay of heavy atoms *

A. Surzhykov[1], *R. H. Pratt*[2], *and S. Fritzsche*[1,3]

[1]Helmholtz Institute Jena, Germany; [2]University of Pittsburgh, Pennsylvania, USA; [3]University of Jena, Germany

Two-photon transitions in atoms and ions have been investigated intensively during recent decades, mainly in order to better understand the non-linear electron-photon interaction. While most of the earlier attention was payed to neutral hydrogen and low-Z atoms, recent interest was focused also upon heavy atoms and ions, and including a detailed analysis of the two-photon decay of helium-like uranium [1]. For highly-charged ions, in particular, the experimental results are hereby typically in very good agreement with predictions based on Dirac's relativistic equation.

However, less agreement between theory and experiment has been found (so far) for the two-photon decay of the K-shell vacancies of neutral atoms. For K-shell ionized gold atoms, for example, Dunford *et al.* [2] measured the differential decay probabilities for the $2s \to 1s$, $3s \to 1s$, $3d \to 1s$ and, respectively, $(4s + 4d) \to 1s$ two-photon transitions, relative to the total decay rate for a hole in the K-shell. While previous (theoretical) estimates were able to explain the general trends for these decay probabilities, they clearly underestimated the $2s \to 1s$ and $3d \to 1s$ rates and, especially, failed in explaining the *anomalous* resonance structure as observed for the $3s \to 1s$ two-photon line.

To understand (the reasons for) these discrepancies, we have calculated the $2s$, $3s \to 1s$ and $3d \to 1s$ decay probabilities for neutral atoms with nuclear charges $47 \le Z \le 85$ as well as for different geometries in detecting the photons. These computations were based on second-order perturbation theory and Dirac's relativistic equation and made use of the relative differential transition probability

$$P = \frac{1}{W_K} \frac{d^3 w}{d\omega_1 \, d\Omega_1 \, d\Omega_2}$$

in order to compare the theoretical preditions with experiment. In this expression, $\frac{d^3 w}{d\omega_1 \, d\Omega_1 \, d\Omega_2}$ refers to the two-photon transition rate under investigation and W_K to the total decay rate for a K-shell hole, including the radiative and Auger channels. For medium and high-Z elements, the Auger contributions to the decay rate is usually suppressed and can hence be estimated in a simple manner.

Using perturbation theory, we especially explored the two-photon decay of K-shell vacancies in heavy atoms and evaluated the (many-electron) transition amplitude within the independent particle approximation. These results can be compared directly with recent data from experiment without any further assumptions about the scaling of these rates. For example, Figure 1 displays the results from our IPA calculations (squares connected by solid line) for the $2s \to 1s$ (top panel) and $3s \to 1s$ (bottom panel), together with experimental data by Dunford *et al.* [2] and other measurements, cf. Ref. [3] for further details.

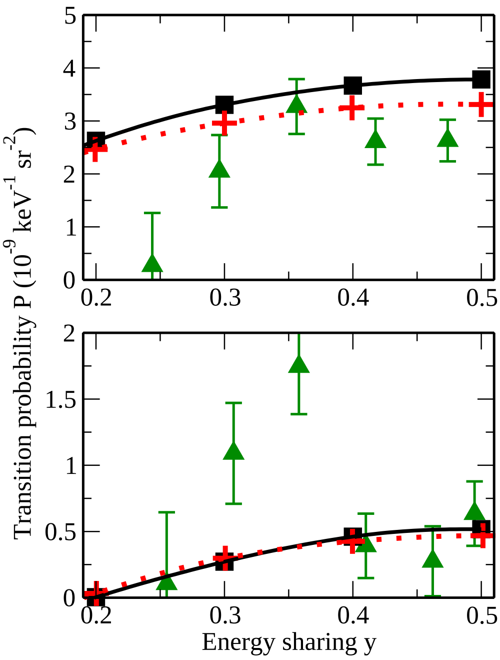

Figure 1: Relative differential probability P at opening angle $\theta = 90^\circ$ for the $2s \to 1s$ (top panel) and $3s \to 1s$ (bottom panel) transitions in gold as function of the energy sharing y. For details, see text and Ref. [3].

Reasonable to good agreement between our theoretical results and the experimental findings was found for the $3d \to 1s$ and $(4s + 4d) \to 1s$ two-photon transitions and for a wide range of the energy sharing. For the $3s \to 1s$ decay, the theoretical and experimental probabilities also agree for most energy sharings apart from the region $0.3 \le y \le 0.38$. The resonance-like structure, reported by Dunford and coworkers [2] for such an energy sharing, could not be confirmed by our computations, cf. Fig. 1. Therefore, the discrepancy between the measured and theoretical values of the $2s \to 1s$ two-photon decay and for $3s \to 1s$ within the 'resonance' region remains at present an open question.

References

[1] S. Trotsenko *et al.*, *Phys. Rev. Lett.* **104**, 033001 (2010).

[2] R. W. Dunford, *Phys. Rev.* **A74**, 012504 (2006).

[3] A. Surzhykov, R. H. Pratt and S. Fritzsche, *Phys. Rev.* **A88**, 042512 (2013).

* Work supported by Helmholtz Institute Jena and the Helmholtz Association under the project VH-NG-421.

Hyperfine-induced effects on the anisotropy of the $K\alpha_1$ x-ray emission *

Z. W. Wu† [1], *A. Surzhykov* [1], *and S. Fritzsche* [1,2]

[1]Helmholtz Institute Jena, Germany; [2]University of Jena, Germany

During the last decades, the angular distribution of the characteristic x-ray emission of highly-charged ions has been investigated extensively. When compared to the total decay rates of these ions, their angular distributions are often found more sensitive with regard to subtle effects in the electron-photon interaction. At the GSI storage ring, therefore, detailed measurements have been performed on the x-ray emission of such ions. While, for example, the observed Ly-α_1 radiation following the radiative electron capture (REC) into the $2p_{3/2}$ state of H-like ions exhibits a quite strong anisotropic angular pattern, an almost isotropic $K\alpha_1$ emission was found for the decay of the excited He-like $1s2p_{3/2}\ ^{1,3}P_{1,2}$ levels. Such a qualitative difference can be understood as the mutual cancelation of the two $1s2p_{3/2}\ ^1P_1 \to 1s_2\ ^1S_0$ and $1s2p_{3/2}\ ^3P_2 \to 1s_2\ ^1S_0$ fine-structure components of the $K\alpha_1$ x-ray emission which have an opposite angular emission behavior.

Until now, however, most studies on the x-ray emission have been made on ions with zero nuclear spin, $I = 0$. Little attention was paid so far to isotopes with $I \neq 0$. In a recent work [1], we have investigated the $K\alpha_1$ emission following the REC into the $1s2p_{3/2}\ ^{1,3}P_{1,2}$ levels of He-like ions with *nonzero* nuclear spin. Emphasis is placed on the question of how the hyperfine interaction affects the anisotropy of the $K\alpha_1$ radiation.

The anisotropy of the $K\alpha_1$ emission can be easily described by means of a (anisotropy) parameter β_2^{eff}, and which can be obtained by taking the average over the corresponding hyperfine- and fine-structure components. For isotopes with $I = 1/2$, for example, this parameter can be expressed as

$$\begin{aligned}\beta_2^{\text{eff}}(I=1/2) &= \frac{1}{3\sqrt{2}} N_1 \mathcal{A}_2(^1P_1) \\ &+ \frac{2}{5}\sqrt{\frac{7}{5}} N_2\, \mathcal{A}_2(^3P_2) \left(\frac{\sqrt{6}}{2} \frac{a_{E1}}{a_{M2}} - \frac{\sqrt{2}}{4} - \frac{3\sqrt{2}}{7} \right), \quad (1)\end{aligned}$$

where N_i is the statistical weight and $\mathcal{A}_2$ the alignment parameter of a given fine-structure level. Moreover, the a_{pL} here denote the reduced amplitudes for the leading M2 and hyperfine-induced E1 channels of the $1s2p_{3/2}\ ^3P_2$, $F_i = 3/2 \to 1s^2\ ^1S_0$, $F_f = 1/2$ hyperfine-resolved transition, and which depends on the nuclear magnetic moment μ_I of the isotopes. For $I = 0$, this parameter simplifies to

$$\beta_2^{\text{eff}}(I=0) = \frac{1}{\sqrt{2}} N_1 \mathcal{A}_2(^1P_1) - \sqrt{\frac{5}{14}} N_2 \mathcal{A}_2(^3P_2)\,. \quad (2)$$

We can use Eqs. (1) and (2) in order to analyze the anisotropy of the overall $K\alpha_1$ emission and to understand the changes in the overall observed $K\alpha_1$ angular emission of ions with non-zero spins owing to the hyperfine interaction. For example, Fig. 1 displays the effective anisotropy parameter β_2^{eff} of the $K\alpha_1$ radiation following the REC into initially H-like projectiles with energy T_p = 50 MeV/u, as functions of μ_I for selected spin-1/2 tin, xenon and thallium isotopes as well as their zero-spin counterparts. While, as seen from this figure, the anisotropy $\beta_2^{\text{eff}}(I=0)$ is nearly the same for all mid- and high-Z elements, the parameters $\beta_2^{\text{eff}}(I=1/2)$ decrease roughly linear with μ_I of the isotopes. For the isotope $^{119}_{50}\text{Sn}^{48+}$, for example, the β_2^{eff} increases from 0.04 to 0.104, when compared to its zero-spin counterpart. Such a change in the β_2^{eff} can be easily detected by using present-day detectors [2].

From this theoretical analysis, we therefore conclude that accurate measurements of the $K\alpha_1$ angular emission at ion storage rings may help determining the nuclear parameters of rare stable or radioactive isotopes with $I \neq 0$ in the future.

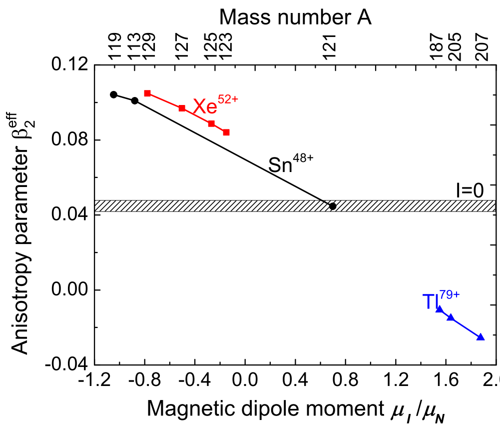

Figure 1: Effective anisotropy parameter β_2^{eff} of the $K\alpha_1$ emission as functions of the magnetic dipole moment μ_I following REC into $1s2p_{3/2}\ ^{1,3}P_{1,2}$ levels of initially H-like projectiles with energy T_p = 50 MeV/u. Results are shown for selected spin-1/2 isotopes as well as their zero-spin counterparts (shadowed area).

References

[1] Z. W. Wu *et al.*, Phys. Rev. A, submitted (2014).

[2] G. Weber *et al.*, Phys. Rev. Lett. **105**, 243002 (2010).

* Work supported by Helmholtz Institute Jena and the Helmholtz Association under the project VH-NG-421.

† wuzhongwen05@126.com

Inelastic Raman scattering of light by highly charged heavy ions *

Th. Jahrsetz† [1,2], *S. Fritzsche*[2,3], *and A. Surzhykov* [2]

[1]Physikalisches Institut, Ruprecht-Karls-Universität Heidelberg, Germany; [2]Helmholtz-Institut Jena, Germany;
[3]Theoretisch-Physikalisches Institut, Friedrich-Schiller-Universität Jena, Germany

The scattering of photons on atoms, ions, or molecules may lead to an excitation of the target. In atomic physics, most of the studies of this so called Raman scattering were focused on low-Z systems such as neutral hydrogen [1, 2]. Owing to the recent advances in electron beam ion traps (EBITs), brilliant x-ray sources, and x-ray detector technology, novel possibilities arise to investigate inelastic photon scattering by heavy highly-charged ions. Such experiments would allow a detailed analysis of relativistic, higher multipole, and even QED effects in the high-Z regime. To support these future studies we examined the total and differential cross section of Raman scattering by H-like ions.

A theoretical analysis of the light scattering by atomic or ionic targets is usually performed within the framework of second-order perturbation theory. In this theory, all properties of the photon can be traced back to the matrix element:

$$M_{fi} = \sum_{\nu} \frac{\left\langle f \left| \hat{R}_2^{\dagger}(\mathbf{k_2}, \epsilon_\mathbf{2}) \right| \nu \right\rangle \left\langle \nu \left| \hat{R}_1(\mathbf{k_1}, \epsilon_\mathbf{1}) \right| i \right\rangle}{E_i + \omega_1 - E_\nu} + \frac{\left\langle f \left| \hat{R}_1(\mathbf{k_1}, \epsilon_\mathbf{1}) \right| \nu \right\rangle \left\langle \nu \left| \hat{R}_2^{\dagger}(\mathbf{k_2}, \epsilon_\mathbf{2}) \right| i \right\rangle}{E_i - \omega_2 - E_\nu}, \quad (1)$$

which describes the transition between an initial state $|i\rangle \equiv |n_i j_i \mu_i\rangle$ and a final state $|f\rangle \equiv |n_f j_f \mu_f\rangle$ under the absorption of a photon $|\omega_1, \epsilon_\mathbf{1}\rangle$ with energy ω_1 and polarization $\epsilon_\mathbf{1}$, and emission of the photon $|\omega_2, \epsilon_\mathbf{2}\rangle$. In order to calculate the matrix element (1) one has to perform a summation over the complete spectrum $|\nu\rangle \equiv |n_\nu j_\nu \mu_\nu\rangle$ of the ion. In the present work, this summation is carried out with the help of the Green's function approach [3].

By making use of the transition matrix amplitude (1), we studied the angle-differential:

$$\frac{d\sigma}{d\Omega} = \frac{1}{2(2j_i+1)} \frac{\omega_2}{\omega_1} \sum_{\epsilon_1, \epsilon_2} \sum_{\mu_i, \mu_f} |M_{fi}|^2, \quad (2)$$

and the total, $\sigma = \int \frac{d\sigma}{d\Omega} d\Omega$, cross sections for the inelastic scattering of initially unpolarized light. In Fig. 1 these cross sections are shown for the process $\gamma + U^{91+}(1s_{1/2}) \to \gamma' + U^{91+}(2s_{1/2})$. Calculations have been performed for incident photon energies ranging from $0.7 \cdot E_{ion}$ to $0.97 \cdot E_{ion}$ where E_{ion} refers to the $1s_{1/2}$ ionization threshold. As seen from the top panel of the figure, the total cross section is very sensitive to the photon energy and exhibits a clear resonant behavior. The resonances arise at energies that correspond to single photon excitation of the $np_{1/2}$, $np_{3/2}$ or $nd_{5/2}$ intermediate states. In the resonant region, moreover, one may observe a drastic change of the angular distribution of scattered photons. While, as seen from the bottom panels of Fig. 1, the photons with incident energy below the $3p_{1/2}$ resonance are scattered predominantly in the forward and backward directions, the Raman scattering prefers the perpendicular direction, $\theta \approx 90°$, for $\hbar\omega_1 \tilde{>} E_{3p_{1/2}} - E_{1s_{1/2}}$. Such an effect is caused by interference between the transition amplitude contributions from the $3p_{1/2}$ and the $3p_{3/2}$ intermediate states and can be observed with the help of available x-ray detectors.

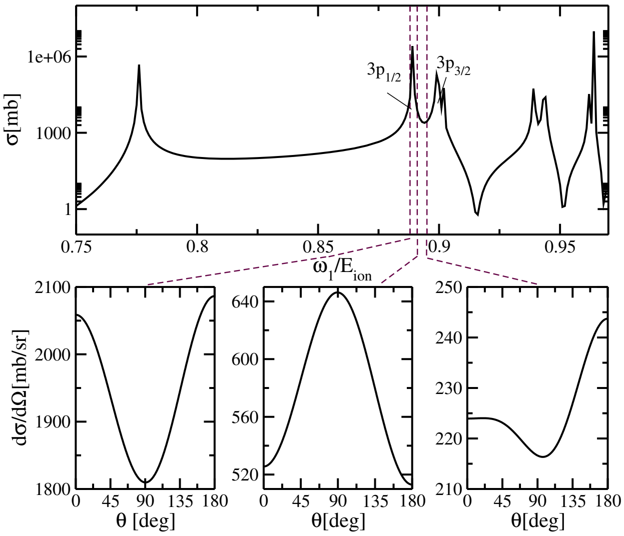

Figure 1: Top panel: Total cross section of the $\gamma + U^{91+}(1s_{1/2}) \to \gamma' + U^{91+}(2s_{1/2})$ Raman scattering as a function of incident photon energy in units of the ionization energy. Bottom panels: Angular-differential cross section for incident photon energies around the $3p_{1/2}$ and $3p_{3/2}$ resonances as a function of scattering angle θ.

References

[1] B.A. Zon et al., Sov. Phys. JETP **28**, 480-482 (1969)

[2] H. Sadeghpour et al, J. Phys. B: At. Mol. Opt. Phys. **25**, 4801 (1992)

[3] A. Surzhykov et al., Phys. Rev. A **71**, 022509 (2005)

* Work supported by the Helmholtz Gemeinschaft (Nachwuchsgruppe VH-NG-421) and the BMBF (Contract No. 05K13VHA)

† jahrsetz@physi.uni-heidelberg.de

Polarization transfer in elastic Rayleigh scattering *

A. Surzhykov[†1], *V. A. Yerokhin*[2], *Th. Jahrsetz*[1,3], *Th. Stöhlker*[1,4,5], *and S. Fritzsche*[1,4]

[1]Helmholtz Institute Jena, Germany; [2]St. Petersburg State Polytechnical University, Russia; [3]University of Heidelberg, Germany; [4]University of Jena, Germany; [5]GSI Helmholtzzentrum, Darmstadt, Germany

Studies on the elastic Rayleigh scattering of photons by bound atomic (or ionic) electrons have a long tradition. Since the mid 1930's, a large number of experimental and theoretical works have dealt with the total as well angle–differential Rayleigh cross sections [1]. More recent investigations were focused, moreover, on the linear polarization of the scattered photons. Of particular interest here is the question of how this polarization is affected if the incident light is itself (linearly) polarized. Owing to recent advances in coherent light sources and efficient detection techniques, a new generation of experiments has currently become feasible, in which such a "polarization transfer" can be explored for heavy atomic targets and the radiation in the x–ray region. Polarization analysis of the Rayleigh scattering in the high–Z—and—high–energy domain may serve as a valuable tool for exploring this second–order quantum electrodynamical (QED) process in very strong electromagnetic fields.

In order to analyze the current and future experiments on the polarization transfer in elastic Rayleigh scattering of x–rays by heavy targets, detailed theoretical study has been performed by us based on the second–order perturbation theory and Dirac relativistic equation [2]. The practical application of such a perturbative approach requires the knowledge about the *complete* Dirac spectrum of an atom (or ion), including not only bound– but also positive and negative energy continuum–states. In our study, this spectrum was represented by means of the Coulomb Green's function:

$$G_E(\boldsymbol{r}, \boldsymbol{r}') = \sum\!\!\!\!\!\!\int_{\nu} \frac{\psi_\nu^\dagger(\boldsymbol{r})\, \psi_\nu(\boldsymbol{r}')}{E_\nu - E}\,, \tag{1}$$

constructed from the eigensolutions $\psi_\nu(\boldsymbol{r}) \equiv \psi_{n_\nu j_\nu,\mu_\nu}(\boldsymbol{r})$ of the Dirac Hamiltonian. By using the analytical representation of $G_E(\boldsymbol{r}, \boldsymbol{r}')$ in terms of the regular and irregular Whittaker functions [3] we were able to perform an accurate perturbative calculations of the angular as well as polarization properties of scattered Rayleigh photons.

With the help of the relativistic Green's function approach we investigated, in particular, the elastic scattering of completely linearly polarized x–rays on hydrogen–like ions in their ground state. For example, Fig. 1 displays the angular distribution (left panel) and the degree of linear polarization (right panel) of scattered photons for the case of xenon Xe^{53+} target and three different energies $\hbar\omega$ of the incident light. As seen from the figure, both (angular and polarization) properties appear to be very sensitive to the photon energy. In particular, if $\hbar\omega \cong 45$ keV, which is just 10 % above the $1s$ ionization threshold, the Rayleigh photons are strongly polarized over the entire angular range, except for $\theta \approx 80$–$100°$, and their emission pattern is almost dipole–like, $W(\theta) \sim \cos^2\theta$. In contrast, the increase of the energy leads to (i) a strongly enhanced forward emission and to (ii) a significant *reduction* of the polarization of outgoing radiation. This reduction is largest for the backward scattering but may also reach 20–30 % for the emission angles in the range $30° \lesssim \theta \lesssim 60°$, where the photon yield is high. Based on our theoretical analysis, we argue that such a "depolarization" of light in the course of elastic scattering is caused mainly by the higher, non–dipole components of the electromagnetic field. The measurements of the depolarization effects, which is feasible today with the help of available solid–state detectors, can reveal, therefore, useful information about the details of photon–matter interactions in the extreme relativistic regime; the topic which attracts currently much attention both in intense–laser and heavy–ion physics.

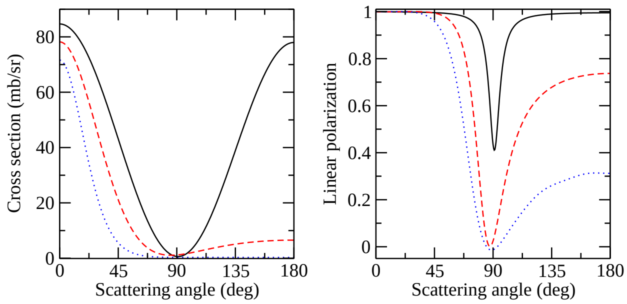

Figure 1: The angle–differential cross section (left panel) and the degree of linear polarization (right panel) of elastically scattered x–rays on hydrogen–like xenon Xe^{53+} ions in their ground state. Relativistic calculations were performed for the completely linearly polarized incident light with energies $\hbar\omega$ = 1.1 I_{1s} (solid line), 5 I_{1s} (dashed line) and 10 I_{1s}, where $I_{1s} \cong 41$ keV refers to the $1s$ ionization threshold. Data from Ref. [2].

References

[1] R. Pratt, Rad. Phys. Chem. **74**, 411 (2005).

[2] A. Surzhykov *et al.*, Phys. Rev. A **88**, 062515 (2013).

[3] P. Koval and S. Fritzsche, Comp. Phys. Commun. **152**, 191 (2003).

* Work supported by Helmholtz Association under the project VH–NG–421 and by the BMBF under the project No. 05K13VHA.

† a.surzhykov@gsi.de

Compton scattering of X-ray photons assisted by a strong laser pulse

D. Seipt[1,2] *and B. Kämpfer*[2,3]

[1]Helmholtz-Institut Jena, Fröbelstieg 3, 07743 Jena, Germany; [2]Helmholtz-Zentrum Dresden-Rossendorf, P.O. Box 510119, 01314 Dresden, Germany; [3]TU Dresden, Institut für Theoretische Physik, 01062 Dresden, Germany

Compton scattering, i.e. the scattering of X-rays off free electrons $X + e \to X' + e'$ is one of the fundamental interaction processes of photons with charged particles. If the scattering happens in the the presence of an additional strong laser pulse (L) both the spectral distribution and the polarization properties of the radiation are modified. In the strong laser pulse the electron moves on a figure-8 trajectory and laser assisted Compton scattering can be related to the scattering of X-ray photons off accelerated particles.

Such experiments could be realized at the planned Helmholtz international beamline for extreme fields (HIBEF) [1] at the European XFEL, where a PW class Ti:Sapphire laser is to be installed at one of the XFEL endstations. We have studied theoretically the laser assisted Compton process $X + L + e \to X' + e'$ [2]. The calculations were performed within the framework of strong field QED employing Volkov states to describe the electrons in the strong laser field and X-ray field fully taking into account the finite pulse length of both the laser and X-ray pulses.

Depending on the number ℓ of involved laser photons the frequency ω' of the scattered photon reads

$$\omega'(\ell, \vartheta) = \frac{\omega_X + \ell\omega_L}{1 + \frac{\omega_X + \ell\omega_L}{m}(1 - \cos\vartheta)}\,, \qquad (1)$$

with the scattering angle ϑ. Values of $\ell \neq 0$ refer to sidebands in the spectral distribution in the vicinity of the main Klein-Nishina line ($\ell = 0$).

A stationary phase analysis of the scattering amplitude reveals that spectral distribution forms a plateau for $\ell_- \leq \ell \leq \ell_+$ with $\ell_\pm \sim \varkappa a_L$ being the relevant multi-photon parameter. Thus, multi-photon effects are strongly enhanced by a large frequency ratio $\varkappa = \omega_X/\omega_L \sim 3000$. Even for moderately strong laser fields with $a_L = 0.3$ ($a_L = 0.68\sqrt{I_L[10^{18}\mathrm{W/cm^2}]}$) up to 1000 laser photons are participating in a single scattering event and the width of the plateau of side-bands can reach several keV, see Fig. 1 (upper panel). This is in contrast to non-linear Compton scattering where the multi-photon parameter is a_L itself.

The polarization of the photon X' is rotated as compared to Compton scattering without the laser. This rotation can be quantified experimentally by measuring the Stokes parameter

$$P_2 = \frac{I_{45^\circ} - I_{135^\circ}}{I_{45^\circ} + I_{135^\circ}}\,. \qquad (2)$$

In Fig. 1 (lower panel) the Stokes parameter P_2 is exhibited as a function of ω'. The value of P_2 is zero at the KN line and increases with increasing distance from it, i.e., in the region where more laser photons are involved. The maximum value of $P_2 \approx 0.15$ corresponds to a rotation angle of 5° towards the scattering plane (note that $P_1 \approx -1$).

The modification of the spectral distribution and the polarization properties of the scattered photons reported here and in [2] are a new way to observe $\mathcal{O}(1000)$ multi-photon effects experimentally with moderately strong laser fields.

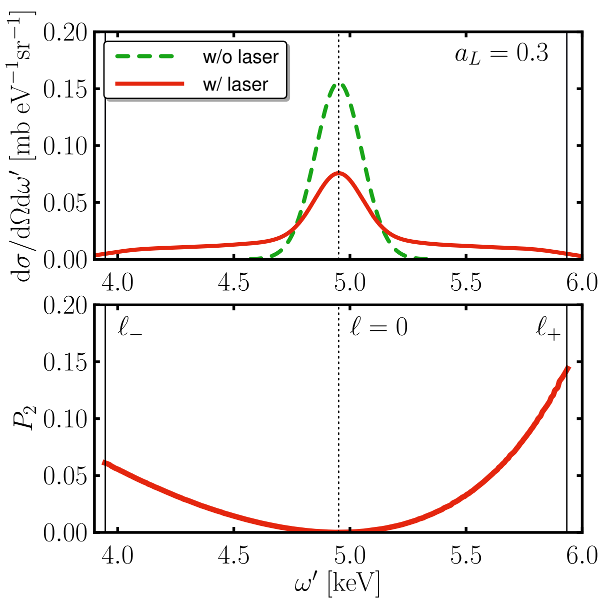

Figure 1: Upper panel: The frequency spectrum of laser assisted Compton scattering for 90° scattering (red curve) shows a prominent plateau of side-bands in the vicinity of the main Klein-Nishina line ($\ell = 0$) with a total width of 2 keV. The main line is reduced in intensity as compared to the laser free Compton scattering (green dashed curve). The spectra have been averaged with a resolution of 100 eV. Lower panel: Rotation of the polarization of the scattered photon, quantified via the Stokes parameter P_2 as a function of ω' for 90° scattering. Without the laser pulse $P_2 \equiv 0$. The photon energies are $\omega_L = 1.55$ eV and $\omega_X = 5$ keV; the FWHM pulse lengths are $T_L = 20$ fs and $T_X = 50$ fs.

References

[1] "The HIBEF project", www.hzdr.de/hgfbeamline/.

[2] D. Seipt and B. Kämpfer, "Laser assisted Compton scattering of X-ray photons", (2013), arXiv:1309.2092; Phys. Rev. A., in print.

Photon polarization tensor in a homogeneous magnetic or electric field

F. Karbstein[1,2]

[1]Helmholtz-Institut Jena, Fröbelstieg 3, D-07743 Jena, Germany; [2]Theoretisch-Physikalisches Institut, FSU Jena, Max-Wien-Platz 1, D-07743 Jena, Germany

We study the photon polarization tensor in a homogeneous external magnetic or electric field. Our focus is on explicit analytical insights for both on- and off-the-light-cone dynamics in a wide range of well-specified physical parameter regimes, ranging from the perturbative to the manifestly nonperturbative strong field regime. The basic ideas underlying well-established approximations to the photon polarization tensor are carefully examined and critically reviewed. We point out the limitations of such approximations and manage to go beyond at several instances.

The photon polarization tensor is a central object in quantum electrodynamics (QED). It contains essential information about the renormalization properties of QED and, accounting for the vacuum fluctuations of the underlying theory, it encodes quantum corrections to Coulomb's force law. In the presence of an external electromagnetic field, the photon polarization tensor acquires a dependence on the external field, which couples to the quantum fluctuations involving charged particles (cf. Fig. 1). Correspondingly, it gives rise to a variety of dispersive (associated with its real part) and absorptive (associated with its imaginary part) effects affecting photon propagation in electromagnetic fields.

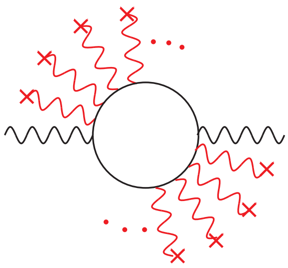

Figure 1: One-loop photon polarization tensor in the presence of an external electromagnetic field indicated by the red wiggly lines ending at crosses.

As long as the external field is homogeneous, translational invariance implies that the polarization tensor in momentum space depends only on the transferred four-momentum and the respective field vectors [1]. In the case of a pure magnetic or electric field, the photon polarization tensor in momentum space can then be decomposed into three independent tensor structures, that can be associated with three distinct polarization modes, and the corresponding scalar functions. Thus, the vacuum subject to an external field exhibits medium-like properties. The difference in the momentum dependence of these modes gives rise to striking observable consequences, such as vacuum birefringence and dichroism.

Even for pure and homogeneous fields, the associated scalar functions at one-loop accuracy are highly non-trivial. In case of a pure magnetic field the entire field dependence of the scalar functions is via trigonometric functions. Analogously, for a pure electric field the dependence is via the corresponding hyperbolic functions. Both situations are related by an electric-magnetic duality allowing for their uniform treatment [2].

While the generic analytic properties of the photon polarization tensor in a magnetic field and its different representations: propertime, dispersion-sum, and Landau or spectral sum representation, have been studied in great detail in the literature, handy analytical expressions and controlled approximations that hold within certain, well-constrained parameter regimes are still very rare – even more so beyond on-the-light-cone dynamics.

Triggered by the seminal works of Tsai and Erber [3] in the 1970s, ongoing efforts have sought to find adequate approximations for the photon polarization tensor in the presence of an external magnetic or electric field (e.g., [4]) in various limits. However, their derivation in general involves constraints to a certain momentum regime and most of these approximations are tailored to on-the-light-cone dynamics. While there are some motivations and indications concerning their regimes of applicability, so far more systematic studies of their regimes of validity – particularly beyond on-the-light-cone dynamics – have not been performed. In [2] we managed to go beyond. Our focus was threefold: to thoroughly investigate the regimes of validity of established approximations, to generalize them beyond on-the-light-cone dynamics, and to obtain new analytical results, particularly into the nonperturbative regime.

Besides providing for reliable analytical results into various physical parameter regimes for homogeneous electric and magnetic fields, our study is also relevant beyond the constant field limit, namely for inhomogeneous field configurations that may locally be approximated by a constant As in QED the relevant reference length scale is the Compton wavelength of the electron, $\lambda_c \approx 3.9 \cdot 10^{-13}$m, this holds for a vast range of field configurations attainable in the laboratory.

References

[1] I. A. Batalin and A. E. Shabad, Sov. Phys. JETP **33**, 483 (1971).

[2] F. Karbstein, Phys. Rev. D **88**, 085033 (2013).

[3] W. y. Tsai and T. Erber, Phys. Rev. D **10**, 492 (1974) and Phys. Rev. D **12**, 1132 (1975).

[4] V. N. Baier and V. M. Katkov, Phys. Rev. D **75**, 073009 (2007) and Phys. Lett. A **374**, 2201 (2010).

Quantum Reflection as a New Signature of Quantum Vacuum Nonlinearity

Holger Gies[1,2], *Felix Karbstein*[1,2], *and Nico Seegert*[1,2]

[1]Helmholtz Institut Jena, Fröbelstieg 3, D-07743 Jena, Germany; [2]Theoretisch-Physikalisches Institut, FSU Jena, Max-Wien-Platz 1, D-07743 Jena, Germany

We show that photons subject to a spatially inhomogeneous electromagnetic field can experience quantum reflection. Based on this observation, we propose quantum reflection as a novel means to probe the nonlinearity of the quantum vacuum in the presence of strong electromagnetic fields.

The commonly accepted theory of the interaction of light and matter, quantum electrodynamics (QED), predicts the vacuum to be permeated by virtual photons as well as particle-antiparticle fluctuations. As these fluctuations can couple to real electromagnetic fields, they have the potential to affect the propagation and interactions of real fields and particles [1]. Currently, a number of experiments and proposals aim at probing different signatures of the QED vacuum such as vacuum magnetic birefringence, photon splitting and light-by-light scattering. The observables depend on the intensities involved and are proportional to at least $(I/I_{\rm cr})^2$, where $I_{\rm cr} \approx 5 \times 10^{29}\,{\rm W/cm^2}$. However, the presently rapid development of high-intensity laser facilities with intensities exceeding $10^{22}\,{\rm W/cm^2}$ offers promising future possibilities to, for the first time, verify *directly* the nonlinear nature of the pure QED vacuum.

In a first study [2], we have aimed at introducing quantum reflection as a new optical signature of the quantum vacuum nonlinearity. The envisaged setup requires the crossing of two high-intensity lasers: An intense background laser ('pump') creates a strong electromagnetic field in its focal spot which modifies the QED vacuum to act as an effective, attractive potential for traversing probe photons. Due to the spatial inhomogeneity of the background field, a fraction of the probe photons will be reflected and can be registered by a suitably placed detector. The inherent physical separation of photons carrying the signature (reflected) from photons unaffected by the modified vacuum (transmitted) yields a highly sensitive setup and should prove to be of a major advantage compared to standard experiments dealing with photon propagation.

We have specialized to the case of a time independent, one-dimensional inhomogeneity $\vec{B}(x)$ (see Fig. 1). Starting from the one-loop effective QED action and requiring the magnetic background field to vary on scales much larger than the Compton wavelength $\lambda_c = 1/m \approx 3.9 \times 10^{-13}$m, we derived a formula for the reflection coefficient R_p for incoming probe photons of arbitrary frequency ω in the perturbative limit $eB/m^2 \ll 1$,

$$\begin{Bmatrix} R_\parallel \\ R_\perp \end{Bmatrix} \approx \left| \frac{\alpha}{180\pi} \frac{\omega^2}{\tilde{\omega}} \begin{Bmatrix} 7 \\ 4 \end{Bmatrix} \int \mathrm{d}x\, \mathrm{e}^{i2\tilde{\omega}x} \left(\frac{eB(x)}{m^2} \right)^2 \right|^2 . \qquad (1)$$

This formula is valid for specific setups which do not induce mixing between photon polarization modes parallel

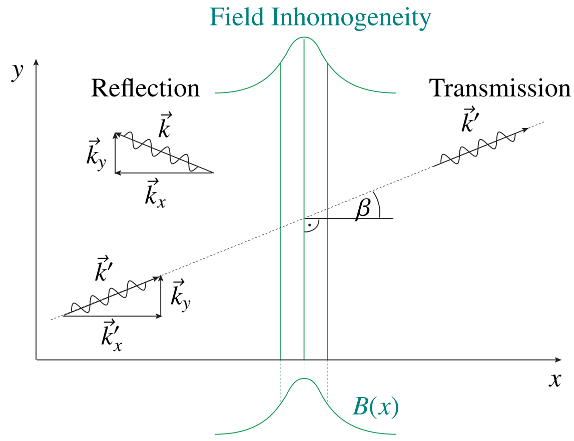

Figure 1: The static, one dimensional field inhomogeneity of amplitude $B(x)$ is infinitely extended in the transversal directions, but falls off to zero asymptotically for large values of $|x|$. The probe photons with wave vector $\vec{k}'$ hit the inhomogeneity under an angle β. The reflected photons with wave vector $\vec{k}$ are measured by a suitably placed detector spanning the y-z plane.

($\parallel$) and perpendicular ($\perp$) to the plane spanned by $\vec{k}'$ and $\vec{B}$. The dependence on the incidence angle β via $\tilde{\omega} = \omega \cos\beta$ is similar to the case of atomic quantum reflection [3]: We encounter an exponential suppression of R_p with $\tilde{\omega}$, which usually can be overcome by shining the probe beam onto the background at large angles β.

We employed Eq. (1) to obtain first estimates of the effect, exemplarily adopting design parameters of the two high-intensity laser systems to be available in Jena: POLARIS (background: $P = 1\,$PW) and JETI200 (probe: $P = 200\,$TW). By choosing a generic Gaussian field profile with a certain spatial modulation and adjusting the incoming angle β, we arrived at a reflection coefficient of $R_p = \mathcal{O}(10^{-20})$, and a number $N_{\rm ref} = \mathcal{O}(1)$ of reflected photons of per shot.

These preliminary figures suggest to make quantum reflection a promising candidate to probe the quantum vacuum nonlinearity. After establishing the existence of quantum reflection and obtaining first estimates, work is currently underway to generalize the treatment to two and three dimensional, time-dependent inhomogeneities in order to make reliable predictions for realistic experimental setups.

References

[1] W. Heisenberg and H. Euler, Z. Phys. **98**, 714 (1936).

[2] H. Gies, F. Karbstein and N. Seegert, New J. Phys. **15**, 083002 (2013) [arXiv:1305.2320 [hep-ph]].

[3] C. Henkel, C. I. Westbrook, and A. Aspect, J. Opt. Soc. Am. B **13**, 233 (1996).

Electron positron pair production in rotating electric fields

Alexander Blinne[2] *and Holger Gies*[1,2]
[1]Helmholtz Institut Jena, Fröbelstieg 3, D-07743 Jena, Germany; [2]Theoretisch-Physikalisches Institut, FSU Jena, Max-Wien-Platz 1, D-07743 Jena, Germany

We explore Schwinger pair production in rotating time-dependent electric fields using the real-time DHW formalism. We determine the time evolution of the Wigner function as well as asymptotic particle distributions neglecting back-reactions on the electric field. Whereas qualitative features can be understood in terms of effective Keldysh parameters, the field rotation leaves characteristic imprints in the momentum distribution that can be interpreted in terms of interference and multiphoton effects. These phenomena may seed characteristic features of QED cascades created in the antinodes of a high-intensity standing wave laser field.

We consider for the first time Schwinger pair production in a time-dependent rotating spatially homogeneous electric field [1]. This constitutes a substantial step towards bringing the quantum field theory studies closer to QED cascade calculations.

The real-time off-equilibrium DHW (or simply Wigner) formalism on a mean-field level (neglecting back-reactions on the electromagnetic field) as developed in [2] can be used to derive a set of modified quantum kinetic equations which describe pair production in homogeneous electric field with arbitrary polarization and time dependence.

A numerical solution yields the momentum distribution of produced pairs at infinite time,

$$f_{\lim}(\vec{p}) = \lim_{t\to\infty} f(\vec{p}),$$

which, upon integration over $\vec{p}$, gives the total number of produced pairs $\mathcal{N}$ per unit volume.

Figure 1: Momentum density of produced pairs per unit volume.

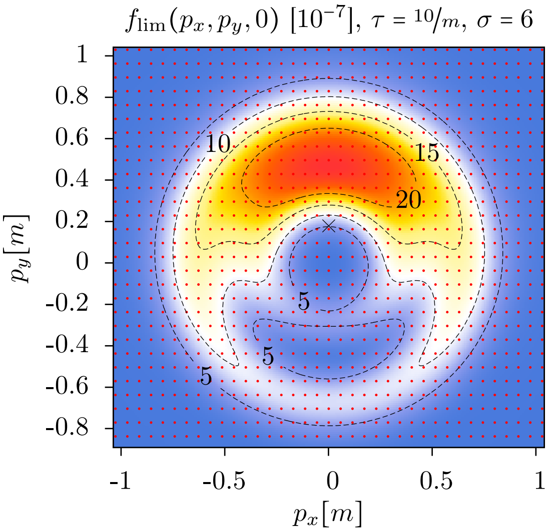

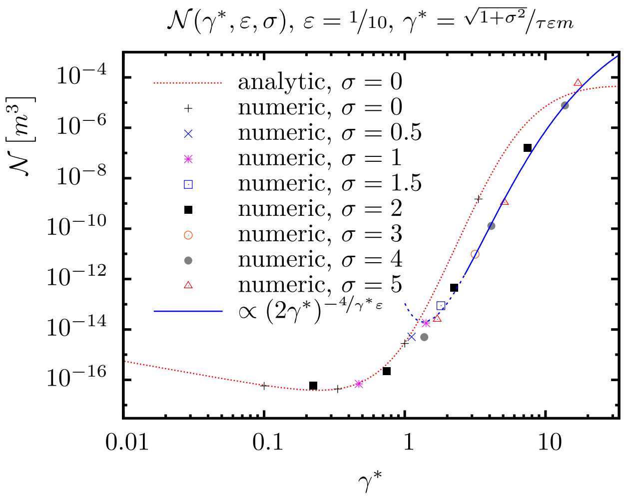

Figure 2: Particle yield for varying parameters. Comparison to power law and analytic solution for $\sigma = 0$.

We consider field configurations with with a field amplitude $\varepsilon = eE/m^2$ and σ rotation cycles inside a smooth pulse envelope of period τ. The rotating field leaves several characteristic imprints on the momentum distribution; as an example see Fig. 1. Rotation can in particular be read off from the shape of the distribution, and from resulting interference patterns. For rotation frequencies $\Omega\tau \gg 1$ the momentum distribution is anisotropic with particles predominantly created at momenta $p_x^2 + p_y^2 = (\frac{n}{2}\Omega)^2 - m^2$. This can be understood in a multiphoton picture, involving n photons in the production process.

We find that rotation generically enhances pair production compared to a linearly polarized field, since rotation introduces more Fourier modes that stimulate multiphoton effects. Fig. 2 shows a collection of integrated particle yields for a wide range of parameters $\sigma = \Omega\tau$ and τ. When viewed as a function of a modified Keldysh parameter $\gamma^* = \frac{\sqrt{1+\Omega^2\tau^2}}{\tau\varepsilon m}$, a universal behaviour emerges that is similar to the multiphoton power law.

The characteristic momentum space patterns of the distribution function, predicted for the first time in this work, can serve as a decisive fingerprint of Schwinger pair production.

References

[1] A. Blinne and H. Gies, Phys. Rev. D in press (2014), arXiv:1311.1678 [hep-ph].

[2] I. Bialynicki-Birula, P. Gornicki and J. Rafelski, Phys. Rev. D **44**, 1825 (1991).

Generation of Physical Conditions Similar to Interior of Superearth Extrasolar Planets by Imploding Solid Iron in LAPLAS Experiments at FAIR *

N.A. Tahir[1], *A. Shutov*[2], *A.R. Piriz*[3], *and Th. Stöhlker*[1,4]

[1]GSI, Darmstadt, Germany; [2]IPCP, Chernogolovka, Russia; [3]UCLM, Ciudad Real, Spain; [4]IOQ Friedrich-Schiller Universität and Helmholtz Institute, Jena, Germany

Due to the discovery of a huge number of Extrasolar planets of different types (gas giants, frozen water rich and earth like rocky planets) over the past two decades, the subject of planetary science has entered into a new very exciting era. This contribution presents numerical calculations using the LAPLAS experimental scheme [1-3] to implode solid Fe to physical conditions that are predicted to exist in the interior of Extrasolar rocky planets named "Superearths" or "Exoearths". The target consists of a solid Fe cylinder having L = 4 mm and r = 0.2 mm that is enclosed in a W cylinder having an outer radius of 3 mm.

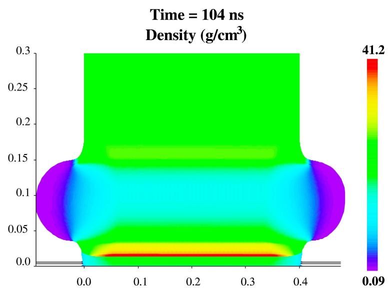

Figure 1: T vs time (Density distribution at the time of maximum compression 5 $\times$ 10^{11} ions.

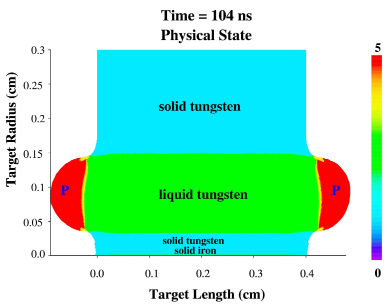

Figure 2: Phase state of the target corresponding to Fig. 1.

A hollow beam of 1 GeV/u U ions (that will be available at FAIR) that has an annular focal spot is used to implode the target. The beam intensity is considered to be 5 $\times$ 10^{11} ions per bunch where the bunch length is 50 ns. Numerical simulations have been done using the 2D hydrodynamic code, BIG2.

In Fig. 1 we present the target density at the time of maximum compression. It is seen that a shell of tungsten tamper with a density of about 40 g/cm^2 has been generated around uniformly compressed Fe. Fig. 2 shows the material phase corresponding to conditions presented in Fig. 1. It is seen that the compressed Fe and the compressed tungsten tamper are in solid phase whereas the tungsten region directly heated by the target is in liquid state.

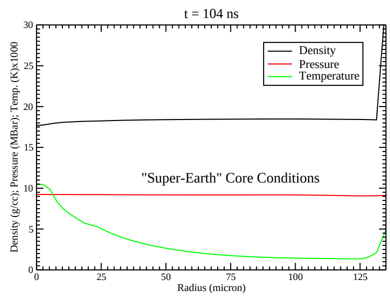

Figure 3: ρ, T and P vs r in Fe region using 5 $\times$ 10^{11} ions.

In Fig. 3 we plot the density, temperature and pressure vs radius in the iron region at L = 2 mm (target middle). It is seen that Fe has been compressed to twice the solid density where as the pressure is around 10 Mbar. These are conditions that are expected to exist in the interiors of huge earthlike Exoplanets.

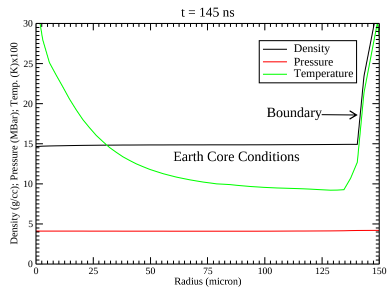

Figure 4: ρ, T and P vs r in Fe region using 2 $\times$ 10^{11} ions.

In Fig. 4 we plot the same parameters as in Fig. 3, but using a lower beam intensity of 2 $\times$ 10^{11} per bunch. In this case one achieves conditions similar to that in the earth core. LAPLAS experiment is a very efficient scheme to study planetary physics at FAIR.

References

[1] N.A. Tahir et al., PRE 63 (2001) 016402.
[2] N.A. Tahir et al., High Energy Density Phys. 2 (2006) 21.
[3] N.A. Tahir et al., New J. Phys. 12 (2010) 073022.

* Work supported by the BMBF

Publications

A. N. Artemyev, V. M. Shabaev, I. I. Tupitsyn, G. Plunien, A. Surzhykov, and S. Fritzsche
Ab initio calculations of the $2p_{3/2} - 2p_{1/2}$ fine-structure splitting in boronlike ions
Phyical Review A **88**, 032518 (2013).

D. R. Atanasov, D. Balabanski, L. Batist, K. Blaum, F. Bosch, D. Boutin, C. Brandau, C. Dimopoulou, H. G. Essel, T. Faestermann, H. Geissel, S. Hagmann, R. Hess, P.-M. Hillenbrand, P. Kienle, R. Knöbel, C. Kozhuharov, J. Kurcewicz, M. Lestinsky, S. A. Litvinov, Y. A. Litvinov, X. Ma, R. Märtin, M. Mazzocco, G. Münzenberg, F. Nolden, T. Ohtsubo, Z. Patyk, M. S. Sanjari, C. Scheidenberger, D. Shubina, U. Spillmann, M. Steck, Th. Stöhlker, B. Sun, T. Suzuki, S. Torilov, M. Trassinelli, S. Trotsenko, X. Tu, I. Tupitsyn, H. Weick, N. Winckler, M. Winkler, D. F. A. Winters, N. Winters, H. Xu, T. Yamaguchi, X. Yan, Y. Yuan, and Y. Zhang
Half-life measurements of highly charged radionuclides
Physica Scripta **2013**, 014026 (2013).

B. Aurand, B. Elkin, L.-O. Heim, B. Lommel, B. Kindler, M. Tomut, C. Rödel, S. Kuschel, O. Jäckel, J. Barz, and T. Kühl
Preparation and characterization of nanometer-thin freestanding polymer foils for laser-ion acceleration
Journal of Polymer Science Part B: Polymer Physics **51**, 1355 (2013).

B. Aurand, S. Kuschel, O. Jäckel, C. Rödel, H. Y. Zhao, S. Herzer, A. E. Paz, J. Bierbach, J. Polz, B. Elkin, G. G. Paulus, A. Karmakar, P. Gibbon, T. Kühl, and M. C. Kaluza
Radiation pressure-assisted acceleration of ions using multi-component foils in high-intensity laser-matter interactions
New Journal of Physics **15**, 033031 (2013).

K. Baker, G. Cantatore, S. A. Cetin, M. Davenport, K. Desch, B. Döbrich, H. Gies, I. G. Irastorza, J. Jäckel, A. Lindner, T. Papaevangelou, M. Pivovaroff, G. Raffelt, J. Redondo, A. Ringwald, Y. Semertzidis, A. Siemko, M. Sulc, A. Upadhye, and K. Zioutas
The quest for axions and other new light particles
Annalen der Physik **525**, A93 (2013).

D. Banaś, A. Gumberidze, S. Trotsenko, A. V. Volotka, A. Surzhykov, H. F. Beyer, F. Bosch, A. Bräuning-Demian, S. Fritzsche, S. Hagmann, C. Kozhuharov, A. Kumar, X. Ma, R. Mann, P. H. Mokler, D. Sierpowski, U. Spillmann, S. Tashenov, Z. Stachura, A. Warczak, and Th. Stöhlker
Two-photon energy distribution from the decay of the $2\,^1S_0$ state in He-like uranium
Phyical Review A **87**, 062510 (2013).

D. Banaś, M. Pajek, A. Gumberidze, A. Surzhykov, and Th. Stöhlker
Differential L-shell radiative recombination rate coefficients for bare uranium ions interacting with low-energy electrons
The European Physical Journal - Special Topics **222**, 2317 (2013).

D. Banaś, M. Pajek, A. Gumberidze, A. Surzhykov, and Th. Stöhlker
K-shell differential radiative recombination rates for bare uranium ions interacting with low-energy electrons
Physica Scripta **2013**, 014045 (2013).

S. Banerjee, J. Koerner, M. Siebold, Q. Yang, K. Ertel, P. D. Mason, P. J. Phillips, M. Loeser, H. Zhang, S. Lu, J. Hein, U. Schramm, M. C. Kaluza, and J. L. Collier
Temperature dependent emission and absorption cross section of Yb^{3+} doped yttrium lanthanum oxide (YLO) ceramic and its application in diode pumped amplifier
Optics Express **21**, 726 (2013).

K. H. Blumenhagen, E. Badura, H. Bräuning, J. Hoffmann, K. Koch, N. Kurz, R. Märtin, S. Minami, W. Ott, U. Spillmann, Th. Stöhlker, G. Weber, and M. Weber
Fully digital readout of segmented solid state detectors
Physica Scripta **2013**, 014102 (2013).

F. Bosch, D. R. Atanasov, C. Brandau, I. Dillmann, C. Dimopoulou, T. Faestermann, H. Geissel, S. Hagmann, P.-M. Hillenbrand, P. Kienle, R. Knöbel, C. Kozhuharov, J. Kurcewicz, M. Lestinsky, S. Litvinov, Y. A. Litvinov, X. Ma, F. Nolden, T. Ohtsubo, Z. Patyk, R. Reuschl, M. S. Sanjari, C. Scheidenberger, D. Shubina, U. Spillmann, M. Steck, Th. Stöhlker, B. Sun, M. Trassinelli, S. Trotsenko, X. L. Tu, H. Weick, N. Winckler, M. Winkler, D. Winters, T. Yamaguchi, and X. L. Yan
Beta decay of highly charged ions
Physica Scripta **2013**, 014025 (2013).

F. Bosch, Yu. A. Litvinov, and Th. Stöhlker
Nuclear physics with unstable ions at storage rings
Progress in Particle and Nuclear Physics **73**, 84 (2013).

N. Brambilla, F. Karbstein, and A. Vairo
Symmetries of the three-heavy-quark system and the color-singlet static energy at next-to-next-to-leading logarithmic order
Physical Review D **87**, 074014 (2013).

C. Brandau, C. Kozhuharov, A. Müller, D. Bernhardt, D. Banas, F. Bosch, F. J. Currell, C. Dimopoulou, A. Gumberidze, S. Hagmann, P.-M. Hillenbrand, M. Heil, M. Lestinsky, Y. A. Litvinov, R. Märtin, F. Nolden, R. Reuschl, S. Sanjari, S. Schippers, D. Schneider, D. Shubina, H. Simon, U. Spillmann, Z. Stachura, M. Steck, Th. Stöhlker, G. Weber, M. Wiedeking, N. Winckler, and D. F. A. Winters
Probing nuclear properties by resonant atomic collisions between electrons and ions
Physica Scripta **2013**, 014050 (2013).

S. Busold, D. Schumacher, O. Deppert, C. Brabetz, S. Frydrych, F. Kroll, M. Joost, H. Al-Omari, A. Blažević, B. Zielbauer, I. Hofmann, V. Bagnoud, T. E. Cowan, and M. Roth
Focusing and transport of high-intensity multi-MeV proton bunches from a compact laser-driven source
Physical Review Special Topics - Accelerators and Beams **16**, 101302 (2013).

W. Chen, G. Vorobyev, D. Guo, P.-M. Hillenbrand, F. Herfurth, S. Hagmann, U. Spillmann, S. Trotsenko, A. Gumberidze, and Th. Stöhlker
Charge transfer of slow highly charged xenon ions in collisions with magnesium atoms
Physical Review A **88**, 052703 (2013).

J. Colgan, J. Abdallah, A. Ya. Faenov, S. A. Pikuz, E. Wagenaars, N. Booth, O. Culfa, R. J. Dance, R. G. Evans, R. J. Gray, T. Kämpfer, K. L. Lancaster, P. McKenna, A. L. Rossall, I. Yu. Skobelev, K. S. Schulze, I. Uschmann, A. G. Zhidkov, and N. C. Woolsey
Exotic Dense-Matter States Pumped by a Relativistic Laser Plasma in the Radiation-Dominated Regime
Physical Review Letters **110**, 125001 (2013).

S. Demmler, J. Rothhardt, S. Hädrich, M. Krebs, A. Hage, J. Limpert, and A. Tünnermann
Generation of high photon flux coherent soft x-ray radiation with few-cycle pulses
Optics Letters **38**, 5051 (2013).

B. Döbrich, H. Gies, N. Neitz, and F. Karbstein
Magnetically amplified light-shining-through-walls via virtual minicharged particles
Physical Review D **87**, 025022 (2013).

L. B. Fletcher, E. Galtier, P. Heimann, H. J. Lee, B. Nagler, J. Welch, U. Zastrau, J. B. Hastings, and S. H. Glenzer
Plasmon measurements with a seeded x-ray laser
Journal of Instrumentation **8**, C11014 (2013).

S. Fuchs, C. Rödel, M. Krebs, S. Hädrich, J. Bierbach, A. E. Paz, S. Kuschel, M. Wünsche, V. Hilbert, U. Zastrau, E. Förster, J. Limpert, and G. G. Paulus
Sensitivity calibration of an imaging extreme ultraviolet spectrometer-detector system for determining the efficiency of broadband extreme ultraviolet sources
Review of Scientific Instruments **84**, 023101 (2013).

S. Gardiner, H. Gies, J. Jäckel, and C. Wallace
Tunnelling of the 3rd kind: A test of the effective non-locality of quantum field theory
Europhysics Letters **101**, 61001 (2013).

R. Geithner, D. Heinert, R. Neubert, W. Vodel, and P. Seidel
Low temperature permeability and current noise of ferromagnetic pickup coils
Cryogenics **54**, 16 (2013).

H. Gies, F. Karbstein, and N. Seegert
Quantum Reflection as a New Signature of Quantum Vacuum Nonlinearity
New Journal of Physics **15**, 083002 (2013).

A. Gopal, S. Herzer, A. Schmidt, P. Singh, A. Reinhard, W. Ziegler, D. Brömmel, A. Karmakar, P. Gibbon, U. Dillner, T. May, H.-G. Meyer, and G. G. Paulus
Observation of Gigawatt-Class THz Pulses from a Compact Laser-Driven Particle Accelerator
Physical Review Letters **111**, 074802 (2013).

A. Gopal, P. Singh, S. Herzer, A. Reinhard, A. Schmidt, U. Dillner, T. May, H.-G. Meyer, W. Ziegler, and G. G. Paulus
Characterization of 700 μJ T rays generated during high-power laser solid interaction
Optics Letters **38**, 4705 (2013).

A. Gumberidze, D. Thorn, C. Fontes, B. Najjari, H. Zhang, A. Surzhykov, A. Voitkiv, S. Fritzsche, D. Banaś, H. Beyer, W. Chen, R. DuBois, S. Geyer, R. Grisenti, S. Hagmann, M. Hegewald, S. Hess, C. Kozhuharov, R. Märtin, I. Orban, N. Petridis, R. Reuschl, A. Simon, U. Spillmann, M. Trassinelli, S. Trotsenko, G. Weber, D. Winters, N. Winters, D. Yu, and Th. Stöhlker
Electron- and Proton-Impact Excitation of Hydrogenlike Uranium in Relativistic Collisions
Physical Review Letters **110**, 213201 (2013).

J. Gunst, A. Surzhykov, A. Artemyev, S. Fritzsche, S. Tashenov, A. Maiorova, V. M. Shabaev, and Th. Stöhlker
Parity-nonconservation effects on the radiative recombination of heavy hydrogenlike ions
Phyical Review A **87**, 032714 (2013).

S. Hädrich, A. Klenke, A. Hoffmann, T. Eidam, T. Gottschall, J. Rothhardt, J. Limpert, and A. Tünnermann
Nonlinear compression to sub-30-fs, 0.5 mJ pulses at 135 W of average power
Optics Letters **38**, 3866 (2013).

S. Hagmann, Th. Stöhlker, Y. Litvinov, C. Kozhuharov, P.-M. Hillenbrand, U. Spillmann, V. Shabaev, K. Stiebing, M. Lestinsky, A. Surzhykov, A. Voitkiv, B. Franzke, D. Fischer, D. Schneider, D. Jakubassa, A. Artiomov, E. DeFilippo, X. Ma, R. Dörner, and H. Rothard
Few-body quantum dynamics of high-Z ions studied at the future relativistic high-energy storage ring
Physica Scripta **2013**, 014086 (2013).

A. G. Hayrapetyan and S. Fritzsche
Bessel beams of laser-driven two-level atoms
Physica Scripta **2013**, 014067 (2013).

A. G. Hayrapetyan K. K. Grigoryan, R. G. Petrosyan, and S. Fritzsche
Propagation of sound waves through a spatially homogeneous but smoothly time-dependent medium
Annals of Physics **333**, 47 (2013).

A. G. Hayrapetyan, O. Matula, A. Surzhykov, and S. Fritzsche
Bessel beams of two-level atoms driven by a linearly polarized laser field
The European Physical Journal D **67**, 1 (2013).

K. Heeg, H.-C. Wille, K. Schlage, T. Guryeva, D. Schumacher, I. Uschmann, K. S. Schulze, B. Marx, T. Kämpfer, G. Paulus, R. Röhlsberger, and J. Evers
Vacuum-Assisted Generation and Control of Atomic Coherences at X-Ray Energies
Physical Review Letters **111**, 073601 (2013).

V. Hilbert, A. Blinne, S. Fuchs, T. Feigl, T. Kämpfer, C. Rödel, I. Uschmann, M. Wünsche, G. Paulus, E. Förster, and U. Zastrau
An extreme ultraviolet Michelson interferometer for experiments at free-electron lasers
Review of Scientific Instruments **84**, 095111 (2013).

P. M. Hillenbrand, S. Hagmann, Th. Stöhlker, Y. Litvinov, C. Kozhuharov, U. Spillmann, V. Shabaev, K. Stiebing, M. Lestinsky, A. Surzhykov, A. Voitkiv, B. Franzke, D. Fischer, C. Brandau, S. Schippers, A. Mueller, D. Schneider, D. Jakubassa, A. Artiomov, E. DeFilippo, X. Ma, R. Dörner, and H. Rothard
Future experiments using forward electron spectroscopy to study the quantum dynamics of high- Z ions at the ESR/CRYRING storage rings
Physica Scripta **2013**, 014087 (2013).

D. C. Hochhaus, B. Aurand, M. Basko, B. Ecker, T. Kühl, T. Ma, F. Rosmej, B. Zielbauer, and P. Neumayer
X-ray radiographic expansion measurements of isochorically heated thin wire targets
Physics of Plasmas **20**, 062703 (2013).

I. Hofmann
Halo coupling and cleaning by a space charge resonance in high intensity beams
Physical Review Special Topics - Accelerators and Beams **16**, 084201 (2013).

I. Hofmann
Performance of solenoids versus quadrupoles in focusing and energy selection of laser accelerated protons
Physical Review Special Topics - Accelerators and Beams **16**, 041302 (2013).

M. Hornung, S. Keppler, R. Bödefeld, A. Kessler, H. Liebetrau, J. Körner, M. Hellwing, F. Schorcht, O. Jäckel, A. Sävert, J. Polz, A. K. Arunachalam, J. Hein, and M. C. Kaluza
High-intensity, high-contrast laser pulses generated from the fully diode-pumped Yb:glass laser system POLARIS
Optics Letters **38**, 718 (2013).

F. Jansen, F. Stutzki, H.-J. Otto, C. Jauregui, J. Limpert, and A. Tünnermann
High-power thermally guiding index-antiguiding-core fibers
Optics Letters **38**, 510 (2013).

C. Jauregui, J. Limpert, and A. Tünnermann
High-power fibre lasers
Nature Photonics **7**, 861 (2013).

C. Jauregui, H.-J. Otto, F. Stutzki, F. Jansen, J. Limpert, and A. Tünnermann
Passive mitigation strategies for mode instabilities in high-power fiber laser systems
Optics Express **21**, 19375 (2013).

A. Jochmann, A. Irman, M. Bussmann, J. P. Couperus, T. E. Cowan, A. D. Debus, M. Kuntzsch, K. W. D. Ledingham, U. Lehnert, R. Sauerbrey, H. P. Schlenvoigt, D. Seipt, Th. Stöhlker, D. B. Thorn, S. Trotsenko, A. Wagner, and U. Schramm
High Resolution Energy-Angle Correlation Measurement of Hard X Rays from Laser-Thomson Backscattering
Physical Review Letters **111**, 114803 (2013).

A. Jochmann, A. Irman, U. Lehnert, J. P. Couperus, M. Kuntzsch, S. Trotsenko, A. Wagner, A. D. Debus, H.-P. Schlenvoigt, U. Helbig, S. Bock, K. W. D. Ledingham, T. E. Cowan, R. Sauerbrey, and U. Schramm
Operation of a picosecond narrow-bandwidth Laser–Thomson-backscattering X-ray source
Nuclear Instruments and Methods in Physics Research Section B: Beam Interactions with Materials and Atoms **309**, 214 (2013).

S. Kahaly, S. Monchoce, H. Vincenti, T. Dzelzainis, B. Dromey, M. Zepf, Ph. Martin, and F. Quere
Direct Observation of Density-Gradient Effects in Harmonic Generation from Plasma Mirrors
Physical Review Letters **110**, 175001 (2013).

S. Kar, K. F. Kakolee, M. Cerchez, D. Doria, A. Macchi, P. McKenna, D. Neely, J. Osterholz, K. Quinn, B. Ramakrishna, G. Sarri, O. Willi, X. H. Yuan, M. Zepf, and M. Borghesi
Experimental investigation of hole boring and light sail regimes of RPA by varying laser and target parameters
Plasma Physics and Controlled Fusion **55**, 124030 (2013).

F. Karbstein
Photon polarization tensor in a homogeneous magnetic or electric field
Physical Review D **88**, 085033 (2013).

D. Kiefer, M. Yeung, T. Dzelzainis, P. S. Foster, S. G. Rykovanov, C. L. S. Lewis, R. S. Marjoribanks, H. Ruhl, D. Habs, J. Schreiber, M. Zepf, and B. Dromey
Relativistic electron mirrors from nanoscale foils for coherent frequency upshift to the extreme ultraviolet
Nature Communications **4**, 1763 (2013).

T. Kiefer, T. Schlegel, and M. C. Kaluza
Plasma expansion into vacuum assuming a steplike electron energy distribution
Physical Review E **87**, 043110 (2013).

M. Kienel, A. Klenke, T. Eidam, M. Baumgartl, C. Jauregui, J. Limpert, and A. Tünnermann
Analysis of passively combined divided-pulse amplification as an energy-scaling concept
Optics Express **21**, 29031 (2013).

P. Kienle, F. Bosch, P. Bühler, T. Faestermann, Yu. A. Litvinov, N. Winckler, M. S. Sanjari, D. B. Shubina, D. Atanasov, H. Geissel, V. Ivanova, X. L. Yan, D. Boutin, C. Brandau, I. Dillmann, Ch. Dimopoulou, R. Hess, P.-M. Hillebrand, T. Izumikawa, R. Knöbel, J. Kurcewicz, N. Kuzminchuk, M. Lestinsky, S. A. Litvinov, X. W. Ma, L. Maier, M. Mazzocco, I. Mukha, C. Nociforo, F. Nolden, Ch. Scheidenberger, U. Spillmann, M. Steck, Th. Stöhlker, B. H. Sun, F. Suzaki, T. Suzuki, S. Yu. Torilov, M. Trassinelli, X. L. Tu, M. Wang, H. Weick, D. F. A. Winters, N. Winters, P. J. Woods, T. Yamaguchi, G. L. Zhang, and T. Ohtsubo
High-resolution measurement of the time-modulated orbital electron capture and of the β^+ decay of hydrogen-like ^{142}Pm^{60+} ions
Physics Letters B **726**, 638 (2013).

A. Klenke, S. Breitkopf, M. Kienel, T. Gottschall, T. Eidam, S. Hädrich, J. Rothhardt, J. Limpert, and A. Tünnermann
530 W, 1.3 mJ, four-channel coherently combined femtosecond fiber chirped-pulse amplification system
Optics Letters **38**, 2283 (2013).

A. Klenke, M. Kienel, T. Eidam, S. Hädrich, J. Limpert, and A. Tünnermann
Divided-pulse nonlinear compression
Optics Letters **38**, 4593 (2013).

J. Körner, J. Hein, H. Liebetrau, R. Seifert, D. Klöpfel, M. Kahle, M. Loeser, M. Siebold, U. Schramm, and M. C. Kaluza
Efficient burst mode amplifier for ultra-short pulses based on cryogenically cooled Yb^{3+}:CaF_2
Optics Express **21**, 29006 (2013).

Y. S. Kozhedub, I. I. Tupitsyn, V. M. Shabaev, S. Hagmann, G. Plunien, and Th. Stöhlker
Relativistic calculations of inner-shell atomic processes in low-energy ion–atom collisions
Physica Scripta **2013**, 014053 (2013).

D. Kraus, J. Vorberger, D. O. Gericke, V. Bagnoud, A. Blazevic, W. Cayzac, A. Frank, G. Gregori, A. Ortner, A. Otten, F. Roth, G. Schaumann, D. Schumacher, K. Siegenthaler, F. Wagner, K. Wünsch, and M. Roth
Probing the Complex Ion Structure in Liquid Carbon at 100 Gpa
Physical Review Letters **111**, 255501 (2013).

M. Krebs, S. Hädrich, S. Demmler, J. Rothhardt, A. Zaïr, L. Chipperfield, J. Limpert, and A. Tünnermann
Towards isolated attosecond pulses at megahertz repetition rates
Nature Photonics **7**, 555 (2013).

M. Kübel, N. G. Kling, K. J. Betsch, N. Camus, A. Kaldun, U. Kleineberg, I. Ben-Itzhak, R. R. Jones, G. G. Paulus, T. Pfeifer, J. Ullrich, R. Moshammer, M. F. Kling, and B. Bergues
Nonsequential double ionization of N_2 in a near-single-cycle laser pulse
Physical Review A **88**, 023418 (2013).

S. Kuhn, A. Herrmann, J. Hein, M. C. Kaluza, and C. Rüssel
Sm^{3+}-doped La_2O_3–Al_2O_3–SiO_2-glasses: structure, fluorescence and thermal expansion
Journal of Materials Science **48**, 8014 (2013).

P. Linusson, S. Fritzsche, J. H. D. Eland, M. Mucke, and R. Feifel
Single-photon multiple ionization forming double vacancies in the 2p subshell of argon
Phyical Review A **87**, 043409 (2013).

Yu. A. Litvinov, S. Bishop, K. Blaum, F. Bosch, C. Brandau, L. X. Chen, I. Dillmann, P. Egelhof, H. Geissel, R. E. Grisenti, S. Hagmann, M. Heil, A. Heinz, N. Kalantar-Nayestanaki, R. Knöbel, C. Kozhuharov, M. Lestinsky, X. W. Ma, T. Nilsson, F. Nolden, A. Ozawa, R. Raabe, M. W. Reed, R. Reifarth, M. S. Sanjari, D. Schneider, H. Simon, M. Steck, T. Stöhlker, B. H. Sun, X. L. Tu, T. Uesaka, P.M. Walker, M. Wakasugi, H. Weick, N. Winckler, P. J. Woods, H.S. Xu, T. Yamaguchi, Y. Yamaguchi, and Y.H. Zhang
Nuclear physics experiments with ion storage rings
Nuclear Instruments and Methods in Physics Research Section B: Beam Interactions with Materials and Atoms **317**, 603 (2013).

A. V. Maiorova, A. Surzhykov, S. Tashenov, V. M. Shabaev, and Th. Stöhlker
Production and diagnostics of spin-polarized heavy ions in the sequential two-electron radiative recombination
Physica Scripta **2013**, 014046 (2013).

I. A. Maltsev, G. B. Deyneka, I. I. Tupitsyn, V. M. Shabaev, Y. S. Kozhedub, G. Plunien, and Th. Stöhlker
Relativistic calculations of charge transfer probabilities in U^{92+}–U^{91+}(1s) collisions using the basis set of cubic Hermite splines
Physica Scripta **2013**, 014056 (2013).

R. Märtin, G. Weber, R. Barday, Y. Fritzsche, J. Enders, U. Spillmann, and Th. Stöhlker
Target-thickness effects in electron–atom bremsstrahlung
Physica Scripta **2013**, 014070 (2013).

B. Marx, K. S. Schulze, I. Uschmann, T. Kämpfer, R. Lötzsch, O. Wehrhan, W. Wagner, C. Detlefs, T. Roth, J. Härtwig, E. Förster, Th. Stöhlker, and G. G. Paulus
High-Precision X-Ray Polarimetry
Physical Review Letters **110**, 254801 (2013).

O. Matula, A. G. Hayrapetyan, V. G. Serbo, A. Surzhykov, and S. Fritzsche
Atomic ionization of hydrogen-like ions by twisted photons: angular distribution of emitted electrons
Journal of Physics B: Atomic, Molecular and Optical Physics **46**, 205002 (2013).

S. Mondal, R. Ma, K. Motomura, H. Fukuzawa, A. Yamada, K. Nagaya, S. Yase, Y. Mizoguchi, M. Yao, A. Rouzée, A. Hundertmark, M. J. J. Vrakking, P. Johnsson, M. Nagasono, K. Tono, T. Togashi, Y. Senba, H. Ohashi, M. Yabashi, T. Ishikawa, I. P. Sazhina, S. Fritzsche, N. M. Kabachnik, and K Ueda
Photoelectron angular distributions for the two-photon sequential double ionization of xenon by ultrashort extreme ultraviolet free electron laser pulses
Journal of Physics B: Atomic, Molecular and Optical Physics **46**, 164022 (2013).

Y. Nakano, Y. Takano, T. Ikeda, Y. Kanai, S. Suda, T. Azuma, H. Bräuning, A. Bräuning-Demian, D. Dauvergne, Th. Stöhlker, and Y. Yamazaki
Resonant coherent excitation of the lithiumlike uranium ion - A scheme for heavy-ion spectroscopy
Phyical Review A **87**, 060501 (2013).

W. Nörtershäuser, M. Lochmann, R. Jöhren, C. Geppert, Z. Andelkovic, D. Anielski, B. Botermann, M. Bussmann, A. Dax, N. Frömmgen, M. Hammen, V. Hannen, T. Kühl, Y. A. Litvinov, J. Volbrecht, Th. Stöhlker, R. C. Thompson, C. Weinheimer, W. Wen, E. Will, D. Winters, and R. M. Sánchez
First observation of the ground-state hyperfine transition in $^{209}Bi^{80+}$
Physica Scripta **2013**, 014016 (2013).

H.-J. Otto, C. Jauregui, F. Stutzki, F. Jansen, J. Limpert, and A. Tünnermann
Controlling mode instabilities by dynamic mode excitation with an acousto-optic deflector
Optics Express **21**, 17285 (2013).

H.-J. Otto, F. Jansen, F. Stutzki, C. Jauregui, J. Limpert, and A. Tünnermann
Improved Modal Reconstruction for Spatially and Spectrally Resolved Imaging
Journal of Lightwave Technology **31**, 1295 (2013).

S. Pikuz, A. Faenov, J. Colgan, R. Dance, J. Abdallah, E. Wagenaars, N. Booth, O. Culfa, R. Evans, R. Gray, T. Kämpfer, K. Lancaster, P. McKenna, A. Rossall, I. Skobelev, K. Schulze, I. Uschmann, A. Zhidkov, and N. Woolsey
Measurement and simulations of hollow atom X-ray spectra of solid-density relativistic plasma created by high-contrast PW optical laser pulses
High Energy Density Physics **9**, 560 (2013).

T. Rathje, A. M. Sayler, S. Zeng, P. Wustelt, H. Figger, B. D. Esry, and G. G. Paulus
Coherent Control at Its Most Fundamental: Carrier-Envelope-Phase-Dependent Electron Localization in Photodissociation of a H_2^+ Molecular Ion Beam Target
Physical Review Letters **111**, 093002 (2013).

R. Reuschl, T. Gassner, U. Spillmann, A. Bräuning-Demian, A. Ananyeva, H. Beyer, K.-H. Blumenhagen, W. Chen, S. Hagmann, M. Hegewald, P. Indelicato, M. Schwemlein, S. Toleikis, M. Trassinelli, S. Trotsenko, D. Winters, N. Winters, and Th. Stöhlker
Lifetime measurement of the 2 $^3P_0$ state in He-like uranium
Physica Scripta **2013**, 014024 (2013).

R. Riedel, A. Al-Shemmary, M. Gensch, T. Golz, M. Harmand, N. Medvedev, M. J. Prandolini, K. Sokolowski-Tinten, S. Toleikis, U. Wegner, B. Ziaja, N. Stojanovic, and F. Tavella
Single-shot pulse duration monitor for extreme ultraviolet and X-ray free-electron lasers
Nature Communications **4**, 1731 (2013).

R. Riedel, M. Schulz, M. J. Prandolini, A. Hage, H. Höppner, T. Gottschall, J. Limpert, M. Drescher, and F. Tavella
Long-term stabilization of high power optical parametric chirped-pulse amplifiers
Optics Express **21**, 28987 (2013).

V. Rodriguez, A. Bernhard, A. Keilmann, P. Peiffer, R. Rossmanith, C. Widmann, T. Baumbach, M. Nicolai, and M. C. Kaluza
Development of a Superconducting Transverse-Gradient Undulator for Laser-Wakefield Accelerators
IEEE Transactions on Applied Superconductivity **23**, 4101505 (2013).

J. Rothhardt, S. Demmler, S. Hädrich, T. Peschel, J. Limpert, and A. Tünnermann
Thermal effects in high average power optical parametric amplifiers
Optics Letters **38**, 763 (2013).

A. Rouzée, P. Johnsson, L. Rading, A. Hundertmark, W. Siu, Y. Huismans, S. Düsterer, H. Redlin, F. Tavella, N. Stojanovic, A. Al-Shemmary, F. Lépine, D. M. P. Holland, T Schlatholter, R. Hoekstra, H. Fukuzawa, K. Ueda, and M. J. J. Vrakking
Towards imaging of ultrafast molecular dynamics using FELs
Journal of Physics B: Atomic, Molecular and Optical Physics **46**, 164029 (2013).

S. Salem, Th. Stöhlker, A. Bräuning-Demian, S. Hagmann, C. Kozhuharov, D. Liesen, and A. Gumberidze
Angular distribution of photons for the simultaneous excitation and ionization of He-like uranium ions in relativistic ion-atom collisions
Physical Review A **88**, 012701 (2013).

G. Sarri, W. Schumaker, A. Di Piazza, K. Poder, J. M. Cole, M. Vargas, D. Doria, S. Kushel, B. Dromey, G. Grittani, L. Gizzi, M. E. Dieckmann, A. Green, V. Chvykov, A. Maksimchuk, V. Yanovsky, Z. H. He, B. X. Hou, J. A. Nees, S. Kar, Z. Najmudin, A. G. R. Thomas, C. H. Keitel, K. Krushelnick, and M. Zepf
Laser-driven generation of collimated ultra-relativistic positron beams
Plasma Physics and Controlled Fusion **55**, 124017 (2013).

G. Sarri, W. Schumaker, A. Di Piazza, M. Vargas, B. Dromey, M. E. Dieckmann, V. Chvykov, A. Maksimchuk, V. Yanovsky, Z. H. He, B. X. Hou, J. A. Nees, A. G. R. Thomas, C. H. Keitel, M. Zepf, and K. Krushelnick
Table-Top Laser-Based Source of Femtosecond, Collimated, Ultrarelativistic Positron Beams
Physical Review Letters **110**, 255002 (2013).

M. B. Schwab, A. Sävert, O. Jäckel, J. Polz, M. Schnell, T. Rinck, L. Veisz, M. Möller, P. Hansinger, G. G. Paulus, and M. C. Kaluza
Few-cycle optical probe-pulse for investigation of relativistic laser-plasma interactions
Applied Physics Letters **103**, 191118 (2013).

M. Schnell, A. Sävert, I. Uschmann, M. Reuter, M. Nicolai, T. Kämpfer, B. Landgraf, O. Jäckel, O. Jansen, A. Pukhov, M. C. Kaluza, and C. Spielmann
Optical control of hard X-ray polarization by electron injection in a laser wakefield accelerator
Nature Communications **4**, 2421 (2013).

D. Seipt and B. Kämpfer
Asymmetries of azimuthal photon distributions in nonlinear Compton scattering in ultra-short intense laser pulses
Physical Review A **88**, 012127 (2013).

D. Shubina, R. B. Cakirli, Yu. A. Litvinov, K. Blaum, C. Brandau, F. Bosch, J. J. Carroll, R. F. Casten, D. M. Cullen, I. J. Cullen, A. Y. Deo, B. Detwiler, C. Dimopoulou, F. Farinon, H. Geissel, E. Haettner, M. Heil, R. S. Kempley, C. Kozhuharov, R. Knöbel, J. Kurcewicz, N. Kuzminchuk, S. A. Litvinov, Z. Liu, R. Mao, C. Nociforo, F. Nolden, Z. Patyk, W. R. Plass, A. Prochazka, M. W. Reed, M. S. Sanjari, C. Scheidenberger, M. Steck, Th. Stöhlker, B. Sun, T. P. D. Swan, G. Trees, P. M. Walker, H. Weick, N. Winckler, M. Winkler, P. J. Woods, T. Yamaguchi, and C. Zhou
Schottky mass measurements of heavy neutron-rich nuclides in the element range $70 \leq Z \leq 79$ at the GSI Experimental Storage Ring
Physical Review C **88**, 024310 (2013).

N. Sirse, J. P. Booth, P. Chabert, A. Surzhykov, and P. Indelicato
Chlorine atom densities in the $(3p^5)^2P^0_{1/2}$ excited spin-orbit state measured by two-photon absorption laser-induced fluorescence in a chlorine inductively coupled plasma
Journal of Physics D: Applied Physics **46**, 295203 (2013).

U. Spillmann, K. H. Blumenhagen, E. Badura, M. Balzer, H. Bräuning, J. Hoffmann, K. Koch, N. Kurz, R. Märtin, S. Minami, W. Ott, Th. Stöhlker, G. Weber, and M. Weber
Employing digital pulse processing electronics for the readout of a Si(Li)–Compton–polarimeter for the SPARC collaboration
Physica Scripta **2013**, 014103 (2013).

Th. Stöhlker, Y. A. Litvinov, V. Bagnoud, U. Bechstedt, C. Dimopoulou, A. Dolinskii, C. Geppert, S. Hagmann, T. Katayama, T. Kühl, R. Maier, W. Nörtershäuser, D. Prasuhn, R. Schuch, M. Steck, and H. Stockhorst
SPARC experiments at the high-energy storage ring
Physica Scripta **2013**, 014085 (2013).

F. Stutzki, F. Jansen, C. Jauregui, J. Limpert, and A. Tünnermann
2.4 mJ, 33 W Q-switched Tm-doped fiber laser with near diffraction-limited beam quality
Optics Letters **38**, 97 (2013).

A. Surzhykov, Y. Litvinov, Th. Stöhlker, and S. Fritzsche
Hyperfine-induced effects on the linear polarization of $K\alpha_1$ emission from heliumlike ions
Phyical Review A **87**, 052507 (2013).

A. Surzhykov, A. V. Maiorova, V. M. Shabaev, Th. Stöhlker, and S. Fritzsche
Parity violation in beryllium-like heavy ions
Physica Scripta **2013**, 014027 (2013).

A. Surzhykov, R. H. Pratt, and S. Fritzsche
Two-photon decay of inner-shell vacancies in heavy atoms
Phyical Review A **88**, 042512 (2013).

A. Surzhykov, V. A. Yerokhin, T. Jahrsetz, P. Amaro, Th. Stöhlker, and S. Fritzsche
Polarization correlations in the elastic Rayleigh scattering of photons by hydrogenlike ions
Physical Review A **88**, 062515 (2013).

N. A. Tahir, A. Shutov, A. P. Zharkov, P. Spiller, A. R. Piriz, G. Rodriguez Prietoc, C. Deutsch, and Th. Stöhlker
Ion Beam Driven High Energy Density Physics Studies at FAIR at Darmstadt: The HEDge-HOB Collaboration
Contributions to Plasma Physics **53**, 292 (2013).

S. Tashenov, T. Bäck, R. Barday, B. Cederwall, J. Enders, A. Khaplanov, Yu. Fritzsche, K.-U. Schässburger, A. Surzhykov, V. A. Yerokhin, and D. Jakubassa-Amundsen
Bremsstrahlung polarization correlations and their application for polarimetry of electron beams
Phyical Review A **87**, 022707 (2013).

M. Tiegel, A. Herrmann, C. Russel, J. Korner, D. Klopfel, J. Hein, and M. C. Kaluza
Magnesium aluminosilicate glasses as potential laser host material for ultrahigh power laser systems
Journal of Materials Chemistry C **1**, 5031 (2013).

W. Q. Wen, M. Lochmann, X. Ma, M. Bussmann, D. F. A. Winters, W. Nörtershäuser, B. Botermann, C. Geppert, N. Frömmgen, M. Hammen, V. Hannen, R. Jöhren, Th. Kühl, Yu. A. Litvinov, R. Sanchez, Th. Stöhlker, J. Vollbrecht, C. Weinheimer, C. Dimopoulou, F. Nolden, and M. Steck
Optical measurement of the longitudinal ion distribution of bunched ion beams in the ESR
Nuclear Instruments and Methods in Physics Research Section A: Accelerators, Spectrometers, Detectors and Associated Equipment **90**, 711 (2013).

D. F. A. Winters, V. Bagnoud, B. Ecker, U. Eisenbarth, S. Götte, T. Kühl, P. Neumayer, C. Spielmann, Th. Stöhlker, and B. Zielbauer
A beamline for x-ray laser spectroscopy at the experimental storage ring at GSI
Physica Scripta **2013**, 014089 (2013).

N. Winters, A. Warczak, J. A. Tanis, T. Gassner, A. Gumberidze, S. Hagmann, P. M. Hillenbrand, C. Kozhuharov, N. Petridis, R. Reuschl, M. Schwemlein, D. Sierpowski, U. Spillmann, R. Strzalka, S. Trotsenko, G. Weber, D. F. A. Winters, Z. Yin, and Th. Stöhlker
A study of radiative double electron capture in bare chromium ions at the ESR
Physica Scripta **2013**, 014048 (2013).

V. A. Yerokhin, A. Surzhykov, R. Märtin, S. Tashenov, and G. Weber
Bremsstrahlung of polarized positrons scattered off atoms
Physica Scripta **2013**, 014072 (2013).

M. Yeung, B. Dromey, D. Adams, S. Cousens, R. Hörlein, Y. Nomura, G. D. Tsakiris, and M. Zepf
Beaming of High-Order Harmonics Generated from Laser-Plasma Interactions
Physical Review Letters **110**, 165002 (2013).

M. Yeung, B. Dromey, C. Rödel, J. Bierbach, M. Wünsche, G. Paulus, T. Hahn, D. Hemmers, C. Stelzmann, G. Pretzler, and M. Zepf
Near-monochromatic high-harmonic radiation from relativistic laser-plasma interactions with blazed grating surfaces
New Journal of Physics **15**, 025042 (2013).

Y. L. Shi, C.-Z. Dong, X.-Y. Ma, Z.-W. Wu, L.-Y. Xie, and S. Fritzsche
Polarization of M2 Line Emitted Following Electron-Impact Excitation of Beryllium-Like Ions
Chinese Physics Letters **30**, 063401 (2013).

U. Zastrau, A. Woldegeorgis, E. Förster, R. Loetzsch, H. Marschner, and I. Uschmann
Characterization of strongly-bent HAPG crystals for von-Hámos x-ray spectrographs
Journal of Instrumentation **8**, P10006 (2013).

M. Zürch, C. Kern, and C. Spielmann
XUV coherent diffraction imaging in reflection geometry with low numerical aperture
Optics Express **21**, 21131 (2013).